# Contents of issue 1 vol. XLVII

Polish Academy of Sciences
Institute of Fundamental Technological Research

# Archives of Mechanics


## Archiwum Mechaniki Stosowanej

volume 47 issue 1

Polish Scientific Publishers PWN
Warszawa 1995

ARCHIVES OF MECHANICS IS DEVOTED TO
Theory of elasticity and plasticity • Theory of nonclassical continua • Physics of continuous media • Mechanics of discrete media • Nonlinear mechanics • Rheology • Fluid gas-mechanics • Rarefied gas • Thermodynamics

---




Printed in Poland, Editorial Office: Świętokrzyska 21,
00-049 Warszawa (Poland)

---

Arkuszy wydawniczych 11. Arkuszy drukarskich 9,5.
Papier offset. kl. III 70 g. B1. Oddano do składania w styczniu 1995 r.
Druk ukończono w marcu 1995 r.
Druk i oprawa: Drukarnia Braci Grodzickich, Żabieniec ul. Przelotowa 7

---

Arch. Mech., 47, 1, pp. 3–11, Warszawa 1995

# Finite-difference analysis of the stability of flow in a curved channel wide-gap problem

M.A. ALI (BAHRAIN), V.M. SOUNDALGEKAR (THANE)
and H.S. TAKHAR (MANCHESTER)

THE FINITE-DIFFERENCE solution to an eigenvalue problem governing the stability of flow between two concentric stationary cylinders separated by a wide gap is presented. The flow is due to a circumferential pressure gradient and is known as the Dean problem. Our results agree well with the earlier results derived by using the Galerkin method. The cell-patterns and radial and tangential velocity perturbations are shown graphically for different values of $\eta(= R_1/R_2)$ where $R_1$ and $R_2$ are the radii of the inner and outer cylinders, respectively. It is observed that the flow remains more stable when the gap width is increased. The effects of gap width on the cell pattern and the perturbations are discussed.

## 1. Introduction

THE THEORETICAL and experimental investigation of the stability of viscous flow between two concentric cylinders separated by a narrow gap was first investigated by TAYLOR [11]. He assumed that the inner cylinder is rotating and the outer one is stationary. Subsequently, this problem was again solved by CHANDRASEKHAR [1] using a trigonometric series method, by DIPRIMA [5] employing the Galerkin method, and by Harris and Reid (1964) using an asymptotic and numerical method, respectively. The corresponding wide gap problem was also solved by CHANDRASEKHAR [2], CHANDRASEKHAR and ELBERT [3], and WALOWIT *et al.* [12] using the Galerkin method, and by SPARROW *et al.* [8] using a numerical method. TAKHAR *et al.* [9, 10] showed the cell patterns etc. in the wide gap stability problem between rotating concentric cylinders.

If the flow between two concentric stationary cylinders is due to transverse pressure gradient, then the question arises as to how the stability of such a flow is affected. This was first studied by DEAN [4] for a narrow gap case and the eigenvalue problem was solved by Dean who employed a Fourier series and determined the critical value of the parameter $\Lambda_c = 93053$ at which the instability sets in. This was later confirmed by REID [7] who again studied Dean's problem by solving the eigenvalue problem using a set of orthogonal functions. The corresponding wide gap Dean's problem was later solved by WALOWIT *et al.* [12] by using a Galerkin method, and by GIBSON and COOK [6] by using a Chebychef collocation method. However, in these last two papers, the cell pattern, the radial and tangential velocity perturbations at the onset of instability are not shown graphically. These graphs are important in understanding the physical phenomenon. Hence we have again attempted to solve this wide gap Dean stability problem by

using a finite-difference method. The results agree very well with those derived by WALOWIT *et al.* [12]. In Sec. 2, the mathematical analysis is presented and in Sec. 3, the conclusions are set out.

## 2. Mathematical analysis

We consider two concentric cylinders of radii $R_1$, $R_2$ of inner and outer cylinders, respectively. Let $(r, \theta, z)$ be the usual cylindrical coordinates, with the $z$-axis coinciding with the axis of the cylinders. If $u_r$, $u_\theta$ and $u_z$ denote the components of velocity in the increasing $r, \theta$ and $z$-directions and $p$ denotes the pressure, then the steady state solutions of the Navier-Stokes equation are (Fig. 1)

$$u_r = u_z = 0, \qquad u_\theta = V(r), \qquad \frac{\partial p}{\partial r} = \rho V^2/r, \tag{2.1}$$

where $\rho$ is the density.

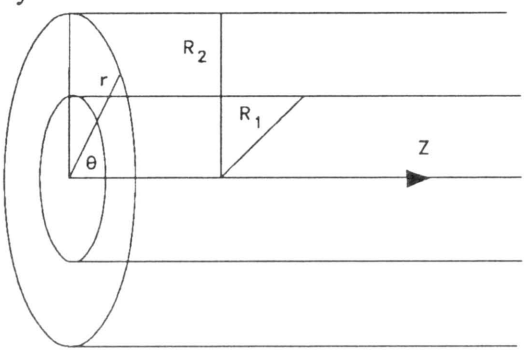


FIG. 1. Schematic diagram.

To study the stability, we assume that a small rotationally symmetric disturbance in the $\theta$-direction is superimposed on the steady motion. Mathematically this is represented by

$$u_\theta(r, z, t) = V(r) + v(r)e^{\sigma t} \cos \lambda z, \tag{2.2}$$

where $\sigma$ is the growth rate of the disturbance and $\lambda$ is the wave number. Usually $\sigma$ is a complex quantity $(\sigma_r + i\sigma_i)$ and the stability of the motion depends on $\sigma$. If the solution of the resultant eigenvalue problem exist such that $\mathrm{Re}(\sigma) > 0$, then the motion is unstable and if $\mathrm{Re}(\sigma) < 0$, then the motion is stable. It has been observed experimentally that there occurs a new steady secondary motion and the marginal state is said to occur at $\sigma = 0$.

Substituting Eq. (2.2) in the usual Navier-Stokes equations in cylindrical polar coordinates and linearising the equations for the disturbance velocities, we get

$$(DD^* - \lambda^2)^2 u = \frac{2\lambda^2}{\nu} \Omega(r) v, \tag{2.3}$$

$$(DD^* - \lambda^2)v = \frac{1}{\nu}(D^*V)u, \tag{2.4}$$

where $u$ is the disturbance velocity in the radial direction, $\nu$ is the kinematic viscosity and $\Omega(r) = V(r)/r$. Also

$$D = \frac{d}{dr}, \qquad D^* = D + \frac{1}{r}. \tag{2.5}$$

The corresponding no-slip boundary conditions are

$$u = v = Du = 0 \tag{2.6}$$

at $r = R_1$ and $r = R_2$.

Considering constant circumferential pressure gradient, the basic velocity is given by

$$V(r) = \frac{1}{2\rho\nu}\frac{\partial p}{\partial \theta}\left(r \ln r + Cr + \frac{E}{r}\right), \tag{2.7}$$

where

$$C = -\frac{R_2^2 \ln R_2 - R_1^2 \ln R_1}{R_2^2 - R_1^2}, \qquad E = \frac{R_1^2 R_2^2}{R_2^2 - R_1^2} \ln \frac{R_2}{R_1}. \tag{2.8}$$

We now introduce the following dimensionless variables:

$$r = R_0 + dx, \qquad a = \lambda d, \tag{2.9}$$

where

$$d = R_2 - R_1 \qquad \text{and} \qquad R_0 = \frac{R_1 + R_2}{2}.$$

Here $d$ is the gap width and $R_0$ is the mean radius.

Again introducing

$$\xi = \frac{r}{R_2} = \eta + (1 - \eta)\left(x + \frac{1}{2}\right), \qquad \eta = \frac{R_1}{R_2}, \tag{2.10}$$

Equations (2.3) and (2.4) in view of relations (2.8)–(2.10), reduce to the following finite gap Dean stability problem:

$$(DD^* - a^2)^2 u = a^2 P[h(x)/\xi]v, \tag{2.11}$$

$$(DD^* - a^2)v = (D^*h)u, \tag{2.12}$$

where

$$V(r) = V_m h(x), \qquad V_m = -\frac{R_2}{2\rho\nu}\frac{\partial p}{\partial \theta}\frac{(1 - \eta^2)^2 - 4\eta^2(\ln \eta)^2}{4(1 - \eta)(1 - \eta^2)},$$

$$h(x) = \frac{4(1-\eta)}{4\eta^2(\ln\eta)^2 - (1-\eta^2)^2}\xi\left\{(1-\eta^2)\ln\xi + \eta^2\ln\eta\left(1-\frac{1}{\xi^2}\right)\right\}, \tag{2.13}$$

where

$$P = 2\left(\frac{V_m d}{\nu}\right)^2 \frac{d}{R_2}.$$

Here $V_m$ is the average velocity, and $u$ is replaced by $(V_m d/\nu)^{-1}u$.

The boundary conditions now reduce to

$$u = v = Du = 0 \qquad \text{at} \qquad x = 0 \text{ and } 1. \tag{2.14}$$

We have now to solve the eigenvalue problem defined by Eqs. (2.11) and (2.12), satisfying the boundary conditions (2.14). We determine $P_c$, the critical value of $P$, which is the minimum value of $P$ over all the positive real values of the wave number $a$, and then the corresponding critical wave number $a_c$. For this purpose, we employ the finite-difference technique as follows:

We write Eqs. (2.11) and (2.12) by expanding in terms of power of $D$ as

$$\left[D^4 + 2KD^3 - \left(3K^2 + 2a^2\right)D^2 + \left(3K^3 - 2a^2K\right)D + \left(2a^2K^2 - 3K^4 + a^4\right)\right]u = a^2P(h(x)/\xi)v, \tag{2.15}$$

$$\left(D^2 + KD - K^2 - a^2\right)v = (D^*h)u, \tag{2.16}$$

where

$$K = \frac{1-\eta}{\xi}.$$

By expressing the derivatives in terms of the central-differences and rearranging them, Eqs. (2.15) and (2.116) reduce to the following:

$$m_1U_{i+2} + m_2U_{i+1} + m_3U_i + m_4U_{i-1} + m_5U_{i-2} = h^4a^2P(h(x)/\xi)V_i, \tag{2.17}$$

$$C_1V_{i+1} + C_2V_i + C_3V_{i-1} = h^2(D^*h)U_i, \tag{2.18}$$

$$\begin{aligned}
m_1 &= 1 + hK,\\
m_2 &= -\left[4 + 2hK + h^2(3K^2 + 2a^2) - \frac{1}{2}h^3(3K^3 - 2a^2K)\right],\\
m_3 &= 6 + 2h^2(3K^2 + 2a^2) + h^4(2a^2K - 2K^4 + a^4),\\
m_4 &= -\left[4 - 2hK + h^2(3K^2 + 2a^2) + \frac{1}{2}h^3(3K^3 - 2a^2K)\right],\\
m_5 &= 1 - hK,\\
C_1 &= 1 + \frac{1}{2}hK, \qquad C_2 = -2 - h^2(K^2 + a^2), \qquad C_3 = 1 - \frac{1}{2}hK.
\end{aligned} \tag{2.19}$$

Here the suffix $i$ stands for the pivoted point under consideration. The step-length $h = 1/N$ where $N$ is the number of intervals into which the range $(0, 1)$ is divided.

The boundary conditions (2.14) can now be written as

$$U_0 = V_0 = U_N = V_N = 0, \qquad U_{-1} = U_1, \qquad U_{N+1} = U_{N-1}. \tag{2.20}$$

The Eqs. (2.17) and (2.18), taking account of (2.19), can be expressed in matrix notation as

$$A_1\overline{U} = h^4 P B_1 \overline{V}, \tag{2.21}$$

$$A_2\overline{V} = h^2 B_2 \overline{U}. \tag{2.22}$$

Here the coefficient matrices $A_1$, $A_2$, $B_1$ and $B_2$ and the column matrices $\overline{U}$, $\overline{V}$ are of order $n \times n$, where $n = N - 1$.

We now express Eqs. (2.21) and (2.22) in the following form

$$(\mathbf{C} - \lambda \mathbf{I})\overline{U} = 0, \tag{2.23}$$

where $\lambda = h^6 P$, and the matrix $\mathbf{C}$ is given by

$$\mathbf{C} = \left[B_1 \, A_2^{-1} \, B_2\right]^{-1} A_1. \tag{2.24}$$

The solution is obtained as follows:

The matrix $\mathbf{C}$ is first reduced to the upper Heissenberg form. The eigenvalues and eigenvectors are then calculated using the QR algorithm. Hence for given wave number $a$, the corresponding $P$ is the lowest value of $\lambda$ obtained from (2.23). The computations are repeated for different values of $a$ until the minimum value $P_c$ and the corresponding $a_c$ are well-defined. The eigenvectors $\overline{U}$ and the corresponding $\overline{V}$ are then computed for $\lambda = P_c$ and normalised to unity. We then use the values of $\overline{U}$ to draw the cell-patterns. Throughout the computations, we have assumed $h = 1/100$.

**Critical values of $(V_m d/\nu)(d/R_2)^{1/2} = (P/2)^{1/2}$ and the corresponding values of $a_c$ for different values of $\eta$.**

| $\eta$ | $a_c$ | $(P/2)^{1/2}$ | $(P/2)^{1/2}$ WALOWIT *et al.* |
|---|---|---|---|
| 0.95 | 3.98 | 36.32 | 36.26 |
| 0.9 | 4.01 | 36.80 | 36.79 |
| 0.8 | 4.08 | 37.89 | 37.88 |
| 0.7 | 4.15 | 39.21 | 39.19 |
| 0.6 | 4.22 | 40.85 | 40.79 |
| 0.5 | 4.29 | 42.89 | 42.79 |
| 0.4 | 4.37 | 45.51 | 45.18 |
| 0.3 | 4.45 | 49.02 | 48.75 |
| 0.2 | 4.56 | 54.0 | 53.60 |
| 0.1 | 4.73 | 61.50 | 60.92 |

The cell patterns are shown in Figs. 2–4 for different values of $\eta$ and $z(= z/d)$, and the radial and tangential velocity perturbations at the onset of instability are shown in Figs. 5 and 6, respectively. It is observed that an increaase in the gap width leads to an increase in the value of critical wave number $a_c$ and the flow also remains more stable as the values of $(P/2)^{1/2}$ increase.

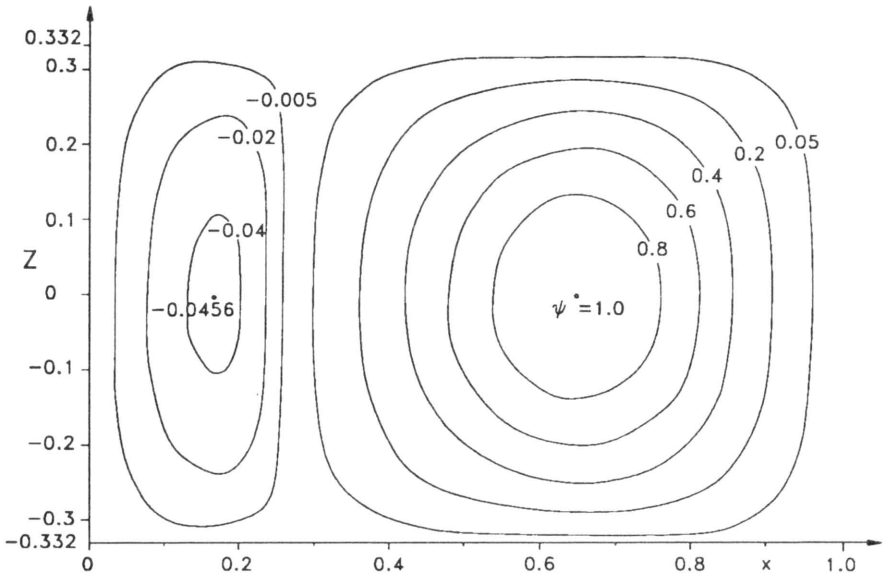


FIG. 2. The cell pattern at the onset of instability $\eta = 0.1$, $\psi = u(x)\cos az$.

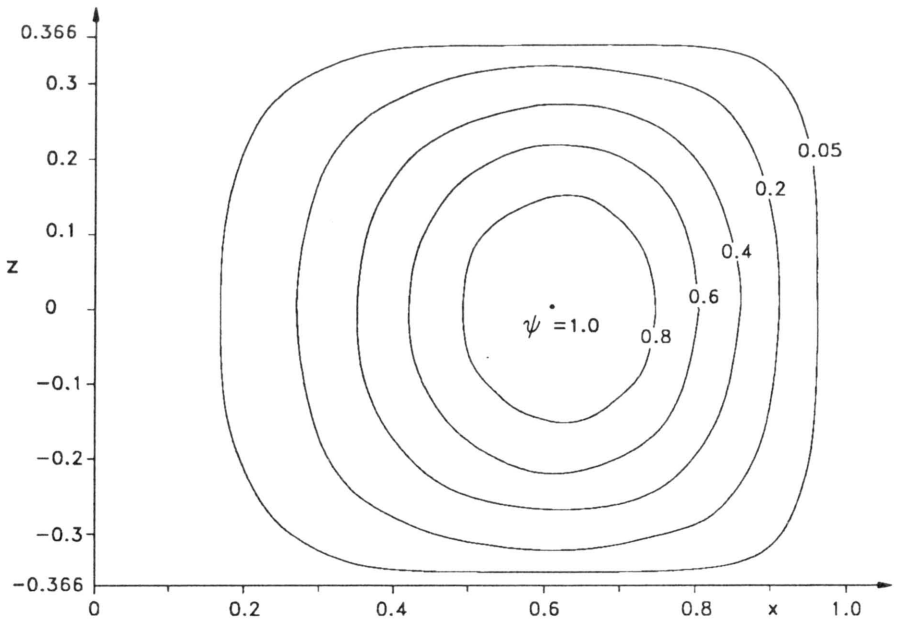


FIG. 3. The cell pattern at the onset of instability $\eta = 0.5$, $\psi = u(x)\cos az$.

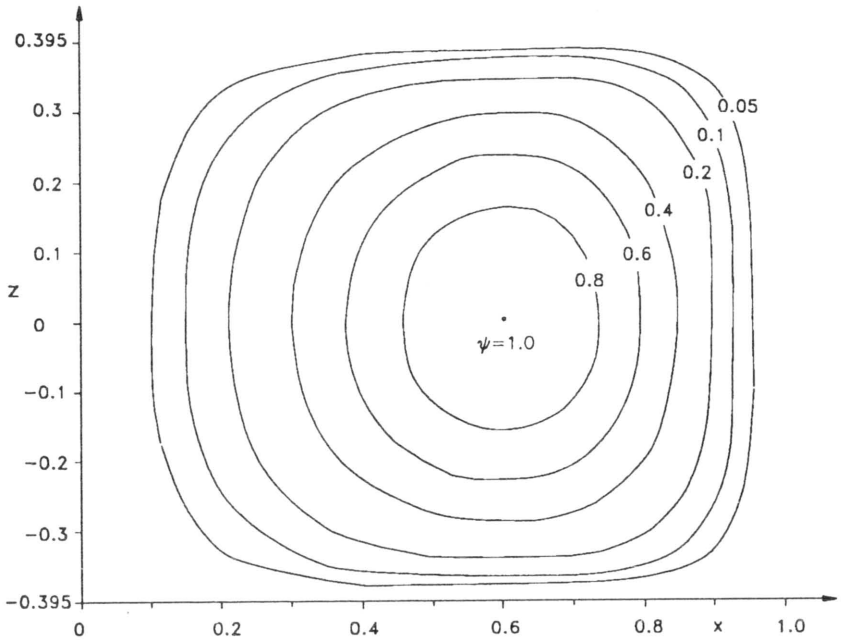


FIG. 4. The cell pattern at the onset of instability $\eta = 0.95$, $\psi = u(x)\cos az$.

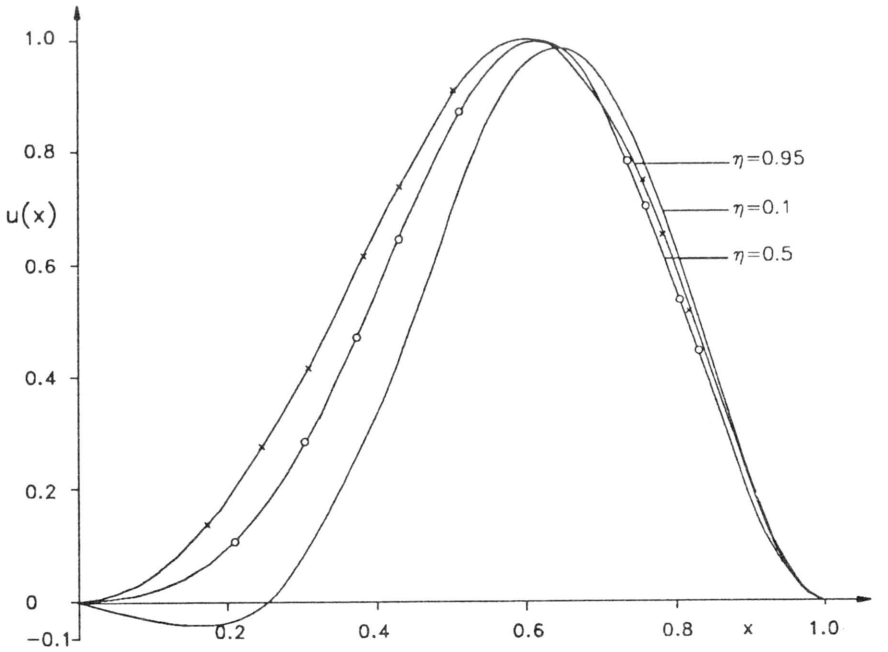


FIG. 5. The radial velocity perturbation $u(x)$ at the onset of instability.

From Figs. 2–4, we also observe that as the gap width decreases, the cells become elongated. From Fig. 5 we observe that the radial velocity perturbation is maximum in a narrow gap region and increases with the decreasing gap width near the inner cylinder. Again from Fig. 6 it is observed that near the inner cylinder, the tangential velocity perturbation increases as the gap width increases, whereas in the central region, it decreases with increasing the gap width.

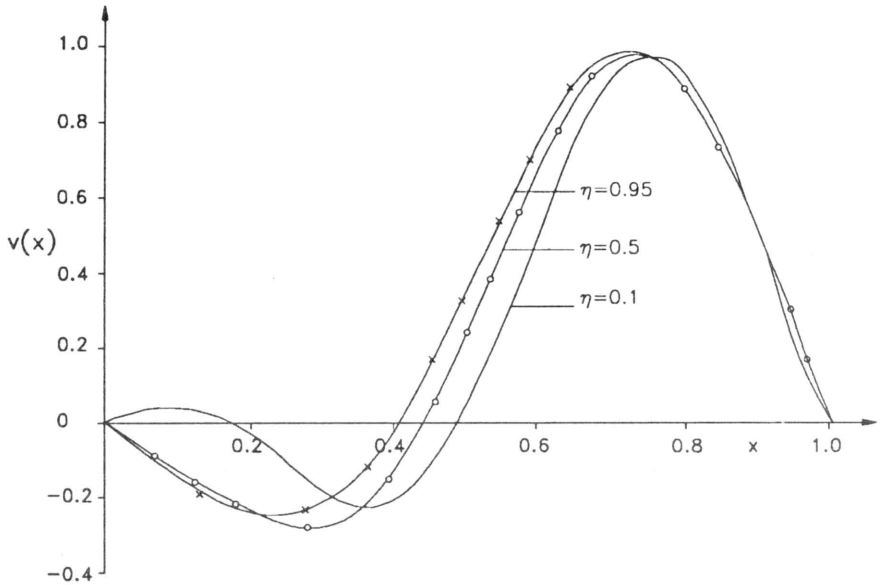


FIG. 6. The tangential velocity perturbation $v(x)$ at the onset of instability.

## 3. Conclusions

Our results obtained by the finite-difference method agree very well with those of WALOWIT *et al.* [12]. The method is also quite simple compared with other earlier methods as the NAG library subroutines are available for use.

## References

1. S. CHANDRASEKHAR, *The stability of viscous flow between rotating cylinders*, Mathematika, **1**, 5-13, 1954.
2. S. CHANDRASEKHAR, *The stability of viscous flow between rotating cylinders*, Proc. Roy. Soc. (London), **A246**, 301–311, 1958.
3. S. CHANDRASEKHAR and D. ELBERT, *The stability of viscous flow between rotating cylinders*, II, Proc. Roy. Soc. (London), **A268**, 145–152, 1962.
4. W.R. DEAN, *Fluid motion in a curved channel*, Proc. Roy. Soc. (London), **A121**, 402–420, 1928.
5. R.C. DIPRIMA, *Application of the Galerkin method to problems in hydrodynamic stability*, Quart. Appl. Math., **13**, 55–62, 1955.
6. R.D. GIBSON and A.E. COOK, *The stability of curved channel flow*, Quart. J. Mech. Appl. Math., **27**, 149–160, 1974.

7. W.R. REID, *On the stability of viscous flow in a curved channel*, Proc. Roy. Soc. (London), **A244**, 186–198, 1958.
8. E.M. SPARROW, W.D. MUNRO and V.K. JOHNSSON, *Instability of flow between rotating cylinders; The wide gap problem*, J. Fluid Mech., **20**, 35–46, 1964.
9. H.S. TAKHAR, M.A. ALI and V.M. SOUNDALGEKAR, *Stability of the flow between rotating cylinders – wide gap problem*, ASME, J. Fluid Engng., **111**, 97–99, 1989.
10. H.S. TAKHAR, V.M. SOUNDALGEKAR and M.A. ALI, *Some cell-patterns in a wide gap Taylor stability problem*, Physics Letters A, **137**, 389–392, 1989.
11. G.I. TAYLOR, *Stability of a viscous liquid contained between two rotating cylinders*, Phil. Trans. Roy. Soc., **A223**, 289–343, 1923.
12. J. WALOWIT, S. TSAO and R.C. DIPRIMA, *Stability of flow between arbitrarily spaced concentric cylindrical surfaces including the effect of a radial temperature gradient*, J. Appl. Mech. (Tr.ASME), **31E**, 585–593, 1964.

**DEPARTMENT OF MATHEMATICS, UNIVERSITY OF BAHRAIN,**
**BRINDAVAN SOCIETY, THANE, INDIA**
**and**
**DEPARTMENT OF ENGINEERING, UNIVERSITY OF MANCHESTER, ENGLAND.**

*Received February* 15, 1994; *new version September* 29, 1994.

Arch. Mech., 47, 1, pp. 13–26, Warszawa 1995

# Experimental evaluation of the influence of stress state type on creep characteristics of copper at 523 K

Z. L. KOWALEWSKI (WARSZAWA)

RESULTS OF the experimental programme concerning creep process of M1E copper manufactured according to Polish Standards are presented. Creep tests were carried out in the plane stress state at elevated temperature equal to 523 K. It has been found that for creep process conducted at the same effective stress, the type of stress state plays a significant role. The variations in lifetime obtained for uni-axial tension and pure torsion tests exceeded one order of magnitude, in spite of initial isotropy of the material in the sense of basic mechanical properties obtained from monotonic tension investigations.

## 1. Introduction

THE VAST MAJORITY of the creep-to-rupture investigations have been carried out under uni-axial stress states [1, 2, 3, 4]. Results of such tests have been subsequently used to determine material constants existing in different theoretical models with the objective to reflect precisely the creep behaviour of the material considered. These models are often generalized into multi-axial stress states under the assumption of isotropy of the body examined [5, 6, 7, 8]. In practice, however, the isotropic materials exist rather seldom, since the manufacturing processes used to produce semi-finished products such as rods, tubes, sheets etc., induce anisotropy which cannot be often removed by any heat treatment subsequently applied. In some cases the material can be isotropic in the sense of plastic parameters such as the yield limit and ultimate tensile stress, but during creep it can exhibit anisotropic properties [9, 10]. In these situations, carring out only uni-axial creep tests to obtain material constants for constitutive model describing the material behaviour, may lead to significant errors.

In the paper creep results from tests under plane stress state are presented for pure electrolytic copper (M1E) which exhibits isotropic mechanical properties such as Young's modulus, yield limit and tensile strength.

## 2. Material, specimen and testing devices

The material investigated was electrolytic copper (M1E) of 99.9% purity. It was annealed for two hours at 673 K and furnace cooled to achieve a uniform grain size, and next it was aged at constant room temperature for five years. Creep investigations were carried out on thin-walled tubular testpieces shown in Fig. 1 in the biaxial creep testing machine, which makes it possible to realize plane

stress conditions by simultaneous loading of the testpieces by an axial force and torsional moment at elevated temperature (523 K). Details of the experimental apparatus are presented in [11], whereas the information concerning measurement technique applied – in [13].

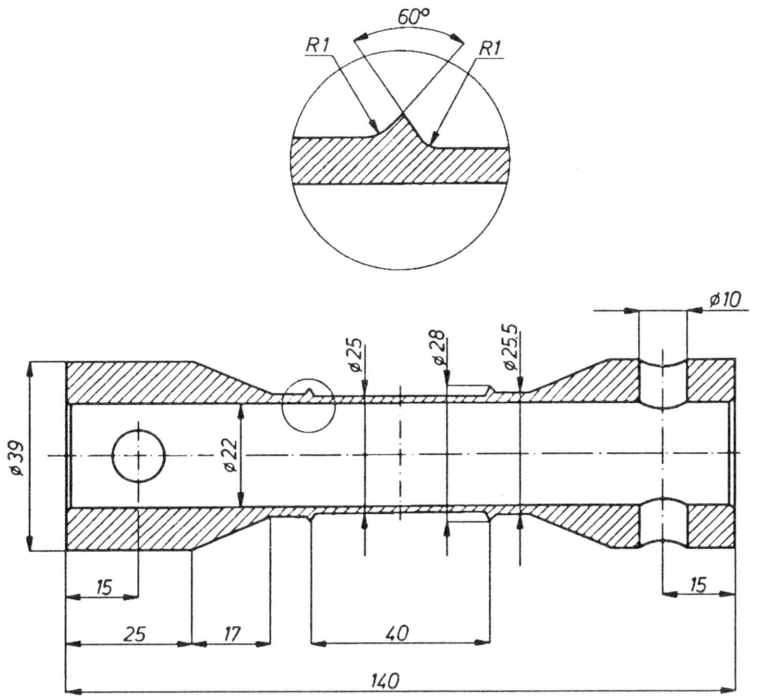


FIG. 1. Dimensions of the testpiece.

## 3. Experimental procedure

Experimental programme contained creep tests up to rupture for copper specimens, subjected to biaxial stress state obtained by various combinations of an axial force and torsional moment required to give three different values of effective stress ($\sigma_i$ = 70.0; 72.5; 75.0 [MPa]) defined by the Huber-Mises condition in the following form:

$$\sigma_i = \left(\frac{3}{2} S_{ij} S_{ij}\right)^{1/2} = \left(\sigma^2 + 3\tau^2\right)^{1/2}, \tag{3.1}$$

where $S_{ij}$ – stress deviator, $\sigma$ – axial stress, $\tau$ – shear stress. Diagram of the experimental programme is shown in Fig. 2. Creep tests under tension, torsion and combination of these loadings were carried out. The complex stress states in the two-dimentional stress space $(\sigma, \sqrt{3}\tau)$ correspond to the points located on

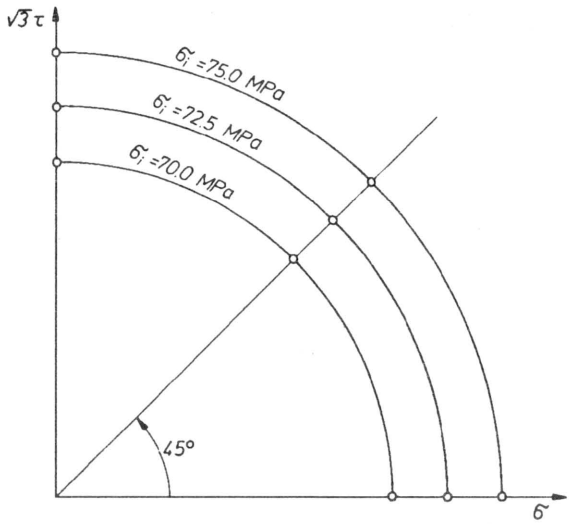


FIG. 2. Scheme of the creep tests programme.

the rectilinear path of slope $\Theta_\sigma = 45°$ with respect to the $\sigma$ stress axis. The angle $\Theta_\sigma$ was determined from the relation

$$\Theta_\sigma = \arctan\left(\frac{\sqrt{3}\tau}{\sigma}\right). \tag{3.2}$$

Prior to creep test, each specimen was heated uniformly at the test temperature (523 K) for 24 hours. Creep investigations were carried out until rupture of the testpieces was achieved, giving as a consequence the whole creep characteristics. All creep tests were performed at stress levels which were lower than the value of yield point of the material at 523 K ($R_{0.2} = 76$ [MPa]). Thus, the total strain has been expressed as a sum of the elastic and creep strain components in the form:

$$\varepsilon_{ij} = \varepsilon_{ij}^{(e)} + \varepsilon_{ij}^{(c)}, \tag{3.3}$$

where strain components with the superscripts $e$ and $c$ denote elastic and creep strain, respectively.

## 4. Creep tests results and their discussion

The creep curves up to rupture for copper are presented in Figs. 3, 4, 5. Creep characteristics obtained under effective stress equal to $\sigma_i = 70.0$ [MPa] for stress states, which correspond to uniaxial tension, combination of tension and torsion, and pure torsion are shown in Fig. 3. Creep curves obtained for the same types of stress states under effective stress equal to $\sigma_i = 72.5$ [MPa] and $\sigma_i = 75.0$ [MPa]

are plotted in Fig. 4 and Fig. 5, respectively. The vertical axes in Figs. 3, 4, 5 correspond to the effective creep strain defined by the well known relation in the following form:

$$\varepsilon_i^{(c)} = \left(\frac{2}{3}\varepsilon_{ij}^{(c)}\varepsilon_{ij}^{(c)}\right)^{1/2} = \sqrt{\varepsilon^2 + \left(\frac{1}{3}\right)\gamma^2}, \tag{3.4}$$

where $\varepsilon$ and $\gamma$ denote axial and shear strain, respectively, and the horizontal axes correspond to the time.

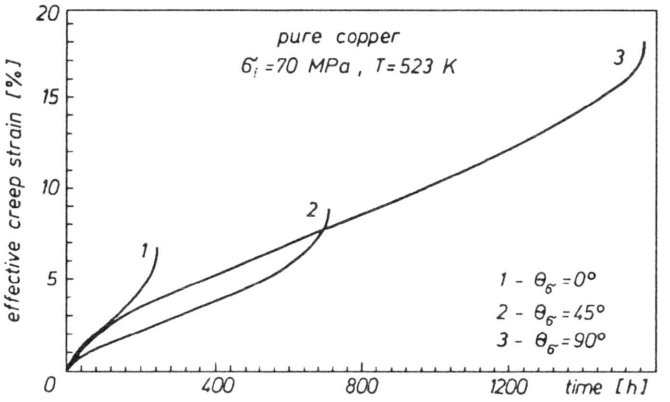


FIG. 3. Creep curves at the effective stress $\sigma_i$ = 70.0 MPa.

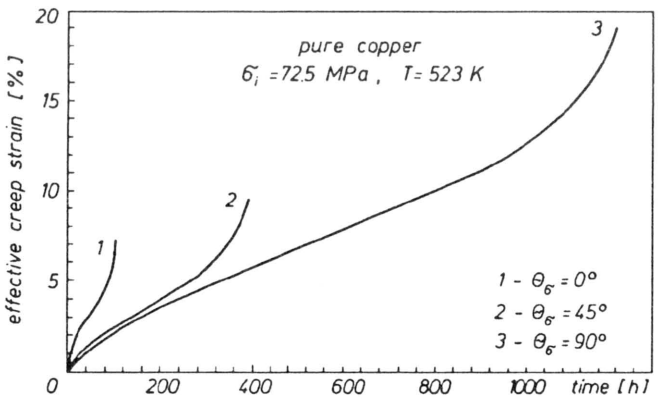


FIG. 4. Creep curves at the effective stress $\sigma_i$ = 72.5 MPa.

The creep characteristics obtained at the same effective stress but under different stress states exhibit drastic differences for all the stress levels considered. In all cases the shortest lifetimes and, moreover, the lowest ductility have been achieved for tensioned testpieces. The opposite effect was observed for testpieces subjected to pure torsion. It has to be emphasized that differences in creep curves due to different loading types applied are considerable, and they are discussed shortly in the following sections.

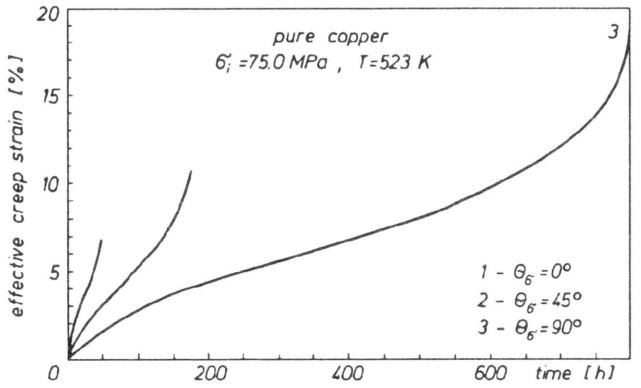


FIG. 5. Creep curves at the effective stress $\sigma_i = 75.0$ MPa.

### 4.1. Primary creep period

The difference between the creep curves already appears at the primary creep period in which strain rate gradually decreases. Variations of these curves can be identified in the form of a plot showing duration of primary creep versus

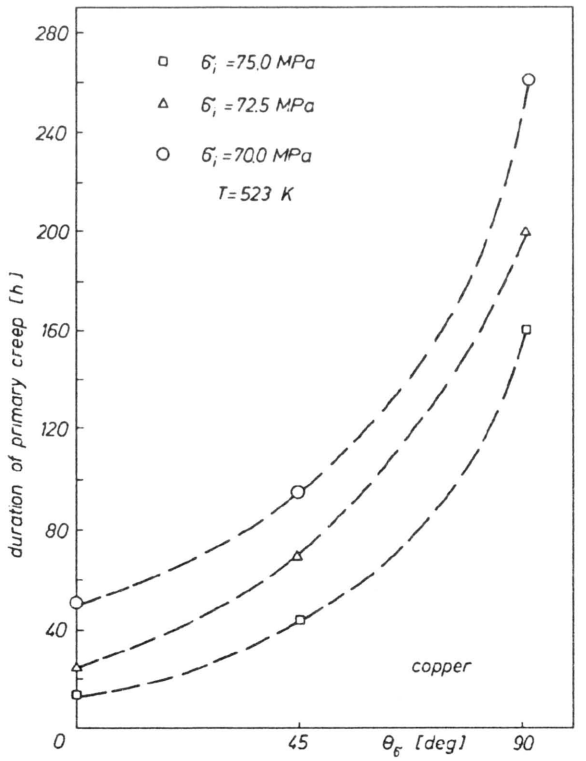


FIG. 6. Duration of primary creep period as a function of the angle defining the type of stress state.

the angle of $\Theta_\sigma$ which defines the type of stress state, Fig. 6. As it is shown, the minimum creep rate has been achieved in the shortest time period during tension creep tests while in the longest time at pure torsion creep tests. The ratio of the primary creep durations at pure torsion and uni-axial tension showed tendency to increase with the increasing stress level. It was equal 5.2 for $\sigma_i$ = 70.0 [MPa] and 10.7 for $\sigma_i$ = 75.0 [MPa]. Marked decrease of the primary creep duration with the increase of stress level has been obtained for each type of stress state defined by the angle $\Theta_\sigma$.

#### 4.2. Secondary creep period

The difference in mutual location of the creep curves during primary creep period is also observed in the secondary creep. It can be studied by comparison of the times to tertiary creep period as a function of the stress state type, Fig. 7 for all the tests carried out. The longest times to tertiary creep under the same stress

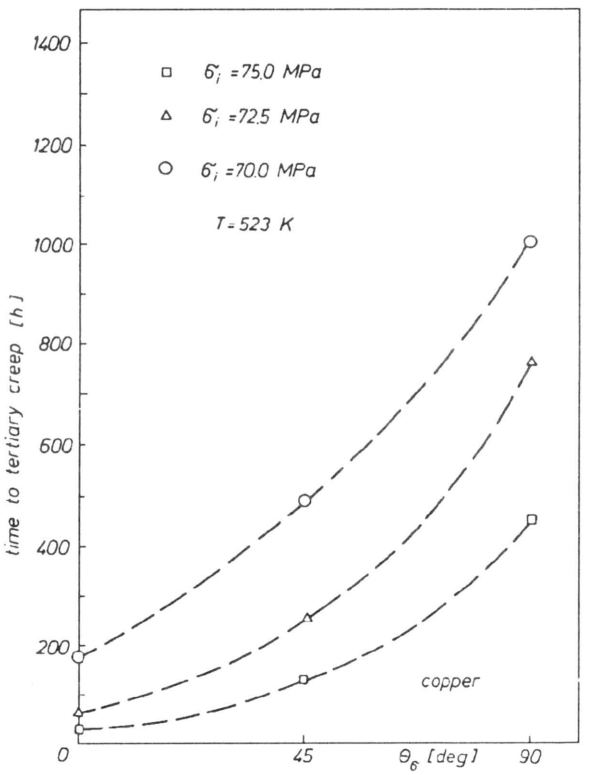


FIG. 7. Time to tertiary creep period as a function of the angle defining the type of stress state.

level considered were obtained at pure torsion creep tests; shorter values of this time were achieved at complex stress states being a combination of tension and torsion and the shortest ones at uni-axial tension creep tests. The sum of primary and secondary creep periods obtained at tension test referred to the same sum

obtained for creep tests, either at combination of tension and torsion ($\Theta_\sigma = 45°$) or at pure torsion ($\Theta_\sigma = 90°$), gives the best evaluation of the degree of creep curves variations depending on the stress state. In the case of $\sigma_i = 70.0$[MPa] these ratios equal 2.8, 5.9, respectively, while in the case of $\sigma_i = 75.0$[MPa]: 3.6, 12.9, respectively, and they are shown to exhibit a tendency to increase with the increasing stress level.

The next parameter which characterises the creep process in its secondary period is the steady creep strain rate achieved at the end of primary creep and held during the entire secondary period. Variations of this parameter as functions of $\Theta_\sigma$ are presented in Fig. 8. The greatest value of steady creep strain rate for the chosen stress level was obtained in the tension creep test, but the lowest – in

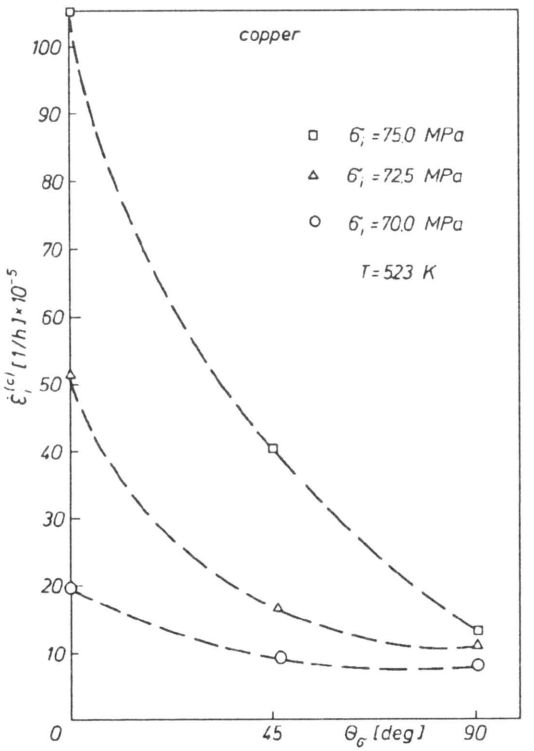


FIG. 8. Minimum effective creep strain rate as a function of the angle defining the type of stress state.

pure torsion creep test. Such difference expressed as the ratio of the strain rates at tension and torsion was 8.1 for $\sigma_i = 75$ [MPa] and 2.3 for $\sigma_i = 70$ [MPa]. From these results it may be seen that the tested material is more sensitive to the stress variations under tension, since the ratio of the effective steady creep rates obtained in tension tests at stress levels $\sigma_i = 75$ [MPa] and $\sigma_i = 70$ [MPa] was 5.7, whereas in the case of torsion tests it was only 1.6. It is interesting to note that, taking into consideration the particular stress state type in the logarithmic

diagram $\log \dot{\varepsilon}_i^{(c)} = f(\log(\sigma_i))$, all the effective steady creep rates can be located on a straight line, Fig. 9. It suggests that the creep deformation process for the

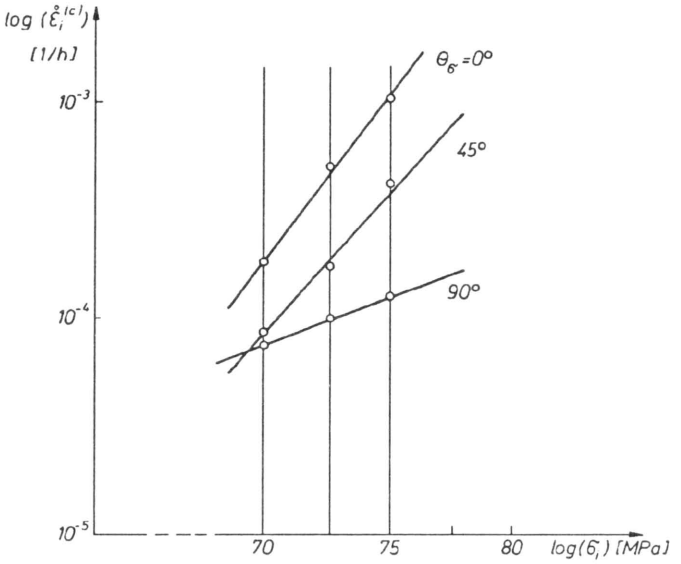


FIG. 9. Logarithmic diagram of the minimum effective creep strain rate versus effective stress.

loading type taken into account is controlled by the special creep deformation mechanism which seems to be different at tension, different at torsion and also different at the combinations of these loading components. This result is not surprising, since it confirms the experimental data previously obtained for this material at higher temperature (573 K) [10, 12]. Detailed results concerning the secondary creep period are presented in Table 1.

**Table 1. Creep tests results for copper.**

| | $\sigma_i$ = 70.0 [MPa] | | | $\sigma_i$ = 72.5 [MPa] | | | $\sigma_i$ = 75.0 [MPa] | | |
|---|---|---|---|---|---|---|---|---|---|
| | $\Theta_\sigma$=0° | $\Theta_\sigma$=45° | $\Theta_\sigma$=90° | $\Theta_\sigma$=0° | $\Theta_\sigma$=45° | $\Theta_\sigma$=90° | $\Theta_\sigma$=0° | $\Theta_\sigma$=45° | $\Theta_\sigma$=90° |
| $\dot{\varepsilon}_i^{(c)} \times 10^{-5}$ [1/h] | 18.4 | 8.5 | 8.0 | 51.0 | 16.6 | 10.2 | 105.0 | 41.2 | 13.0 |
| $\dot{\varepsilon} \times 10^{-5}$ [1/h] | 18.4 | 6.1 | – | 51.0 | 12.7 | – | 105.0 | 31.0 | – |
| $\dot{\gamma} \times 10^{-5}$ [1/h] | – | 10.2 | 13.9 | – | 18.5 | 17.7 | – | 47.0 | 22.5 |
| $t_R$ [h] | 254 | 700 | 1560 | 101 | 391 | 1187 | 47 | 175 | 799 |
| $t_I$ [h] | 50 | 90 | 260 | 25 | 65 | 200 | 15 | 45 | 160 |
| $t_{II}$ [h] | 170 | 480 | 1000 | 70 | 255 | 760 | 35 | 125 | 450 |
| $\varepsilon_i^{(c)}$ [%] | 6.8 | 8.6 | 17.5 | 7.3 | 9.3 | 18.1 | 6.7 | 10.6 | 19.0 |

Notation in the Table 1: $\dot{\varepsilon}_i^{(c)}$ – minimum effective creep strain rate, $\dot{\varepsilon}$ – minimum axial creep strain rate, $\dot{\gamma}$ – minimum shear creep strain rate, $t_R$ – time to rupture, $t_{\mathrm{I}}$ – duration of primary creep period, $t_{\mathrm{II}}$ – time to tertiary creep, $\varepsilon_i^{(c)}$ – creep strain at rupture.

### 4.3. Tertiary creep period

The increase of strain rate characterises the tertiary period of the creep process, at the end of which rupture of the specimen tested occurs after the time period $t_R$ (time to rupture). Such development of the phenomenon in this period is connected with the increase of structure degradation velocity of a material which is manifested by the development of voids and microcracks existing mainly at the grain boundaries. The material continuity is disturbed by the propagation of microcracks and due to other structural defects, what in consequence leads to the reduction of stiffness, and finally to rupture.

Time-to-rupture is the parameter which reflects the whole creep process. Variation of this parameter as a function of the stress state type is presented in Fig. 10.

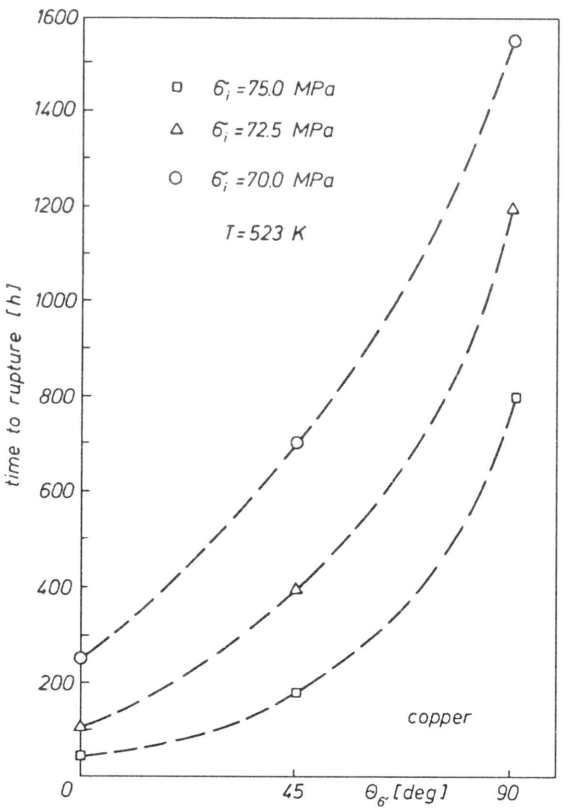


FIG. 10. Time to creep rupture as a function of the angle defining the type of stress state.

It is shown that the longest lifetimes under the same effective stress considered were obtained at creep under pure torsion, while the shortest ones – at uni-axial tension. Using the same data analysis procedure as in the time to tertiary creep period considerations, namely, for the same effective stress level dividing the lifetimes obtained from tests at combination of loadings ($\Theta_\sigma = 45°$) and at pure torsion ($\Theta_\sigma = 90°$) by the value of time-to-rupture at tension, the following values of these proportions have been calculated: 2.8; 6.1 in case of $\sigma_i = 70.0$ [MPa], and 3.7; 17.0 in case of $\sigma_i = 75.0$ [MPa], respectively.

The differences in creep properties of copper depending on the stress state type are also visible by comparing the effective creep strains obtained at the specimen rupture versus angle $\Theta_\sigma$, Fig. 11. The lowest effective creep strains were obtained at uni-axial tension creep tests, the greatest ones at pure torsion creep tests, Table 1.

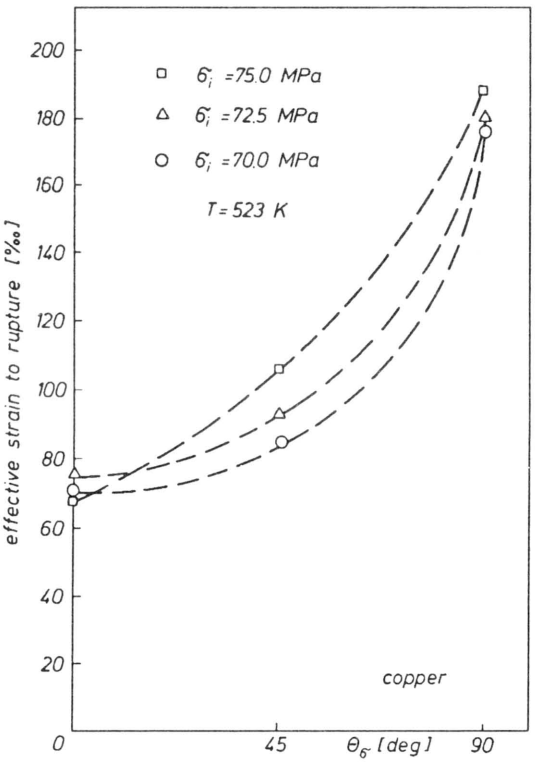


FIG. 11. Effective creep strain as a function of the angle defining the type of stress state.

All of the macroscopic creep parameters discussed up to now prove the anisotropy of the copper tested under creep conditions which possessed isotropic properties at monotonic loading in the sense of Young's modulus, yield limit, etc. The reason of such behaviour may by connected, to a certain degree, with the type of deformation, since the material during creep may be controlled by different

deformation mechanisms, the activation of which depends on the selected type of stress state. It seems that this conclusion can be also confirmed by the shapes of the specimen cross-section in places where rupture occurred. In case of creep tension tests, the failure line was perpendicular to the main specimen axis; in case of the complex stress states this line was inclined by angles equal 15 – 20°, measured with respect to the line perpendicular to the main specimen axis, whereas for testpieces subjected to pure torsion these angles were approximatelly equal to 30 – 45°, Fig. 12.

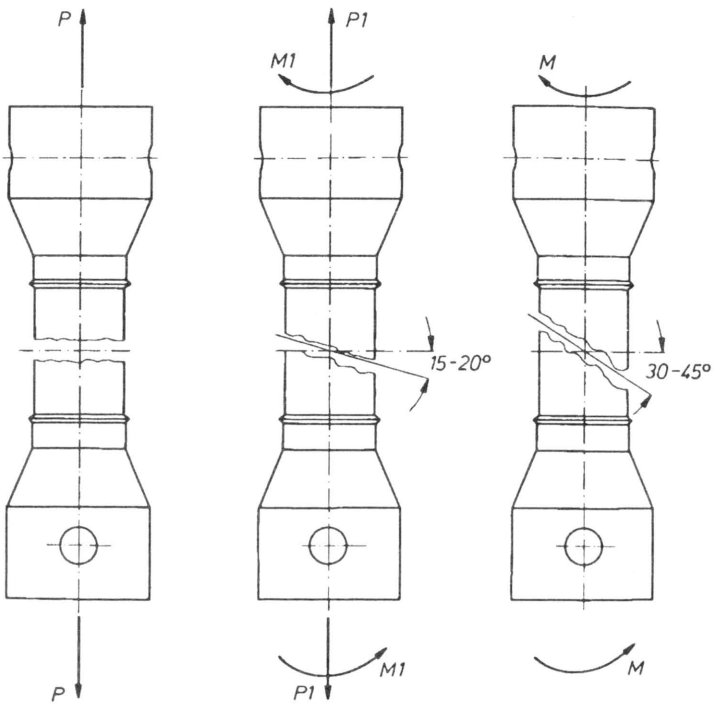


FIG. 12. Variations of the testpiece failure line during creep at different types of stress state.

On the other hand, however, it has to be noted that the comparison of creep test results obtained at uni-axial tension with those achieved at pure torsion becomes complicated, since it is difficult to maintain a constant stress during the tension tests. These situations often exist in tests conducted on standard creep testing machines, where stress level variations are caused by the reduction of specimen cross-section area during the deformation process. An error in stress level selected for investigation of the material is relatively small when the axial deformations are smaller than 10%. However, the value of strain obtained at the creep process is often much greater. It depends either on the materials tested or on certain conditions of tests. Relatively large creep deformations have been observed in superplastic materials and in materials examined at high stress

levels exceeding their yield limit. In order to compare the creep results from tension tests with those at torsion, it is required to apply in creep testing machines such devices which will be capable of compensating the changes of the specimen cross-section and, consequently, to maintain the required constant stress level. Such creep machines are known especially in case of uni-axial tension [14, 15]. Creep devices in which loadings are applied in more than one direction require further engineering studies.

The entire creep strains of copper tested for all uni-axial tension creep experiments did not exceed 7.5%. The change of the specimen cross-sectional area was uniform at the whole gauge length and relatively small. It means that all specimens failed without significant necking and, moreover, the variations of stress level did not exceed 2 [MPa]. Knowing this value, all data at tension creep tests, i.e. those obtained at 70.0; 72.5, and 75.0 [MPa], can be treated as obtained under increased stress levels which correspond to the maximum error resulted from the variations of specimen cross-sectional area, i.e. at 72.0; 74.5 and 77.0 [MPa]. Similar procedure has been applied to reconsider the experimental data from creep tests carried out at the biaxial stress state, for which also small reductions of the specimen cross-section area were observed. These reductions induced certain increase of the stress level, not greater, however, than 1 [MPa] at failure.

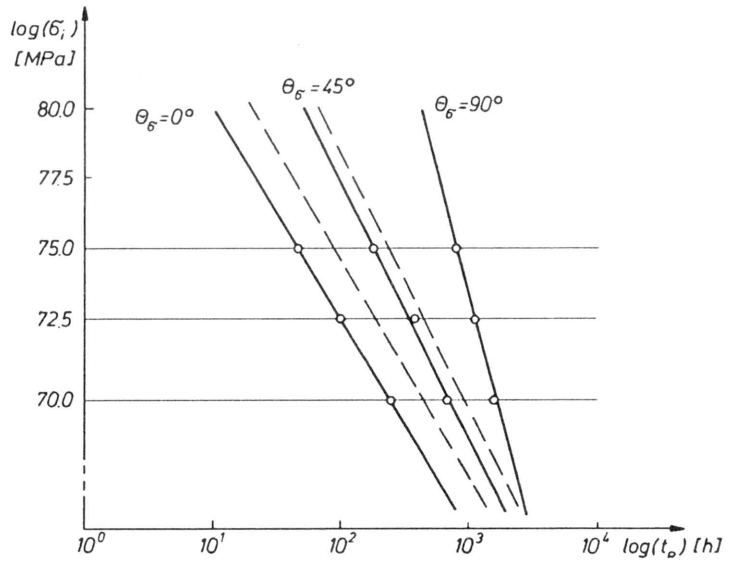


FIG. 13. Logarithmic relation between effective stress and time to creep rupture.

Results for the three types of stress states are presented in Fig. 13 in the form of logarithmic diagrams of the effective stress versus time to rupture. Data points for the chosen type of stress state are located, with relatively high accuracy, on the straight lines which have different location and orientation. Assuming as a reference point the line representing pure torsion results, the remaining straight

lines are shifted and rotated. For both cases of the stress state types where changes in stress level exist, i.e. in uniaxial tension and combination of tension and torsion, the recalculated results which correspond to the same tests as those previously described are drawn in dashed lines. They reflect global variation of the stress level due to reduction of specimen cross-sectional area, measured after the tests are completed. It is shown that these corrections do not change qualitatively the fact of significant differences in creep results for the stress state types considered at the same effective stress.

## 5. Conclusions

The results of creep experiments, performed on pure copper subjected to different stress state types in the two-dimensional stress space $(\sigma, \sqrt{3}\tau)$ at 523 K, have been presented.

For the material tested the parameters which characterise creep such process as duration of primary creep period, steady creep rate, time to rupture and ductility were the functions of the type of stress state. In spite of isotropy of the basic strength properties (yield limit, tensile strength, etc.), the investigations show a strong anisotropic character of the material behaviour during creep. Uni-axial tension was the most dangerous loading type, taking into account lifetime of the material at the same effective stress.

Although the creep curves determined by uniaxial tests provide information about the reological properties of the material, they cannot be generalized to complex stress states. In order to obtain reliable results which could be used to verify the constitutive models required to describe material behaviour under multi-axial loadings, the investigations at complex stress states are necessary.

The differences in creep curves observed for the material tested at the same effective stress but for different stress state types, are connected with the deformation mechanisms. Depending on the type of stress state, different mechanism controls the creep deformation process of copper. In the investigations it was manifested by the failure line of the specimen, the shape of which was strongly sensitive to the type of stress applied.

## References

1. F.H. NORTON, *Creep of steel at high temperatures*, McGrow-Hill, New York 1929.
2. N. MALININ and J. RŻYSKO, *Mechanics of materials* [in Polish], PWN, 1981.
3. Y.N. RABOTNOV, *Creep problems in structural members*, North Holland Publishing Company, Amsterdam 1969.
4. J. GITTUS, *Creep, viscoelasticity and creep fracture in solids*, Applied Science Publishers LTD, 1975.
5. F. GAROFALO, *Fundamentals of creep and creep rupture in metals*, Macmillan, New York 1965.
6. L.M. KACHANOV, *The theory of creep* [English translation edited by A.J. KENNEDY], National Lending Library, Boston Spa 1958.
7. F.K.G. ODQVIST, *Mathematical theory of creep and creep rupture*, Clarendon Press, Oxford 1966.

8. D.R. HAYHURST, *On the role of creep continuum damage in structural mechanics*, [in:] Engineering Approaches to High Temperature Design, B. WILSHIRE, D.R.J. OWEN [Eds.], Pineridge Press, 85–176, Swansea 1983.
9. Z. KOWALEWSKI, *Creep behaviour of copper under plane stress state*, Int. J. Plasticity, **7**, 387–404, 1991.
10. Z. KOWALEWSKI, *The influence of deformation history on creep of pure copper*, [in:] Creep in Structures, M. ŻYCZKOWSKI [Ed.], Proc. 4th IUTAM Symp., Cracow 1990, Springer-Verlag, 115–122, 1991.
11. Z. KOWALEWSKI, *The surface of constant rate of energy dissipation under creep and its experimental determination*, Arch. Mech., **39**, 445–459, 1987.
12. Z. KOWALEWSKI, *The influence of plastic anisotropy on the creep of metals under complex stress states* [in Polish], IFTR Reports 36, 1987.
13. W. TRĄMPCZYŃSKI and Z. KOWALEWSKI, *A tension-torsion testing technique*, Proc. Symp. "Techniques for Multiaxial Creep Testing", Elsevier Applied Science, 79–92, London and New York 1986.
14. T. HOSTINSKY and J. CADEK, *A constant tensile stress creep testing machine*, J. Testing and Evaluation, **4**, 26, 1976.
15. P. YAVARI and T.G. LANGDON, *A constant stress tensile creep machine for very low stresses*, J. Testing and Evaluation, 10, 174, 1982.

POLISH ACADEMY OF SCIENCES
INSTITUTE OF FUNDAMENTAL TECHNOLOGICAL RESEARCH, WARSZAWA.

*Received July* 11, 1994.

Arch. Mech., 47, 1, pp. 27–37, Warszawa 1995

# Rayleigh's integral and effective conductivity of the square array of cylinders

V. V. MITYUSHEV (SŁUPSK)

AN EXACT FORMULA for the effective conductivity of a composite with circular inclusions has been derived. The formula is based on the rigorous definition and calculation of Rayleigh's integral and on the accurate solution of the $\mathbb{R}$-linear problem for a circular domain.

## 1. Introduction

THE DETERMINATION of the effective conductivity $\lambda_e$ of a two-phase composite material consisting of cylindrical particles of one material embedded in a continuous medium of another material has been a subject of many investigations. If the volume fraction $v$ of the inclusions is very small, the interactions between particles may be ignored. This assumption implies the famous Clausius-Mossotti (also known as the Maxwell-Garnett) approximation [1]

$$\frac{\lambda_e}{\lambda} = \frac{1+\rho v}{1-\rho v}, \tag{1.1}$$

where $\lambda$ is the conductivity of the matrix, $\lambda_1$ is the conductivity of the inclusions, $\rho := (\lambda_1-\lambda)/(\lambda_1+\lambda)$. JEFFREY [2], BATCHELOR and O'BRIEN [3], SANGANI and YAO [4, 5] studied statistically homogeneous materials to evaluate $\lambda_e$. MCPHEDRAN, MILTON, PERRINS, POLADIAN, MCKENZIE [6–11] evaluated $\lambda_e$ of the square array of cylinders to improve the formula (1.1). The last authors have been inspired by a classical paper of Lord RAYLEIGH [12]. They obtained an infinite set of linear algebraic equations for the multipole coefficients, which can either be truncated to give various low-order formulae, or solved numerically on a computer. FELDERHOF, FORD and COHEN [20] derive a cluster expansion for $\lambda_e$. BERGMAN and DUNN [21] studied analytical properties of $\lambda_e$ and proposed an efficient method to calculate $\lambda_e$. All previous methods use an infinite set of linear algebraic equations or integral equation, and lead to approximate formulae for $\lambda_e$. In the present paper we continue to study the square array of cylinders. Applying the exact formula of the paper [13], we write an exact formula for $\lambda_e$.

In order to calculate $\lambda_e$, we have to investigate the conditionally convergent Rayleigh's sum

$$S_2 := \sum_{j=1}^{\infty} \operatorname{Re} \frac{1}{(x_j + iy_j)^2},$$

where as $j$ runs from 1 to $\infty$, $(x_j, y_j)$ runs over all cylinder centers, except that at the origin. The sum $S_2$ is related to the integral

$$I_2 := \iint\limits_{\mathbb{R}^2} \operatorname{Re} \frac{1}{(x+iy)^2} dx\, dy = \iint\limits_{\mathbb{R}^2} \frac{y^2 - x^2}{(x^2+y^2)^2} dx\, dy,$$

having a singularity at the origin. Rayleigh calculated $I_2$ by summation over a "needle"-shaped region, infinitely more extended along the $x$-axis than along the $y$-axis. This method of integration is based on physical assumptions. It leads to the equality $I_2 = \pi$. In the present paper we propose a rigorous definition of the integral $I_2$. This definition differs from the classical definition of $v.p.$ integral [15].

## 2. Definition of the integral $I_2$

Let us consider a domain $G$ with the piecewise smooth boundary $\partial G$. Let the function $Q(x, y)$ be defined in the closure $\overline{G}$. Our study is based on the following fundamental

GREEN'S THEOREM. *Let $Q(x, y)$ be continuously differentiable in $\overline{G}$ except the point $(x_0, y_0) \in G$, where the derivative $\partial Q/\partial x$ is represented in the form $\partial Q/\partial x = f(x, y)/r$. Here, $r = ((x - x_0)^2 + (y - y_0)^2)^{1/2}$, $f(x, y)$ is continuous in $\overline{G}$. Then*

$$\iint\limits_G \frac{\partial Q}{\partial x} dx\, dy = \int\limits_{\partial G} Q\, dy. \tag{2.1}$$

In the left-hand part of (2.1) the integral is understood as an improper integral, i.e.

$$\iint\limits_G \frac{\partial Q}{\partial x} dx\, dy := \lim_{\varepsilon \to 0} \iint\limits_{G \setminus U_\varepsilon} \frac{\partial Q}{\partial x} dx\, dy,$$

where $U_\varepsilon$ is a neighbourhood of the point $(x_0, y_0)$, for instance, $U_\varepsilon := \{(x, y) \in \mathbb{R}^2 : r < \varepsilon\}$. Let us note that (2.1) is valid for each function $Q(x, y)$ continuous in $\overline{G}$ and having the derivative $\partial Q/\partial x$ from the Lebesgue space $L_1(G)$.

So we have no problem with an improper integral with a weak singularity. Now let us study a singular integral. At first, let us consider the well-known singular integral [15]

$$-v.p. \iint\limits_U \operatorname{Re} \frac{1}{(x+iy)^2} dx\, dy = v.p. \iint\limits_U \frac{y^2 - x^2}{(x^2+y^2)^2} dx\, dy \tag{2.2}$$

$$:= \lim_{\varepsilon \to 0} \iint\limits_{U \setminus U_\varepsilon} \frac{y^2 - x^2}{(x^2+y^2)^2} dx\, dy,$$

where $U := \{(x, y) \in \mathbb{R}^2 : x^2 + y^2 < 1\}$. The $v.p.$ integral (2.2) exists because the integrand is represented in the form

$$\frac{y^2 - x^2}{(x^2 + y^2)^2} = \frac{f(x, y)}{r^2},$$

where $r^2 = x^2 + y^2$, $f(x, y) = \dfrac{y^2 - x^2}{x^2 + y^2}$ and the following condition

$$\int_{\partial U_\varepsilon} f(x, y)\, d\theta = \int_0^{2\pi} \frac{\sin^2\theta - \cos^2\theta}{\sin^2\theta + \cos^2\theta} d\theta = 0$$

takes place. Here $x = r\cos\theta$, $y = r\sin\theta$, $\partial U_\varepsilon$ is the boundary of $U_\varepsilon$. Let us calculate the integral (2.2)

$$v.p. \iint_U \frac{y^2 - x^2}{r^4} dx\, dy = \lim_{\varepsilon \to 0} \frac{dr}{r} \int_\varepsilon^1 \int_0^{2\pi} (\sin^2\theta - \cos^2\theta)\, d\theta = 0.$$

Let us calculate the following integral

$$\int_{\partial U} \frac{x}{x^2 + y^2} dy = \int_{\partial U} x\, dy = \pi. \tag{2.3}$$

Since $\dfrac{\partial}{\partial x}\left(\dfrac{x}{x^2 + y^2}\right) = \dfrac{y^2 - x^2}{(x^2 + y^2)^2}$, one can see that Green's relation (2.1) is not valid for the $v.p.$ integral (2.2). That is why $v.p.$ integral doesn't correspond to our approach.

Let us consider the function $u(x, y)$ harmonic in $\overline{U}$ except for the origin, where $u(x, y)$ has a singularity of second order. Hence, the function $u(x, y)$ is represented in the form

$$u(x, y) = \operatorname{Re} \frac{f(z)}{z^2} \qquad \text{in} \quad \overline{U},$$

where $z = x + iy$, $f(z)$ is analytic in $\overline{U}$.

DEFINITION

$$\iint_U u(x, y)\, dx\, dy := \lim_{\varepsilon \to 0} \iint_U \operatorname{Re} \frac{f(z)}{(z + \varepsilon)(z - \varepsilon)} dx\, dy, \tag{2.4}$$

*where the last integral is defined as an improper one with weak singularity.*

Let us consider the integral

$$I = \iint\limits_U \frac{y^2 - x^2}{(x^2 + y^2)^2} dx\, dy = -\iint\limits_U \operatorname{Re} \frac{1}{z^2} dx\, dy$$

$$:= -\lim_{\varepsilon \to 0} \iint\limits_U \operatorname{Re} \frac{1}{(z + \varepsilon)(z - \varepsilon)} dx\, dy$$

$$= -\lim_{\varepsilon \to 0} \iint\limits_U \frac{1}{2\varepsilon} \operatorname{Re} \left( \frac{1}{(z + \varepsilon)} - \frac{1}{(z - \varepsilon)} \right) dx\, dy.$$

Applying Green's theorem to the last integral we obtain

$$I = -\lim_{\varepsilon \to 0} \int\limits_{\partial U} \frac{1}{2\varepsilon} \operatorname{Re} \ln \frac{z - \varepsilon}{z + \varepsilon} dy = -\int\limits_{\partial U} \lim_{\varepsilon \to 0} \frac{1}{2\varepsilon} \operatorname{Re} \left( \ln \left( 1 - \frac{\varepsilon}{z} \right) \right.$$

$$\left. - \ln \left( 1 + \frac{\varepsilon}{z} \right) \right) dy = \int\limits_{\partial U} \operatorname{Re} \frac{1}{z} dy = \int\limits_{\partial U} x\, dy = \pi.$$

Comparing with (2.3) we conclude that Green's theorem is valid for the integral $I$.

In the present paper we don't intend to study the general integral (2.4). Attention is paid to calculation of the Rayleigh's integral $I_2$.

Let us calculate the following integral

$$J_r := \iint\limits_{U_r} \frac{y^2 - x^2}{(x^2 + y^2)^2} dx\, dy = -\iint\limits_{U_r} \operatorname{Re} \frac{1}{z^2} dx\, dy,$$

where $U_r := \{(x, y) \in \mathbb{R}^2 : \ x^2 + y^2 < r^2\}$. We have

$$J_r = -\iint\limits_{K_r} \operatorname{Re} \frac{1}{z^2} dx\, dy - \iint\limits_U \operatorname{Re} \frac{1}{z^2} dx\, dy,$$

where the annulus $K_r = U_r \backslash \overline{U}$. Using Green's theorem let us calculate

$$\iint\limits_{K_r} \operatorname{Re} \frac{1}{z^2} dx\, dy = -\int\limits_{\partial K_r} \operatorname{Re} \frac{1}{z} dy = -\int\limits_{\partial U_r} \cos^2 \theta\, d\theta + \int\limits_{\partial U} \cos^2 \theta\, d\theta = 0.$$

Therefore, the integral $J_r$ doesn't depend on $r$ and $J_r = I = \pi$.

Only just now we are prepared to define and calculate the Rayleigh integral

$$I_2 := \lim_{\varepsilon \to 0} \iint\limits_{D_\varepsilon} \operatorname{Re} \frac{1}{(x + iy)^2} dx\, dy,$$

where $D_\varepsilon := \{x + iy \in \overline{\mathbb{C}} : \ |x + iy| > \varepsilon\}$. Let us make the change of variables

$$u - iv = \frac{1}{x + iy} \quad \Longleftrightarrow \quad u = \frac{x}{x^2 + y^2}, \qquad v = \frac{y}{x^2 + y^2}.$$

The Jacobian is equal to $-(u^2 + v^2)^{-2}$. Hence

$$\iint\limits_{D_\varepsilon} \operatorname{Re} \frac{1}{(x + iy)^2} dx\, dy = -\iint\limits_{U_{1/\varepsilon}} \operatorname{Re} \frac{1}{(u + iv)^2} du\, dv = J_{1/\varepsilon} = \pi,$$

where $U_{1/\varepsilon} := \{u + iv \in \overline{\mathbb{C}} : \ |u + iv| < 1/\varepsilon\}$. So we have proved that the Rayleigh integral $I_2 = \lim\limits_{\varepsilon \to 0} J_{1/\varepsilon} = \pi$.

If the sum $S_2$ is defined as a limit of the Riemann sum of the improper integral

$$A_\varepsilon := \iint\limits_{D_\varepsilon} \operatorname{Re} \frac{1}{z^2 - \varepsilon^2 |z^4|} dx\, dy = -\iint\limits_{U_{1/\varepsilon}} \operatorname{Re} \frac{1}{(z - \varepsilon)(z + \varepsilon)} dx\, dy,$$

then $S_2 = \lim\limits_{\varepsilon \to 0} A_\varepsilon = I_2 = \pi$.

### 3. Boundary value problem for a circular domain

Let us consider a multiply connected bounded domain $D$ in the complex plane $\mathbb{C}$ of the complex variable $z = x + iy$. Let the circumferences $\partial D_k := \{t \in \mathbb{C}, \ |t - a_k| = r_k\}$ $(k = 0, 1, ..., n)$ generate the boundary of the domain $D$, the circumference $\partial D_0$ envelopes the remaining circumferences, $D_k := \{z \in \mathbb{C}, \ |z - a_k| < r_k\}$ $(k = 1, 2, ..., n)$, $D_0 := \{z \in \overline{\mathbb{C}}, \ |z - a_0| > r_0\}$. Suppose that the domains $D$ and $D_k$ are occupied by isotropic materials with different conductivities $\lambda$ and $\lambda_k$, respectively. The state of the media is described by the differential equations:

$$\nabla \cdot \mathbf{j} = 0, \qquad \mathbf{j} = \begin{cases} \lambda \mathbf{e} & \text{in } D, \\ \lambda_k \mathbf{e} & \text{in } D_k, \end{cases} \qquad \mathbf{e} = -\nabla u,$$

where $u$ is a potential, $\mathbf{j}$ is a current and $\mathbf{e}$ is a gradient. The function $u(z)$ is harmonic in $D$ and $D_k$, and it is continuously differentiable in $\overline{D}$ and $\overline{D_k}$ $(k = 1, 2, ..., n)$. If the contact between $D$ and $D_k$ is perfect, then the potential $u$ and the current $\mathbf{j}$ are continuous in the circle $G := \{z \in \mathbb{C}, \ |z - a_0| < r_0\}$:

$$(3.1) \qquad u = u_k, \qquad \lambda \frac{\partial u}{\partial n} = \lambda_k \frac{\partial u_k}{\partial n}, \qquad k = 1, 2, ..., n, \quad u = f \ \text{ in } \partial D_0,$$

where $\dfrac{\partial}{\partial n}$ is the normal derivative, $f$ is the given Hölder continuous function.

We shall use the results of the paper [13], where the problem (3.1) has been solved in analytical form for unbounded domain $D$ ($\partial D_0$ is absent), and of the papers [17, 18], where the Dirichlet problem for the domain $D$ has been solved too.

The condition (1.1) is equivalent to the following $\mathbb{R}$-linear problem [13]:

$$\phi(t) = \phi_k(t) - \rho_k \overline{\phi_k(t)}, \qquad |t - a_k| = r_k, \qquad k = 1, 2, ..., n, \tag{3.2}$$

where $\rho_k := (\lambda_k - \lambda)(\lambda_k + \lambda)$, $|\rho_k| < 1$. The last condition (3.1) can be written in the form [19]

$$\phi(t) = \phi_0(t) - \overline{\phi_0(t)} + f^-(t), \qquad |t - a_0| = r_0. \tag{3.3}$$

Here, the unknown harmonic and analytic functions are related by the identities $u(z) = \operatorname{Re}\phi(z)$, $u_k(z) = 2\lambda(\lambda + \lambda_k)^{-1}\operatorname{Re}\phi_k(z)$. The auxiliary unknown function $\phi_0(z)$ is analytic in $D_0$. The function

$$f^-(z) = \frac{1}{\pi i}\int\limits_{\partial D_0} \frac{f(\tau)}{z - \tau} d\tau$$

is analytic in $D_0$, vanishes at infinity and satisfies the boundary condition

$$\operatorname{Re} f^-(t) = f(t), \qquad |t - a_0| = r_0.$$

So, the original problem (3.1) can be written in the following form:

$$\phi(t) = \phi_k(t) - \rho_k \overline{\phi_k(t)} + f_k(t), \qquad |t - a_k| = r_k, \qquad k = 0, 1, ..., n, \tag{3.4}$$

where $f_k(t) = 0$ for $k = 1, 2, ..., n$; $\rho_0 = 1$, $f_0(t) = f^-(t)$.

In the next section we shall see that we need only the derivatives $\phi_k'(z)$ to define the effective conductivity. It is easy to modify the conclusions of [13, 16–18] and to prove the following

THEOREM 3.1. *The functions $\phi_k(z)$ of the problem* (3.4) *satisfy the relations*

$$\phi_k'(z) = -f_k'(z) + \sum_{\substack{k_1=0\\k_1\neq k}}^{n} \rho_{k_1}\left(\overline{f_{k_1}(z_{k_1}^*)}\right)' - \sum_{\substack{k_1=0\\k_1\neq k}}^{n}\sum_{\substack{k_2=0\\k_2\neq k_1}}^{n} \rho_{k_1}\rho_{k_2}\left(f_{k_2}(z_{k_2k_1}^*)\right)' + \ldots$$

$$= \sum_{m=0}^{\infty}\sum_{\substack{k_1=0\\k_1\neq k}}^{n}\sum_{\substack{k_2=0\\k_2\neq k_1}}^{n}\cdots\sum_{\substack{k_m=0\\k_m\neq k_{m-1}}}^{n} \rho_{k_1}\rho_{k_2}\cdots\rho_{k_m}(-1)^{m+1}\left(\mathfrak{C}^m f_{k_m}(z_{k_m\ldots k_1}^*)\right)', \tag{3.5}$$

$$|z - a_k| \le r_k, \quad k = 1, 2, ..., n.$$

Here, $\mathfrak{C}$ is the operator of complex conjugation, $z_k^* := r_k^2/(\overline{z - a_k}) + a_k$ is inversion with respect to the circumference $|z - a_k| = r_k$. $z_{k_mk_{m-1}\ldots k_1}^* := (z_{k_{m-1}\ldots k_1}^*)_{k_m}^*$ is the sequence of inversions with respect to the circumferences with numbers $k_1, k_2, ..., k_m$. There are no equal neighbour numbers in the sequence $k_1, k_2, ..., k_m$. The series converges absolutely and uniformly in the domains indicated.

In our case the series takes the form

$$\phi_k'(z) = g'(z) - \sum_{\substack{k_1=1\\k_1\neq k}}^{n} \rho_{k_1}\left(\overline{g(z_{k_1}^*)}\right) + \sum_{\substack{k_1=0\\k_1\neq k}}^{n}\sum_{\substack{k_2=1\\k_2\neq k_1}}^{n} \rho_{k_1}\rho_{k_2}\left(g(z_{k_2k_1}^*)\right)' - \ldots$$

$$= \sum_{m=0}^{\infty}\sum_{\substack{k_1=0\\k_1\neq k}}^{n}\sum_{\substack{k_2=0\\k_2\neq k_1}}^{n}\cdots\sum_{\substack{k_m=1\\k_m\neq k_{m-1}}}^{n} \rho_{k_1}\rho_{k_2}\cdots\rho_{k_m}(-1)^m\left(\mathfrak{C}^m g(z_{k_m\ldots k_1}^*)\right)',$$

$$|z - a_k| \leq r_k, \quad k = 1, 2, \ldots, n,$$

where $g(z) := \overline{f^-(z_0^*)}$, $g(a_0) = \overline{f^-(\infty)} = 0$. In the particular case when $\rho_k = \rho$ for $k = 1, 2, \ldots, n$, the last series becomes

$$\phi_k'(z) = g'(z) - \rho\sum_{\substack{k_1=1\\k_1\neq k}}^{n}\left(\overline{g(z_{k_1}^*)}\right)' + \rho^2\sum_{\substack{k_1=0\\k_1\neq k}}^{n}\sum_{\substack{k_2=1\\k_2\neq k_1}}^{n}\left(g(z_{k_2k_1}^*)\right)' - \ldots . \tag{3.5}$$

## 4. Effective conductivity

Let us define the value

$$\lambda_e^x(n) = \frac{\langle j\rangle}{\langle e\rangle},$$

where $\langle e\rangle = J + \sum_{k=1}^{n} J_k$, $\langle j\rangle = \lambda J + \sum_{k=1}^{n}\lambda_k J_k$, $J_k := \iint_{D_k}\frac{\partial u_k}{\partial x}dx\,dy$, $J := \iint_{D}\frac{\partial u}{\partial x}dx\,dy$. If the inclusions $D_k$ generate a statistically homogeneous and isotropic structure, then for $r_0 \to \infty$ $(n \to \infty)$ the value $\lambda_e^x(n)$ tends to the effective conductivity $\lambda_e$. By virtue of the mean value of a harmonic function we have

$$\iint_{D_k}\frac{\partial u_k}{\partial x}dx\,dy = \pi r_k^2\frac{\partial u_k}{\partial x}(a_k) = \pi r_k^2\operatorname{Re}\phi_k'(a_k)\,2\lambda(\lambda+\lambda_k)^{-1}.$$

Using Green's theorem and conditions (3.1), let us transform the next integral

$$\iint_{D}\frac{\partial u}{\partial x}dx\,dy = \int_{\partial G}u\,dy - \sum_{k=1}^{n}\int_{\partial D_k}u_k\,dy = \int_{\partial G}f\,dy - \sum_{k=1}^{n}J_k.$$

Hence,

$$\frac{\lambda_e^x(n)}{\lambda} = 1 + 2\pi\sum_{k=1}^{n} r_k^2\rho_k\frac{\operatorname{Re}\phi_k'(a_k)}{P_0}, \tag{4.1}$$

where $P_0 = \int\limits_{\partial G} f\,dy$. If $\rho_k = \rho$ and $r_k = r$ for all $k$, then (4.1) becomes

$$\frac{\lambda_e^x(n)}{\lambda} = 1 + \frac{2\pi r^2 \rho}{P_0} \sum_{k=1}^{n} \operatorname{Re} \phi_k'(a_k)\,. \tag{4.2}$$

The effective conductivity $\lambda_e$ doesn't depend on the boundary function $f$. Let us take $f(x,y) = x - \operatorname{Re} a_0$, then $P_0 = \pi r_0^2$ and $g(z) = z - a_0$. The relation (4.2) implies the equality

$$\frac{\lambda_e^x(n)}{\lambda} = 1 + 2v\rho \frac{1}{n} \sum_{k=1}^{n} \operatorname{Re} \phi_k'(a_k),$$

where $v := \sum\limits_{k=1}^{n} (r/r_0)^2$. According to (3.5) we obtain the series

$$\frac{\lambda_e^x(n)}{\lambda} = 1 + \sum_{m=1}^{\infty} 2\rho^m v^m A_m(n),$$

$$\begin{aligned} &A_1(n) := 1, \qquad A_{m+1}(n) := \frac{1}{n} \sum_{k=0}^{n} \operatorname{Re} B_k(n), \\ &B_k(n) := \frac{1}{n^m} \sum_{\substack{k_1=0 \\ k_1 \neq k}}^{n} \sum_{\substack{k_2=0 \\ k_2 \neq k_1}}^{n} \cdots \sum_{\substack{k_m=1 \\ k_m \neq k_{m-1}}}^{n} \operatorname{Re} \left( \frac{r_0}{a_k - a_{k_1}} \frac{r_0}{\overline{(a_k)_{k_1}^* - a_{k_2}}} \right. \\ &\qquad \left. \cdots \times \frac{r_0}{\mathfrak{C}^{m+1} \left[ (a_k)_{k_{m-1} \ldots k_1}^* - a_{k_m} \right]} \right)^2, \qquad m = 1, 2, \ldots . \end{aligned} \tag{4.3}$$

The formula (4.3) is accurate. It can be applied to any regular structure to calculate the effective conductivity. In the present paper we consider the square array of cylinders with centers $a_k$ which are placed at the points with integer coordinates.

There are two possibilities to study the infinite square array. In the first one $r_0$ is fixed, $n \to \infty$, $r = r_0(v/n)^{1/2} \to 0$. In the second one $r$ is fixed, $n \to \infty$, $r_0 = r(n/v)^{1/2} \to \infty$. In both the cases the volume fraction $v$ is fixed. Let us use the second approach. The first way leads to the same result. Using (4.3) when $n \to \infty$, we have

$$\frac{\lambda_e}{\lambda} = 1 + \sum_{m=1}^{\infty} 2\rho^m v^m A_{m+1},$$

where $A_1 = 1$, $A_{m+1} := \lim_{n\to\infty} A_{m+1}(n) = \mathrm{Re} \lim_{n\to\infty} \frac{1}{n}\sum_{k=0}^{n} B_k(n) = \mathrm{Re} \lim_{n\to\infty} B_k(n)$, because $B_k(n)$ doesn't depend on $k$. So we may assume $a_k = 0$. Hence,

$$A_{m+1} = \mathrm{Re}\,\frac{1}{\pi}\sum_{k_1}{}' \frac{1}{a_{k_1}^2}\,\frac{1}{\pi}\sum_{k_2}{}' \frac{1}{(\overline{0^*_{k_1} - a_{k_2}})^2} \cdots \times \frac{1}{\pi}\sum_{k_m}{}' \frac{1}{\mathfrak{L}^{m+1}[0^*_{k_{m-1}\ldots k_1} - a_{k_m}]^2}, \qquad m = 1, 2, \ldots, \tag{4.4}$$

where $\sum_{k_s}{}' := \sum_{\substack{k_s=0 \\ k_s\neq k_{s-1}}}^{\infty}$. Let $\mathcal{P}(z)$ be the function of Weierstrass for which [22]

$$\mathcal{P}(z) - \frac{1}{z^2} = \sum_{n=2}^{\infty}(2n-1)S_{2n}z^{2(n-1)},$$

where $S_{2n} = \sum_k{}' \frac{1}{a_k^{2n}}$. Let us introduce the function

$$P_1(z) := \frac{1}{\pi}\sum_k{}' \frac{1}{(z-a_k)^2} := \frac{1}{\pi}\sum_k{}' \frac{1}{a_k^2} + \frac{1}{\pi}\sum_k{}' \left(\frac{1}{(z-a_k)^2} - \frac{1}{a_k^2}\right) = 1 + \frac{1}{\pi}\left(\mathcal{P}(z) - \frac{1}{z^2}\right)$$

for $|z| \leq r$ and $P_1(z) = P_1(z - a_k)$ for $|z - a_k| \leq r$. The definition of $P_1(z)$ corresponds to the Rayleigh sum $S_2 = \sum_k{}' \frac{1}{a_k^2} = \pi$. Along similar lines let us introduce the functions

$$P_{s+1}(z) := \frac{1}{\pi}\sum_k{}' \frac{1}{(z-a_k)^2}\overline{P_s(z_k^*)} := \overline{P_s(0)}P_1(z) + \frac{1}{\pi}\sum_k{}' \frac{1}{(z-a_k)^2}\left(\overline{P_s(z_k^*)} - \overline{P_s(a_k)}\right).$$

The last sum converges absolutely because

$$\overline{P_s(z_k^*)} - \overline{P_s(a_k)} = \frac{1}{z-a_k} F\left(\frac{1}{z-a_k}\right),$$

where $F(z)$ is bounded for $|z - a_k| \geq r$. So, the following equality $A_{m+1} = P_m(0)$, $m = 1, 2, \ldots$, correctly defines the infinite sum (4.4).

If the radius $r$ is sufficiently small, then we may assume that $0^*_{k_s k_{s-1}\ldots k_1} - a_{k_s} \approx a_{k_{s-1}} - a_{k_s} =: \mathfrak{C}^{s+1} b_{k_s}$. In that case

$$A_{m+1} \approx \frac{1}{\pi}\sum_{k_1}{}' \frac{1}{a_{k_1}^2}\frac{1}{\pi}\sum_{k_2}{}' \frac{1}{b_{k_2}^2} \ldots \frac{1}{\pi}\sum_{k_m}{}' \frac{1}{b_{k_m}^2} = 1, \qquad m = 1, 2, \ldots .$$

Therefore, $\dfrac{\lambda_e}{\lambda} \approx 1 + \sum\limits_{m=1}^{\infty} 2\rho^m v^m = \dfrac{1+\rho v}{1-\rho v}$. This is the Clausius-Mossotti approximation (1.1).

The accurate formula (4.4) implies

$$A_2 = \frac{1}{\pi}\sum_{k_1}{}' \frac{1}{a_{k_1}^2} = 1,$$

$$A_3 = 1 + \frac{1}{\pi^2}\sum_{n=2}^{\infty}(2n-1)S_{2n}^2 r^{4(n-1)},$$

$$A_4 = 1 + \frac{2}{\pi^2}\sum_{n=2}^{\infty}(2n-1)S_{2n}^2 r^{4(n-1)}.$$

Since $r \leq 0.5$, the formulae $A_3 \approx 1 + 3.01840r^4 + 12.84563r^{12}$, $A_4 \approx 1 + 6.03680r^4 + 25.69126r^{12}$ are quite accurate. The numerical values of $S_{2n}$ are calculated in the paper [7].

## 5. Conclusions

1. A rigorous definition of Rayleigh's integral has been proposed.

2. An exact formula for $\lambda_e$ has been written for each structure. Square array of cylinders has been considered in particular.

## References


1. R. LANDAUER, *Electrical conductivity in inhomogeneous media*, [in:] Electrical Transport and Optical Properties of Inhomogeneous Media, J.C. BERLAND and D.B. TANNER [Eds.], 2–45, New York 1978.
2. D.J. JEFFREY, *Conduction through a random suspension of spheres*, Proc. R. Soc. Lond., **A335**, 355–367, 1973.
3. G.K. BATCHELOR and R.W. O'BRIEN, *Thermal or electrical conduction through a granular material*, Proc. R. Soc. Lond., **A355**, 313–333, 1977.
4. A.S. SANGANI and C. YAO, *Bulk thermal conductivity of composites with spherical inclusions*, J. Appl. Phys., **63**, 5, 1334–1341, 1988.
5. A.S. SANGANI and C. YAO, *Transport properties in random arrays of cylinders. 1. Thermal conduction*, Phys. Fluids, **31**, 9, 2426–2434, 1988.
6. R.C. MCPHEDRAN and D.R. MCKENZIE, *The conductivity of lattices of spheres. 1. The simple cubic lattice*, Proc. R. Soc. Lond., **A359**, 45–63, 1978.

7. W.T. PERRINS, D.R. MCKENZIE and R.C. MCPHEDRAN, *Transport properties of regular arrays of cylinders*, Proc. R. Soc. Lond., **A369**, 207–225, 1979.
8. R.C. MCPHEDRAN, *Transport properties of cylinder pairs and the square array of cylinders*, Proc. R. Soc. Lond., **A408**, 31–43, 1986.
9. R.C. MCPHEDRAN and G.W. MILTON, *Transport properties of touching cylinder pairs and of the square array of touching cylinders*, Proc. R. Soc. Lond., **A411**, 313–326, 1987.
10. R.C. MCPHEDRAN, L. POLADIAN and G.W. MILTON, *Asymptotic studies of closely spaced, highly conducting cylinders*, Proc. R. Soc. Lond., **A415**, 185–196, 1988.
11. L. POLADIAN and R.C. MCPHEDRAN, *Effective transport properties of periodic composite materials*, Proc. R. Soc. Lond., **A408**, 45–59, 1986.
12. RAYLEIGH, Lord, *On the influence of obstacles arranged in rectangular order upon the properties of a medium*, Phil. Mag., **34**, 481–502, 1892.
13. V.V. MITYUSHEV, *Plane problem for the steady heat conduction of material with circular inclusions*, Arch. Mech., **45**, 2, 211–215, 1993.
14. S.G. MIKHLIN, *Integral equations*, Pergamon Press, New York 1964.
15. S.G. MIKHLIN and S. PRÖSSDORF, *Singular integral operators*, Akademic-Verlag, Berlin 1986.
16. V.V. MITYUSHEV and T.N. ZHOROVINA, *A mixed boundary value problem for a multiply connected domain, Differential equations* [to appear] [in Russian].
17. V.V. MITYUSHEV, *A method of functional equations for boundary value problems of continuous media*, Rep. Math. Phys., **33**, 1–2, 137–147, 1993.
18. V.V. MITYUSHEV, *Solution of the Hilbert boundary value problem for a multiply connected domain*, Słupskie Prace Mat.-Przyr., 9a, 37–69, 1994.
19. V.V. MITYUSHEV, *On solution of the $\mathbb{R}$-linear problem for a complex circular contour* [in Russian], Reprint VINITI N7709-B87, Minsk 1987.
20. B.U. FELDERHOF, G.W. FORD and G.D. COHEN, *Cluster expansion for the dielectric constant of a polarizable suspension*, J. Statistical Phys., **28**, 1, 135–164, 1982.
21. D. BERGMAN and K.-J. DUNN, *Bulk effective dielectric constant of a composite with a periodic microgeometry*, Phys. Rev. B, **45**, 23, 13262–13271, 1992.
22. A. HURWITZ and R. COURANT, *Allgemeine Funktionentheorie und elliptische Funktionen*, Springer-Verlag, Berlin 1964.

DEPARTMENT OF MATHEMATICS
PEDAGOGICAL UNIVERSITY, SŁUPSK.

*Received July* 11, 1994.

Arch. Mech., 47, 1, pp. 39–67, Warszawa 1995

# Crack interaction in brittle anisotropic materials

W. K. BINIENDA (AKRON)

METHODOLOGY and rigorous solution formulation for stress intensity factors (SIF) and strain energy release rates (SERR) of a multi-cracked plate, with fully interacting cracks, subjected to a far-field arbitrary stress state is presented. The fundamental perturbation problem is derived, and the steps needed to formulate the system of singular integral equations, whose solution gives rise to the evaluation of the SIF, are identified. Parametric studies are conducted for two, three and four crack problems. Accuracy, sensitivity and characteristics of the model is demonstrated.

## 1. Introduction

CONSIDER MULTIPLE cracks embedded in an infinite anisotropic plate (Fig. 1a). The plate is under a far-field stress denoted by $\sigma^0_{jl}$, (in particular $\sigma^0_{XX}$, $\sigma^0_{YY}$, and $\sigma^0_{XY}$, where $(X, Y)$ is the global coordinate system), and the cracks are defined in their local frames $(x_j, y_j)$ (Fig. 1b). The origin of each local frame is defined by the position vector $\mathbf{r}_j$, and the orientation of the local frame with respect to the global frame is defined by the angle $\varphi_j$. Each crack is symmetrically situated within its own coordinate system and is $2a_j$ long, as shown in Fig. 1b. The material is described by the four independent elastic constants, i.e. $E_{LL}$, $E_{TT}$, $G_{LT}$, and $\nu_{LT}$, where $(L, T)$ is the material coordinate system rotated by the angle $\Omega$ with respect to $(X, Y)$.

The general solution formulation can be outlined in four basic steps. The first step is to derive the local stress equations for each crack in its respective local coordinate system. This derivation is achieved by defining the fundamental problem; that is a single crack in an infinite anisotropic plane (Fig. 1b). The fundamental problem is then decomposed into two subproblems: the problem of the undamaged plate containing an imaginary crack (Fig. 1c) and the perturbation problem (Fig. 1d) of a plate with a single crack subjected to the appropriate crack-surface tractions, which are found from the solution of the complementary undamaged problem. The analysis of the perturbation problem leads to singular stresses that govern local crack tip behaviour.

The second step is to formulate the total perturbation stress field for each crack, which includes the interaction of all cracks by means of summation of the transformed local stresses of all other cracks. In the third step of the formulation, the total stress equations are normalized. A set of Cauchy-type singular integral equations, expressed in terms of unknown auxiliary functions, is obtained by subjecting the total perturbation stress equations to the crack-surface traction field at each crack location. The fourth and final step of the formulation is to

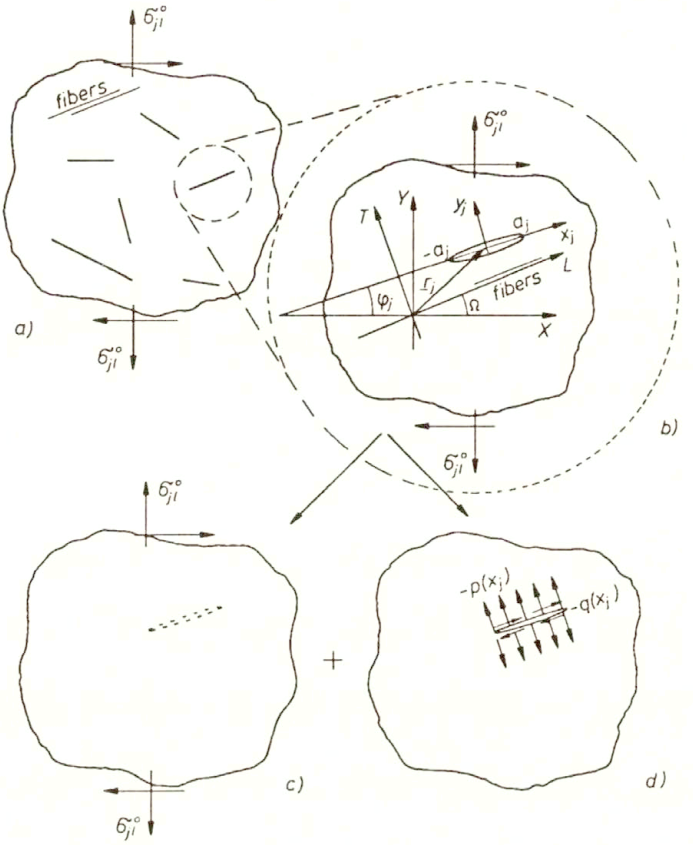


FIG. 1. Multi-cracked plate geometry and method of solution, a) multicracked plate, b) fundamental problem for $j$-th crack, c) undamaged plate, d) perturbation problem.

express the SIF in terms of the discrete auxiliary functions, $H_{\eta j}(\tau_p)$, evaluated at each crack tip. These discrete auxiliary functions are obtained through the implementation of the Lobatto–Chebyshev collocation technique. Finally, the Strain Energy Release Rate (SERR) will be calculated in terms of SIF.

## 2. Local stress formulation

Consider the fundamental problem (Fig. 1b), which is defined as a single crack in an infinite anisotropic plate, whose solution can be obtained by decomposing it into an undamaged problem (Fig. 1c) and a perturbation problem (Fig. 1d). The essence of this decomposition is that the traction forces applied along the crack surface in the perturbation problem are opposite to the obtained stress field of the undamaged plate at the particular location of the imaginary crack. As a result, this undamaged traction field can be defined in terms of the normal $(p_j)$

and shear ($q_j$) stress components along the imaginary crack surface:

$$p_j(x_j) = \sigma_{y_j y_j}(x_j, 0), \tag{2.1}$$

$$q_j(x_j) = \sigma_{x_j y_j}(x_j, 0), \tag{2.2}$$

where

$$\sigma_{y_j y_j}(x_j, 0) = \sigma^0_{XX} \sin^2 \varphi_j + \sigma^0_{YY} \cos^2 \varphi_j - \sigma^0_{XY} \sin 2\varphi_j, \tag{2.3}$$

$$\sigma_{x_j y_j}(x_j, 0) = -\frac{\sigma^0_{XX} - \sigma^0_{YY}}{2} \sin 2\varphi_j + \sigma^0_{XY} \cos 2\varphi_j. \tag{2.4}$$

The mixed boundary conditions for the perturbation part of the fundamental problem (Fig. 1d) are expressed in terms of stresses

$$\sigma_{y_j y_j} = -p_j(x_j) \quad \text{and} \quad \sigma_{x_j y_j} = -q_j(x_j) \tag{2.5}$$

along the crack surface (i.e., $y_j = 0$ and $-a_j \leq x_j \leq a_j$), and in terms of continuity of displacements

$$v^+ = v^- \quad \text{and} \quad u^+ = u^- \tag{2.6}$$

outside of the crack (i.e., $y_j = 0$ and $|x_j| > a_j$). Here + indicates the value of displacement at a point approached from the positive side of the plate, (i.e., $y > 0$), whereas − indicates the same point approached from the negative side of the plate, (i.e., $y < 0$).

The governing equations for the preceding two-dimensional anisotropic plate problem can be expressed in terms of the Airy stress function $F_j(x_j, y_j)$ as

$$\frac{\partial^4 F}{\partial x^4} + \gamma_1 \frac{\partial^4 F}{\partial x^3 \partial y} + \gamma_2 \frac{\partial^4 F}{\partial x^2 \partial y^2} + \gamma_3 \frac{\partial^4 F}{\partial x \partial y^3} + \gamma_4 \frac{\partial^4 F}{\partial y^4} = 0, \tag{2.7}$$

where

$$\gamma_1 = -\frac{2b_{26}}{b_{22}}, \qquad \gamma_2 = \frac{2b_{12} + b_{66}}{b_{22}}, \qquad \gamma_3 = -\frac{2b_{16}}{b_{22}}, \qquad \gamma_4 = \frac{b_{11}}{b_{22}}; \tag{2.8}$$

and

$$\begin{aligned}
b_{11} &= a_{11} \cos^4(\Omega - \varphi) + (2a_{12} + a_{66}) \sin^2(\Omega - \varphi) \cos^2(\Omega - \varphi) \\
&\quad + a_{22} \sin^4(\Omega - \varphi), \\
b_{22} &= a_{22} \cos^4(\Omega - \varphi) + (2a_{12} + a_{66}) \sin^2(\Omega - \varphi) \cos^2(\Omega - \varphi) \\
&\quad + a_{11} \sin^4(\Omega - \varphi), \\
b_{12} &= a_{12} + (a_{11} + a_{22} - 2a_{12} - a_{66}) \sin^2(\Omega - \varphi) \cos^2(\Omega - \varphi), \\
b_{66} &= a_{66} + (a_{11} + a_{22} - 2a_{12} - a_{66}) \sin^2(\Omega - \varphi) \cos^2(\Omega - \varphi),
\end{aligned} \tag{2.9}$$

(2.9) [cont.]
$$b_{16} = \left[a_{22}\sin^2(\Omega-\varphi) - a_{11}\cos^2(\Omega-\varphi) + \frac{1}{2}(2a_{12}+a_{66})\cos 2(\Omega-\varphi)\right]\sin 2(\Omega-\varphi),$$
$$b_{26} = \left[\cos^2(\Omega-\varphi) - \sin^2(\Omega-\varphi) - \frac{1}{2}(2a_{12}+a_{66})\cos 2(\Omega-\varphi)\right]\sin 2(\Omega-\varphi),$$

where

$$a_{11} = \frac{1}{E_{LL}}, \qquad a_{22} = \frac{1}{E_{TT}}, \qquad a_{12} = \frac{-\nu_{LT}}{E_{LL}}, \qquad a_{66} = \frac{1}{G_{LT}}.$$

Consequently, $E_{LL}$, $E_{TT}$, $G_{LT}$ and $\nu_{LT}$ are four independent material constants used for the plate characterization as a fiber-reinforced composite in material coordinate system $L-T$.

A rigorous solution for this stress function can be obtained by employing the Fourier transformation. Assume the stress function to be expressed as:

(2.10)
$$F(x,y) = \frac{1}{2\pi}\int_{-\infty}^{\infty}\sum_{m=1}^{4} C_m e^{r_m y_s} e^{-isx}\,ds;$$

then, upon substitution into (2.7), the characteristic equation is obtained that has four complex roots in the following form

(2.11)
$$r_1 = a + ib, \qquad r_2 = c + id, \qquad r_3 = -a + ib, \qquad r_4 = -c + id,$$

where $a, c > 0$.

The Airy stress function must also satisfy the physical requirement that the stress function is finite throughout the domain of the plate. Therefore, the following form of $F_j(x_j, y_j)$ can be used for the upper half-plane (for $y > 0$)

(2.12)
$$F(x,y^+) = \frac{1}{2\pi}\int_{-\infty}^{\infty}\left[C_1 e^{(ibs-a|s|)y} + C_2 e^{(ids-c|s|)y}\right]e^{-isx}\,ds,$$

and for the lower half-plane (for $y < 0$)

(2.13)
$$F(x,y^-) = \frac{1}{2\pi}\int_{-\infty}^{\infty}\left[C_3 e^{(ibs+a|s|)y} + C_4 e^{(ids+c|s|)y}\right]e^{-isx}\,ds,$$

which are automatically bounded at infinity. Note: constants $C_j$ for $j = 1, 2, 3,$ and 4 are functions of the Fourier variable $s$ and are determined by using the local

stress continuity conditions at the boundaries between the half-planes ($y = 0$) and by using the perturbation boundary conditions subsequent to the determination of the total stresses at each crack location.

The stresses are calculated at the upper and lower half-plane by using the second derivatives of the stress functions [10]. Therefore, the stresses for the upper half-plane are:

$$\sigma_{xx}^{(+)} = \frac{1}{2\pi}\int_{-\infty}^{\infty}\left[C_1(-a|s| + ibs)^2 e^{(ibs-a|s|)y} + C_2(-c|s| + ids)^2 e^{(ids-c|s|)y}\right] e^{-isx}\,ds, \tag{2.14}$$

$$\sigma_{yy}^{(+)} = -\frac{1}{2\pi}\int_{-\infty}^{\infty} s^2\left[C_1 e^{(ibs-a|s|)y} + C_2 e^{(ids-c|s|)y}\right] e^{-isx}\,ds, \tag{2.15}$$

$$\sigma_{xy}^{(+)} = \frac{1}{2\pi}\int_{-\infty}^{\infty} is\left[C_1(-a|s| + ibs)e^{(ibs-a|s|)y} + C_2(-c|s| + ids)e^{(ids-c|s|)y}\right] e^{-isx}\,ds \tag{2.16}$$

and for the lower half-plane are:

$$\sigma_{xx}^{(-)} = \frac{1}{2\pi}\int_{-\infty}^{\infty}\left[C_3(a|s| + ibs)^2 e^{(ibs+a|s|)y} + C_4(c|s| + ids)^2 e^{(ids+c|s|)y}\right] e^{-isx}\,ds, \tag{2.17}$$

$$\sigma_{yy}^{(-)} = -\frac{1}{2\pi}\int_{-\infty}^{\infty} s^2\left[C_3 e^{(ibs+a|s|)y} + C_4 e^{(ids+c|s|)y}\right] e^{-isx}\,ds, \tag{2.18}$$

$$\sigma_{xy}^{(-)} = \frac{1}{2\pi}\int_{-\infty}^{\infty} is\left[C_3(a|s| + ibs)e^{(ibs+a|s|)y} + C_4(c|s| + ids)e^{(ids+c|s|)y}\right] e^{-isx}\,ds. \tag{2.19}$$

The continuity conditions for local stresses, $\sigma_{yy}$ and $\sigma_{xy}$, are identically satisfied, giving

$$C_1 + C_2 = C_3 + C_4 \tag{2.20}$$

and

$$C_1(bs + ia|s|) + C_2(ds + ic|s|) = C_3(bs - ia|s|) + C_4(ds - ic|s|), \tag{2.21}$$

respectively.

The solution of Eqs. (2.20) and (2.21) for $C_3$ and $C_4$ in terms of $C_1$ and $C_2$ can be written in the following form:

$$\begin{aligned} C_3 &= S_1 C_1 + S_2 C_2, \\ C_4 &= S_3 C_1 + S_4 C_2, \end{aligned} \tag{2.22}$$

where

$$\begin{aligned} S_1 &= \frac{|s|(a+c) + i(d-b)s}{|s|(c-a) + i(d-b)s}, \\ S_2 &= \frac{2c|s|}{|s|(c-a) + i(d-b)s}, \\ S_3 &= -\frac{2a|s|}{|s|(c-a) + i(d-b)s}, \\ S_4 &= -\frac{|s|(a+c) - i(d-b)s}{|s|(c-a) + i(d-b)s}. \end{aligned} \tag{2.23}$$

The strains are calculated using generalized Hooke's law. Then normal strains are:

$$\begin{aligned} \varepsilon_{xx} &= b_{11}\sigma_{xx} + b_{12}\sigma_{yy} + b_{16}\sigma_{xy}, \\ \varepsilon_{yy} &= b_{12}\sigma_{xx} + b_{22}\sigma_{yy} + b_{26}\sigma_{xy}. \end{aligned} \tag{2.24}$$

Using the Eqs. (2.24), the strains for upper and lower half-planes can be obtained. Then, using strain-displacement relations [10], the displacement, also for the upper and lower half-plane, are obtained:

$$\begin{aligned} u(x,y) &= \int \varepsilon_{xx}\, dx, \\ v(x,y) &= \int \varepsilon_{yy}\, dy. \end{aligned} \tag{2.25}$$

To obtain the singular integral equations, the following auxiliary functions are introduced,

$$f_1(x) = \frac{\partial}{\partial x}[u^+(x,0) - u^-(x,0)], \tag{2.26}$$

$$f_2(x) = \frac{\partial}{\partial x}[v^+(x,0) - v^-(x,0)]. \tag{2.27}$$

Expressions for the unknown constants $C_1$ and $C_2$ can be determined in terms of the above auxiliary functions, knowing that $f_1(t)$ and $f_2(t)$ are nonzero only

within the crack region (i.e., $-a < t < a$). Therefore,

$$C_1 = \int_{-a}^{a} \frac{D_4 f_1(t) - D_2 f_2(t)}{D_1 D_4 - D_2 D_3} e^{ist}\, dt, \tag{2.28}$$

$$C_2 = -\int_{-a}^{a} \frac{D_3 f_1(t) - D_1 f_2(t)}{D_1 D_4 - D_2 D_3} e^{ist}\, dt, \tag{2.29}$$

where

$$\begin{aligned} D_1 &= 2a|s|[|s|(a+c) + i(d-b)s]b_{11}, \\ D_2 &= 2c|s|[|s|(a+c) + i(d-b)s]b_{11}, \\ D_3 &= 2a\frac{|s|s[s(d-b) - i(a+c)|s|]}{(a^2+b^2)(c|s| + ids)}b_{22}, \\ D_4 &= 2c\frac{|s|s[-s(d-b) - i(a+c)|s|]}{(c^2+d^2)(a|s| + ibs)}b_{22}. \end{aligned} \tag{2.30}$$

Similarly, $C_3$ and $C_4$ can also be expressed in terms of the auxiliary functions using (2.22) with (2.28) and (2.29).

Substituting expressions for the constants $C_j$ into the local stress equations results in the formulation of the set of double integral equations with respect to the Fourier variables $s$ $(-\infty < s < \infty)$ and $t$ $(-a \le t \le a)$. Integrating with respect to $s$ will give a set of singular integral equations with respect to $t$, which are valid for any $j$-th crack within its own local coordinate system $(x_j, y_j)$:

$$\sigma^{(j)}_{x_j x_j} = \frac{1}{2\pi}\int_{-a_j}^{a_j} \left[ f_{j1}(t_j)\frac{Q_1}{b_{11}Q_0} + f_{j2}(t_j)\frac{Q_2}{b_{22}Q_0} \right] dt_j, \tag{2.31}$$

$$\sigma^{(j)}_{y_j y_j} = \frac{1}{2\pi}\int_{-a_j}^{a_j} \left[ f_{j1}(t_j)\frac{Q_3}{b_{11}Q_0} + f_{j2}(t_j)\frac{Q_4}{b_{22}Q_0} \right] dt_j, \tag{2.32}$$

$$\sigma^{(j)}_{x_j y_j} = \frac{1}{2\pi}\int_{-a_j}^{a_j} \left[ f_{j1}(t_j)\frac{Q_5}{b_{11}Q_0} + f_{j2}(t_j)\frac{Q_6}{b_{22}Q_0} \right] dt_j, \tag{2.33}$$

where

$$\begin{aligned} Q_0 = ac\left[(a+c)^2 + (b-d)^2\right]&\left[(t_j - x_j)^2 + 2b(t_j - x_j)y_j + (a^2+b^2)y_j^2\right] \\ &\times \left[(t_j - x_j)^2 + 2d(t_j - x_j)y_j + (c^2+d^2)y_j^2\right], \end{aligned} \tag{2.34}$$

$$Q_1 = R_1(t_j - x_j)^3 + y_j\left[R_2(t_j - x_j)^2 + y_j R_3(t_j - x_j) + y_j^2 R_4\right], \tag{2.35}$$

where

$$
\begin{aligned}
R_1 &= a^2bc + b^3c + 2abc^2 + 2a^2cd + ac^2d + ad^3,\\
R_2 &= a^4c + 2a^2b^2c + b^4c + 2a^3c^2 + 2ab^2c^2 + 2a^2c^3 + ac^4\\
&\quad + 2a^2bcd + 2b^3cd + 2abc^2d + 2a^2cd^2 + 2ac^2d^2 + 2abd^3 + ad^4,\\
R_3 &= a^2bc^3 + b^3c^3 + 2abc^4 + 2a^4cd + 4a^2b^2cd + 2b^4cd + a^3c^2d\\
&\quad + ab^2c^2d + a^2bcd^2 + b^3cd^2 + 4abc^2d^2 + a^3d^3 + ab^2d^3 + 2abd^4\\
R_4 &= (a^2 + b^2)(c^2 + d^2)(a^2c + b^2c + ac^2 + ad^2);
\end{aligned}
$$

$$
(2.36)\qquad Q_2 = R_5\left\{(t_j - x_j)^3R_6 + y_j\left[R_7(t_j - x_j)^2 - y_jR_8(t_j - x_j) + y_j^2R_9\right]\right\},
$$

where

$$
\begin{aligned}
R_5 &= (a^2 + b^2)(c^2 + d^2),\\
R_6 &= (a^2c + b^2c + ac^2 + ad^2),\\
R_7 &= a^2bc + b^3c + 2b^2cd + ac^2d + 2abd^2 + ad^3,\\
R_8 &= a^3c^2 + ab^2c^2 + a^2c^3 - b^2c^3 - 2a^2bcd - 2b^3cd\\
&\quad - 2abc^2d - a^3d^2 - ab^2d^2 + a^2cd^2 - b^2cd^2 - 2abd^3,\\
R_9 &= (a^2 + b^2)(c^2 + d^2)(bc + ad);
\end{aligned}
$$

$$
(2.37)\qquad Q_3 = R_{10}(t_j - x_j)^3 + y_j\left[-(t_j - x_j)^2R_{11} + y_j(t_j - x_j)R_{12} + y_j^2R_{13}\right],
$$

where

$$
\begin{aligned}
R_{10} &= bc + ad,\\
R_{11} &= (a^2 - b^2)c - 2bd(a + c) + a(c^2 - d^2),\\
R_{12} &= bc^3 + a^3d + ab^2d + bcd^2 + 2bd(bc + ad),\\
R_{13} &= (a^2 + b^2)(c^2 + d^2)(a + c);
\end{aligned}
$$

$$
(2.38)\qquad Q_4 = R_5\left\{(t_j - x_j)^3R_{14} + y_j\left[R_{15}(t_j - x_j)^2 + y_j(t_j - x_j)R_{16} + y_j^2R_{17}\right]\right\},
$$

where

$$
\begin{aligned}
R_{14} &= a + c,\\
R_{15} &= 2ab + bc + ad + 2cd,\\
R_{16} &= a^3 + ab^2 + 2a^2c + 2ac^2 + c^3 + 2abd + 2bcd + cd^2,\\
R_{17} &= 2abc^2 + bc^3 + a^3d + ab^2d + 2a^2cd + bcd^2;
\end{aligned}
$$

$$Q_5 = R_{18}(t_j - x_j)^3 + y_j\left[R_{19}(t_j - x_j)^2 - y_j(t_j - x_j)R_{20} + y_j^2 R_9\right], \tag{2.39}$$

where

$$\begin{aligned} R_{18} &= c(a^2 + b^2) + a(c^2 + d^2), \\ R_{19} &= a^2bc + b^3c + 2b^2cd + ac^2d + 2abd^2 + ad^3, \\ R_{20} &= a^3c^2 + ab^2c^2 + a^2c^3 - b^2c^3 - 2a^2bcd - 2b^3cd \\ &\qquad -2abc^2d - a^3d^2 - ab^2d^2 + a^2cd^2 - b^2cd^2 - 2abd^3; \end{aligned}$$

$$Q_6 = R_5\left\{(t_j - x_j)^3 R_{21} + y_j\left[R_{22}(t_j - x_j)^2 + y_j(t_j - x_j)R_{23} + y_j^2 R_{13}\right]\right\}, \tag{2.40}$$

where

$$\begin{aligned} R_{21} &= ad + bc, \\ R_{22} &= -a^2c + b^2c - ac^2 + ad^2 + 2abd + 2bcd, \\ R_{23} &= bc^3 + a^3d + ab^2d + 2b^2cd + 2abd^2 + bcd^2. \end{aligned}$$

Note that the isotropic case can be obtained by substitution $b = d = 0$ and $a = c = 1$, giving $R_1 = R_3 = R_7 = R_9 = R_{10} = R_{12} = R_{15} = R_{17} = R_{19} = R_{21} = R_{23} = 0$, $R_5 = 1$, $R_4 = R_6 = R_8 = R_{11} = R_{13} = R_{14} = R_{18} = R_{20} = -R_{22} = 2$, and $R_2 = R_{16} = 6$. The parameters $Q_i$ then become:

$$Q_0^{(\mathrm{iso})} = 4\left[(t_j - x_j)^2 + y_j^2\right]^2, \tag{2.41}$$

$$Q_1^{(\mathrm{iso})} = 2y_j\left[3(t_j - x_j)^2 + y_j^2\right], \tag{2.42}$$

$$Q_2^{(\mathrm{iso})} = 2(t_j - x_j)\left[(t_j - x_j)^2 - y_j^2\right], \tag{2.43}$$

$$Q_3^{(\mathrm{iso})} = -2y_j\left[(t_j - x_j)^2 - y_j^2\right], \tag{2.44}$$

$$Q_4^{(\mathrm{iso})} = 2(t_j - x_j)\left[(t_j - x_j)^2 + 3y_j^2\right], \tag{2.45}$$

$$Q_5^{(\mathrm{iso})} = 2(t_j - x_j)\left[(t_j - x_j)^2 - y_j^2\right] = Q_2^{(\mathrm{iso})}, \tag{2.46}$$

$$Q_6^{(\mathrm{iso})} = -2y_j\left[(t_j - x_j)^2 - y_j^2\right] = Q_3^{(\mathrm{iso})}, \tag{2.47}$$

and the stresses are reduced to the isotropic stress formulas derived in [2].

This completes the formulation of the fundamental problem (or local stress state) for the $j$-th crack. Henceforth, the formulation of the multiple crack problem will be considered.

### 3. Total stress formulation

The total stress state ${}_p(\sigma^T_{rz})$ for the $p$-th crack is defined as the local stress state of the $p$-th crack $(\sigma^p_{rz})$ plus the contribution to that stress state of all remaining cracks. This may be represented mathematically as

$$(3.1) \qquad {}_p\sigma^T_{rz}(x_p, y_p) = \sigma^p_{rz}(x_p, y_p) + \sum_{j=1}^{n-1} \sigma'^j_{rz}\left[x_j(x_p, y_p),\ y_j(x_p, y_p)\right]$$

for $p = 1, \ldots, n$. Here standard tensor transformation is incorporated, $\sigma'_{rz} = \beta_{lr}\beta_{mz}\sigma_{lm}$, and $\beta_{lr}$, $\beta_{mz}$ are the direction cosines between the $(x_j, y_j)$ and $(x_p, y_p)$ coordinate axes with $j$ identifying the remaining cracks. Note: This statement does not imply that the concept of superposition has been invoked, since the stress perturbation boundary conditions (see Eqs. (2.5)) have not yet been utilized to determine the unknown auxiliary functions.

For functional compatibility within Eq. (3.1), coordinate transformations must be simultaneously applied to all remaining ($j$-th) crack coordinate variables. As a result, the dominant part (i.e., the first term of Eq. (3.1)) possesses a singularity, whereas the regular terms within the summation lose their original singularities and yet still contribute to the total stress state, as one might expect.

The singular terms of the singular integral equations are obtained from the first term of Eq. (3.1) applied for shear, $\sigma_{xy}$, and normal stress, $\sigma_{yy}$, by replacing subscript $j$ by $p$ in Eqs. (2.33) and (2.32), respectively, and evaluating them at $y_p = 0$. Finally, the variables $x$ and $t$ are normalized using $x_p = a_p\xi$ and $t_p = a_p\tau$, where the $\xi$ and $\tau$ are defined between $-1$ and 1. Therefore,

$$(3.2) \qquad \sigma^{(p)}_{x_p y_p} = \frac{1}{\pi}\int_{-1}^{1}\left[E^{p(1)}_{xy}\frac{f_{p1}(\tau_p)}{\tau_p - \xi_p} + E^{p(2)}_{xy}\frac{f_{p2}(\tau_p)}{\tau_p - \xi_p}\right]d\tau_p,$$

$$(3.3) \qquad \sigma^{(p)}_{y_p y_p} = \frac{1}{\pi}\int_{-1}^{1}\left[E^{p(1)}_{yy}\frac{f_{p1}(\tau_p)}{\tau_p - \xi_p} + E^{p(2)}_{yy}\frac{f_{p2}(\tau_p)}{\tau_p - \xi_p}\right]d\tau_p,$$

where $E_{xy}$ and $E_{yy}$ are material related coefficients (superscript $p$ stands for $p$-th local coordinate system), proportional to local $x$-direction stiffness (denoted by superscript 1) or local $y$-direction stiffness (denoted by superscript 2), with respect to the local crack coordinate system. Consequently, they will be called Modified Stiffness Parameters (MSP). The MSP are:

$$(3.4) \qquad E^{(1)}_{xy} = \frac{\left[c(a^2 + b^2) + a(c^2 + d^2)\right]}{2ac\left[(a + c)^2 + (b - d)^2\right]b_{11}},$$

$$(3.5) \qquad E^{(2)}_{xy} = \frac{(a^2 + b^2)(c^2 + d^2)(ad + bc)}{2ac\left[(a + c)^2 + (b - d)^2\right]b_{22}},$$

$$E_{yy}^{(1)} = \frac{(bc + ad)}{2ac\,[(a+c)^2 + (b-d)^2]\,b_{11}}, \tag{3.6}$$

$$E_{yy}^{(2)} = \frac{(a^2 + b^2)(c^2 + d^2)(a + c)}{2ac\,[(a+c)^2 + (b-d)^2]\,b_{22}}. \tag{3.7}$$

For the isotropic and orthotropic cases $E_{xy}^{(2)} = E_{yy}^{(1)} = 0$, and for isotropic case the remaining MSP become:

$$E_{xy}^{(1)} = E_{yy}^{(2)} = \frac{E}{4}. \tag{3.8}$$

The regular terms of the singular integral equations are obtained by transforming the remaining stresses into the local $p$-th crack coordinate system simultaneously with coordinate transformation. The coordinate transformation between the $(x_j, y_j)$ and $(x_p, y_p)$ systems is determined from the following geometric relationship (see Fig. 2):

$$r_{jX} + x_j \cos\varphi_j - y_j \sin\varphi_j = r_{pX} + x_p \cos\varphi_p - y_p \sin\varphi_p, \tag{3.9}$$

$$r_{jY} + x_j \sin\varphi_j + y_j \cos\varphi_j = r_{pY} + x_p \sin\varphi_p + y_p \cos\varphi_p, \tag{3.10}$$

where $r_{jX}$, $r_{jY}$ are the rectangular components of the $j$-th crack position vector referred to the global coordinate system $X - Y$, and $\varphi_j$ is the angle of rotation between the global and local systems.

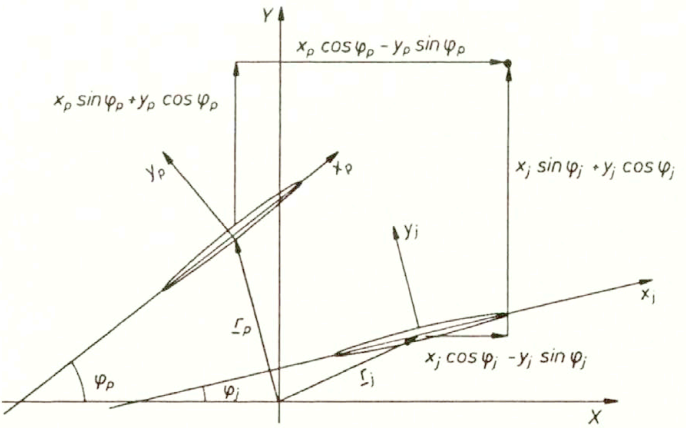


FIG. 2. Geometric relations between a pair of cracks and their local variables.

One component of the regular part of the total stress is obtained by transformation of the stresses from the $j$-th crack local coordinate system into the $p$-th crack local coordinate system,

$$\begin{aligned} \sigma'^{j}_{x_p y_p} &= -\left(\sigma^{(j)}_{x_j x_j} - \sigma^{(j)}_{y_j y_j}\right) \sin\theta\cos\theta + \sigma^{(j)}_{x_j y_j}\left(\cos^2\theta - \sin^2\theta\right), \\ \sigma'^{j}_{y_p y_p} &= \sigma^{(j)}_{x_j x_j} \sin^2\theta + \sigma^{(j)}_{y_j y_j} \cos^2\theta - 2\sigma^{(j)}_{x_j y_j} \sin\theta\cos\theta \end{aligned} \tag{3.11}$$

simultaneously with the coordinate transformation and the substitution $y_p = 0$. Therefore, we can obtain from Eqs. (3.9) and (3.10)

$$
\begin{aligned}
x_j &= p_1 + x_p \cos\theta, \\
y_j &= p_2 + x_p \sin\theta,
\end{aligned}
\tag{3.12}
$$

where $\theta = \varphi_p - \varphi_j$, and $(p_1, p_2)$ is the vector connecting the centers of the $j$-th with $p$-th cracks expressed in $j$-th coordinate system:

$$
\begin{aligned}
p_1 &= (r_{pY} - r_{jY}) \sin\varphi_j + (r_{pX} - r_{jX}) \cos\varphi_j, \\
p_2 &= (r_{pY} - r_{jY}) \cos\varphi_j - (r_{pX} - r_{jX}) \sin\varphi_j.
\end{aligned}
\tag{3.13}
$$

The regular, normalized form of the parameters $Q_i$ for $i = 0, 1, ..., 6$ is obtained using the coordinate normalization $x_p = a_p \xi$ and $t_j = a_j \tau$, in addition to the coordinate transformation, to produce the parameters $Q_i^{(\mathrm{reg})}$:

$$
\begin{aligned}
Q_0^{(\mathrm{reg})} &= ac\left[(a+c)^2 + (b-d)^2\right]\left[(a_j\tau - p_1 - a_p\xi\cos\theta)^2\right. \\
&\quad + 2b(a_j\tau - p_1 - a_p\xi\cos\theta)(p_2 + a_p\xi\sin\theta) + (a^2 + b^2)(p_2 + a_p\xi\sin\theta)^2\Big] \\
&\quad \times \Big[(a_j\tau - p_1 - a_p\xi\cos\theta)^2 + 2d(a_j\tau - p_1 - a_p\xi\cos\theta)(p_2 + a_p\xi\sin\theta) \\
&\quad + (c^2 + d^2)(p_2 + a_p\xi\sin\theta)^2\Big],
\end{aligned}
\tag{3.14}
$$

$$
\begin{aligned}
Q_1^{(\mathrm{reg})} &= R_1(a_j\tau - p_1 - a_p\xi\cos\theta)^3 + (p_2 + a_p\xi\sin\theta) \\
&\quad \times \Big[R_2(a_j\tau - p_1 - a_p\xi\cos\theta)^2 + (p_2 + a_p\xi\sin\theta)R_3(a_j\tau - p_1 - a_p\xi\cos\theta) \\
&\quad + (p_2 + a_p\xi\sin\theta)^2 R_4\Big],
\end{aligned}
\tag{3.15}
$$

$$
\begin{aligned}
Q_2^{(\mathrm{reg})} &= \Big\{(a_j\tau - p_1 - a_p\xi\cos\theta)^3 R_6 + (p_2 + a_p\xi\sin\theta) \\
&\quad \times \Big[R_7(a_j\tau - p_1 - a_p\xi\cos\theta)^2 - (p_2 + a_p\xi\sin\theta)R_8(a_j\tau - p_1 - a_p\xi\cos\theta) \\
&\quad + (p_2 + a_p\xi\sin\theta)^2 R_9\Big]\Big\} R_5,
\end{aligned}
\tag{3.16}
$$

$$
\begin{aligned}
Q_3^{(\mathrm{reg})} &= R_{10}(a_j\tau - p_1 - a_p\xi\cos\theta)^3 + (p_2 + a_p\xi\sin\theta) \\
&\quad \times \Big[-(a_j\tau - p_1 - a_p\xi\cos\theta)^2 R_{11} + (p_2 + a_p\xi\sin\theta)(a_j\tau - p_1 - a_p\xi\cos\theta)R_{12} \\
&\quad + (p_2 + a_p\xi\sin\theta)^2 R_9\Big],
\end{aligned}
\tag{3.17}
$$

$$(3.18)\quad Q_4^{(\mathrm{reg})} = \Big\{(a_j\tau - p_1 - a_p\xi\cos\theta)^3 R_{14} + (p_2 + a_p\xi\sin\theta) \times \Big[R_{15}(a_j\tau - p_1 - a_p\xi\cos\theta)^2 + (p_2 + a_p\xi\sin\theta)(a_j\tau - p_1 - a_p\xi\cos\theta)R_{16} + (p_2 + a_p\xi\sin\theta)^2 R_{17}\Big]\Big\} R_5,$$

$$(3.19)\quad Q_5^{(\mathrm{reg})} = R_{18}(a_j\tau - p_1 - a_p\xi\cos\theta)^3 + (p_2 + a_p\xi\sin\theta) \times \Big[R_{19}(a_j\tau - p_1 - a_p\xi\cos\theta)^2 - (p_2 + a_p\xi\sin\theta)(a_j\tau - p_1 - a_p\xi\cos\theta)R_{20} + (p_2 + a_p\xi\sin\theta)^2 R_9\Big],$$

$$(3.20)\quad Q_6^{(\mathrm{reg})} = \Big\{(a_j\tau - p_1 - a_p\xi\cos\theta)^3 R_{21} + (p_2 + a_p\xi\sin\theta) \times \Big[R_{22}(a_j\tau - p_1 - a_p\xi\cos\theta)^2 + (p_2 + a_p\xi\sin\theta)(a_j\tau - p_1 - a_p\xi\cos\theta)R_{23} + (p_2 + a_p\xi\sin\theta)^2 R_{13}\Big]\Big\} R_5.$$

So the regular normalized component of the shear stress becomes:

$$(3.21)\quad \sigma'^{j}_{x_p y_p} = \int_{-1}^{1} \mathrm{ker}_1 f_{j1}(t_j)\,d\tau_j + \int_{-1}^{1} \mathrm{ker}_2 f_{j2}(t_j)\,d\tau_j,$$

where

$$(3.22)\quad \mathrm{ker}_1 = \frac{a_j}{2\pi}\frac{1}{b_{11}Q_0^{(\mathrm{reg})}}\Big[-\Big(Q_1^{(\mathrm{reg})} - Q_3^{(\mathrm{reg})}\Big)\sin\theta\cos\theta + Q_5^{(\mathrm{reg})}\Big(\cos^2\theta - \sin^2\theta\Big)\Big],$$

$$(3.23)\quad \mathrm{ker}_2 = \frac{a_j}{2\pi}\frac{1}{b_{22}Q_0^{(\mathrm{reg})}}\Big[-\Big(Q_2^{(\mathrm{reg})} - Q_4^{(\mathrm{reg})}\Big)\sin\theta\cos\theta + Q_6^{(\mathrm{reg})}\Big(\cos^2\theta - \sin^2\theta\Big)\Big].$$

The regular normalized normal stress component is:

$$(3.24)\quad \sigma'^{j}_{y_p y_p} = \int_{-1}^{1} \mathrm{ker}_3 f_{j1}(t_j)\,d\tau_j + \int_{-1}^{1} \mathrm{ker}_4 f_{j2}(t_j)\,d\tau_j,$$

where

$$(3.25)\quad \mathrm{ker}_3 = \frac{a_j}{2\pi}\frac{1}{b_{11}Q_0^{(\mathrm{reg})}}\Big[Q_1^{(\mathrm{reg})}\sin^2\theta + Q_3^{(\mathrm{reg})}\cos^2\theta - 2Q_5^{(\mathrm{reg})}\sin\theta\cos\theta\Big],$$

$$(3.26)\quad \mathrm{ker}_4 = \frac{a_j}{2\pi}\frac{1}{b_{22}Q_0^{(\mathrm{reg})}}\Big[Q_2^{(\mathrm{reg})}\sin^2\theta + Q_4^{(\mathrm{reg})}\cos^2\theta - 2Q_6^{(\mathrm{reg})}\sin\theta\cos\theta\Big].$$

The total stresses ($\sigma^T_{yy}$ and $\sigma^T_{xy}$) for $n$ cracks can be written in the following form:

$$(3.27)\qquad {}_n\sigma^T_{xy} = \left\{ \int_{-1}^{1} \ker_1 f_{11}\, d\tau + \int_{-1}^{1} \ker_2 f_{12}\, d\tau + \ldots + \int_{-1}^{1} \ker_1 f_{(n-1)1}\, d\tau \right.$$
$$\left. + \int_{-1}^{1} \ker_2 f_{(n-1)2}\, d\tau + \frac{E^{(1)}_{xy}}{\pi} \int_{-1}^{1} \frac{f_{n1}}{\tau - \xi} d\tau + \frac{E^{(2)}_{xy}}{\pi} \int_{-1}^{1} \frac{f_{n2}}{\tau - \xi} d\tau \right\},$$

$$(3.28)\qquad {}_n\sigma^T_{yy} = \left\{ \int_{-1}^{1} \ker_3 f_{11}\, d\tau + \int_{-1}^{1} \ker_4 f_{12}\, d\tau + \ldots + \int_{-1}^{1} \ker_3 f_{(n-1)1}\, d\tau \right.$$
$$\left. + \int_{-1}^{1} \ker_4 f_{(n-1)2}\, d\tau + \frac{E^{(1)}_{yy}}{\pi} \int_{-1}^{1} \frac{f_{n1}}{\tau - \xi} d\tau + \frac{E^{(2)}_{yy}}{\pi} \int_{-1}^{1} \frac{f_{n2}}{\tau - \xi} d\tau \right\}.$$

The formulation of this system of singular integral equations is complete once the single-valued conditions for the auxiliary functions, $f_{j\eta}$, are chosen. In the case of straight cracks, this single-valuedness condition [8] is:

$$(3.29)\qquad \int_{-1}^{1} f_{j\eta}(\tau)\, d\tau = 0,$$

where $j$ stands for the $j$-th crack and $\eta$ takes on the value of 1 or 2.

## 4. Solution for the stress intensity factors

The integral equations obtained are of the Cauchy type; thus, for sharp cracks the stresses and strains will have a square-root singularity and the classical definition of SIF may be used (see [1, 4, 5, 6]). Therefore, the Modes I and II SIF for the $j$-th crack are

$$(4.1)\qquad k^j_1(1) = \lim_{\xi \to 1} [2(\xi - 1)]^{1/2} \left\{ {}_j\sigma^T_{yy}(\xi, 0) \right\},$$

$$(4.2)\qquad k^j_2(1) = \lim_{\xi \to 1} [2(\xi - 1)]^{1/2} \left\{ {}_j\sigma^T_{xy}(\xi, 0) \right\},$$

$$(4.3)\qquad k^j_1(-1) = \lim_{\xi \to -1} [-2(1 + \xi)]^{1/2} \left\{ {}_j\sigma^T_{yy}(\xi, 0) \right\},$$

$$(4.4)\qquad k^j_2(-1) = \lim_{\xi \to -1} [-2(1 + \xi)]^{1/2} \left\{ {}_j\sigma^T_{xy}(\xi, 0) \right\},$$

where the normal and shear stresses, Eqs. (3.27) and (3.28), are used.

It is well known [8] that the auxiliary functions ($f$) can be expressed as a product of the unknown bounded functions ($H$) and the known singular weight functions $w$:

$$f(\tau) = H(\tau)w(\tau). \tag{4.5}$$

The singular weight function $w$ for a sharp crack is

$$w(\tau) = \left(\tau^2 - 1\right)^{-1/2}. \tag{4.6}$$

ERDOGAN [8] found, for example, that in the case of a Cauchy-type singular integral equations, Eqs. (3.27) and (3.28), the dominant part can be expressed in terms of the function $H$ evaluated at the tips of the $j$-th crack:

$$\frac{1}{\pi}\int_{-1}^{1}\frac{f_{\eta j}\,d\tau}{\tau-\xi} = H_{\eta j}(-1)\frac{e^{i\pi/2}}{\sqrt{2}}(\tau+1)^{-1/2} - H_{\eta j}(1)\frac{1}{\sqrt{2}}(\tau-1)^{-1/2} + O(\tau), \tag{4.7}$$

where $\eta$ is 1 or 2 and $O(\tau)$ is the higher order term, which in subsequent calculations is neglected. The substitution of Eqs. (4.7) for the dominant parts (the last term in Eqs. (3.27) and (3.28)) of the normal and shear components of the total stresses in Eqs. (4.1)–(4.4), and subsequent evaluation of the limits at the crack tips, results in redefining the SIF (normalized with respect to $\sqrt{a_1}$ and $\sigma^{\circ}_{jp}$), expressed in terms of the functions $H_{\eta j}$:

$$k_1^j(1) = \left(E_{yy}^{j(1)}H_{1j}(1) + E_{yy}^{j(2)}H_{2j}(1)\right)\sqrt{a_j/a_1}, \tag{4.8}$$

$$k_2^j(1) = \left(E_{xy}^{j(1)}H_{1j}(1) + E_{xy}^{j(2)}H_{2j}(1)\right)\sqrt{a_j/a_1}, \tag{4.9}$$

$$k_1^j(-1) = \left(E_{yy}^{j(1)}H_{1j}(-1) + E_{yy}^{j(2)}H_{2j}(-1)\right)\sqrt{a_j/a_1}, \tag{4.10}$$

$$k_2^j(-1) = \left(E_{xy}^{j(1)}H_{1j}(-1) + E_{xy}^{j(2)}H_{2j}(-1)\right)\sqrt{a_j/a_1}. \tag{4.11}$$

The Lobatto–Chebyshev collocation integration technique is known to provide excellent results when dealing with Cauchy-type singular integral equations, and so it was used. The unknown function $H_{\eta j}$ is determined at a discrete set of points $\tau_1, \tau_2, \ldots, \tau_m$ called abscissas. In this way, each integral equation is reduced to a set of algebraic equations with unknowns $H_{\eta j}(\tau_1)$, $H_{\eta j}(\tau_2)$, ..., $H_{\eta j}(\tau_m)$, which are the discrete values of the functions $H_{\eta i}$; hence its name, a discrete auxiliary function. It should be noted, that $H_{1j}$ and $H_{2j}$ are proportional, respectively, to shear and normal difference of displacement at the crack tips,

$$\Delta u \sim H_1, \qquad \Delta v \sim H_2. \tag{4.12}$$

Consequently, the $H_{\eta j}$ can be used as a measure of the crack opening displacement rate at the crack tip.

Each of the singular integral equations subjected to the stress boundary conditions (Eqs.(2.5)), is replaced by $m-1$ algebraic equations with $2nm$ unknown parameters (see [2]). In the Lobatto-Chebyshev method, the abscissas are calculated according to

$$\tau_r = \cos\frac{(r-1)\pi}{m-1} \qquad \text{for} \qquad r = 1, \ldots, m, \tag{4.13}$$

with the corresponding weights given by

$$w_1 = w_m = \frac{\pi}{2(m-1)} \qquad \text{and} \qquad w_r = \frac{\pi}{m-1} \quad \text{for } r = 2, 3, \ldots, m-1; \tag{4.14}$$

the collocation points are then found by using the formula

$$\xi_z = \cos\frac{(2z-1)\pi}{2m-2} \qquad \text{for} \quad z = 1, 2, \ldots, m-1. \tag{4.15}$$

In order to have the complete system of $2nm$ algebraic equations, the single-valuedness conditions Eqs. (3.29) are also expressed by using the collocation technique:

$$\sum_{r=1}^{m} H_{\eta j}(\tau_r) w_r = 0. \tag{4.16}$$

Thus, the resulting system of algebraic equations can be written in the form

$$[A]\{H\} = \{\mathcal{R}\}, \tag{4.17}$$

where $[A]$ is a fully populated $2nm \times 2nm$ matrix of coefficients, and $\{\mathcal{R}\}$ is the loading function vector.

The unknown parameter vector $\{H\}$ can be determined through inversion of the $[A]$ matrix; thus,

$$\{H\} = [A]^{-1}\{\mathcal{R}\}, \tag{4.18}$$

although only the appropriate values (i.e., $H_{\eta j}(\pm 1)$) are used to calculate the SIF for the $j$-th crack (see Eqs. (4.8)-(4.11)).

Automatic generation of the associated FORTRAN code for the evaluation of Eq. (4.18) completes the development of the solution for any multi-crack problem. This FORTRAN program was utilized to obtain the following results, which are compared with results obtained by other methods existing in the literature.

## 5. Strain energy release rate

From the fracture point of view, perhaps the most important physical quantity is the Strain Energy Release Rate (SERR), usually denoted by a symbol $G$. CHEREPANOV in [3] discussed the generalized formula for SERR for anisotropic material.

$$G = \frac{1}{2}\int_{a}^{a+da} \{\sigma_{yy}(x,0)[v(x-da,0^+) - v(x-da,0^-)] + \sigma_{xy}(x,0)[u(x-da,0^+) - u(x-da,0^-)]\}\, dx. \tag{5.1}$$

Using the roots of the characteristic equation in terms of the real components (11), it can be shown that:

$$G = \frac{\pi}{2}\left[k_1^2 \frac{(a+c)(ac-bd)+(b+d)(ad+bc)}{(ac-bd)^2+(ad+bc)^2} b_{22} + k_2^2(a+c)b_{11}\right]. \tag{5.2}$$

In the case of isotropic material one may substitute $a = c = 1$, $b = d = 0$ and $b_{11} = b_{22} = \frac{1}{E}$ into (5.2). Consequently, well known fracture mechanics relationship is recovered.

$$G^{(\mathrm{iso})} = \frac{\pi}{E}\left[k_1^2 + k_2^2\right]. \tag{5.3}$$

## 6. Numerical applications

### (i) Two crack interaction

In order to validate the results obtained using the code, the well-known problem of two parallel interacting cracks is considered here. The plate with cracks of length $2a$ and the fiber direction $\Omega = 22°$, is subjected to a normal stress field $(\sigma_{YY}^{\infty})$ as shown in the inserts of Fig. 3. In this figure, SIF does not depend on the rate of anisotropy ratio $E_{LL}/E_{TT}$. Mode-I SIF are exactly the same as the SIF from [9] and [7] at both the inner and outer crack tips, and Mode-II SIF are zero for this configuration.

The shear crack opening as represented by $H_1$ (see (4.12)) is only zero for the ratio of anisotropy $E_{LL}/E_{TT} = 1$ (i.e. isotropic case). Even small anisotropy $E_{LL}/E_{TT} > 1$ produces the shear displacement. This increase is very significant only for $1 < E_{LL}/E_{TT} < 5$ and it becomes constant for $E_{LL}/E_{TT} > 15$. One may say that the two collinear cracks configuration always produces Mode-I crack tip local stress field and Mixed-mode local displacement.

Figure 4 shows the variation of MSP with respect to ratio of anisotropy. One may find the isotropic values of MSP as given in (3.8) for $E_{LL}/E_{TT} = 1$. It also

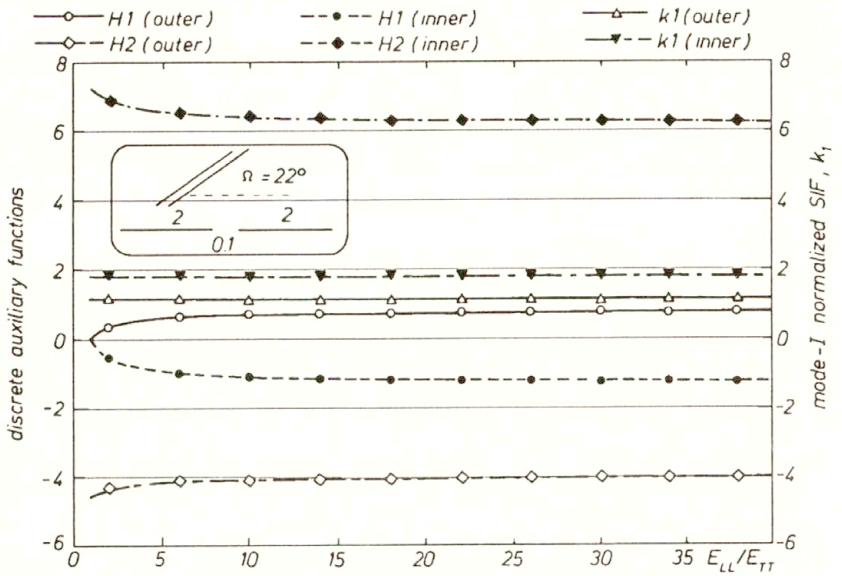


FIG. 3. Discrete auxiliary functions and SIF for two collinear cracks versus rate of anisotropy change.

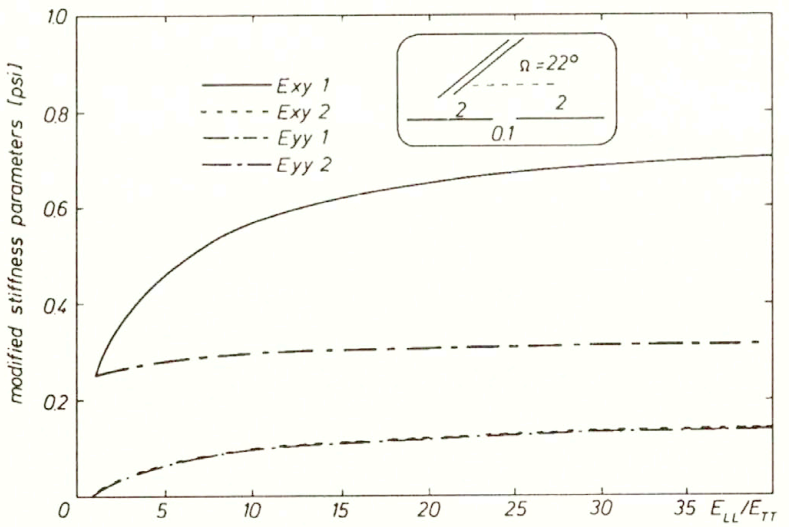


FIG. 4. Modified stiffness parameters for two collinear cracks versus rate of anisotropy change.

may be noted that the rise of anisotropy ratio significantly increases $E_{xy}^{(1)}$, $E_{xy}^{(2)}$ and $E_{yy}^{(1)}$, while $E_{yy}^{(2)}$ is almost constant and that $E_{xy}^{(2)} = E_{yy}^{(1)}$ for all range of $E_{LL}/E_{TT}$.

From the fracture mechanics point of view, cracks propagate driven by the total SERR, shown for the collinear cracks configuration in Fig. 5. Clearly, the maximum SERR occur for the isotropic case, for both the inner and outer crack tips. For anisotropic cases, they are rapidly reduced to almost 50% of the isotropic case within the range $1 < E_{LL}/E_{TT} < 15$, and finally they reach a plateau for $E_{LL}/E_{TT} > 15$.

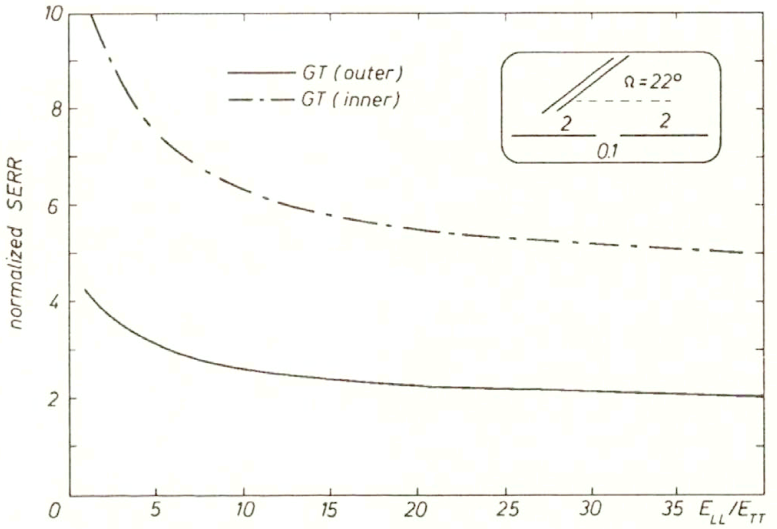


FIG. 5. Total SERR for two collinear cracks versus rate of anisotropy change.

Let us consider now an anisotropic material having ratio $E_{LL}/E_{TT} = 40$ for the same collinear crack configuration, and change the fiber angle $\Omega$. It is shown in Fig. 6 that SIF are still unchanged having only nonzero components. Discrete auxiliary functions show that the crack shear opening displacements are zero only for the orthotopic cases, i.e., $\Omega = 0°, 90°$. Otherwise both openings are not zero. The local shear opening displacements maxima are at $\Omega = 22°$ and 68°, while the local nonzero minimum for the shear opening displacement is at $\Omega = 45°$. The normal opening displacements are the largest at $\Omega = 30°$ but almost the same as for $0 < \Omega < 40$, and are significantly reduced for the remaining range, to reach the value equivalent to 30% of the maximum normal opening.

In Figure 7 the variation of the MSP are shown as a function of the fiber orientation $\Omega$. It may be noticed that the curve representing $E_{xy}^{(1)}$ is symmetrical, with respect to the line $\Omega = 45°$, to the curve representing $E_{yy}^{(2)}$. The remaining MSP are again equal to each other and zero for orthotopic cases. Consequently, $E_{xy}^{(1)}$ and $E_{yy}^{(2)}$ must be related to $b_{16}$ and $b_{26}$ (see Eq. (2.9)).

Since

$$E_{xy}^{(2)} = E_{yy}^{(1)} \tag{6.1}$$

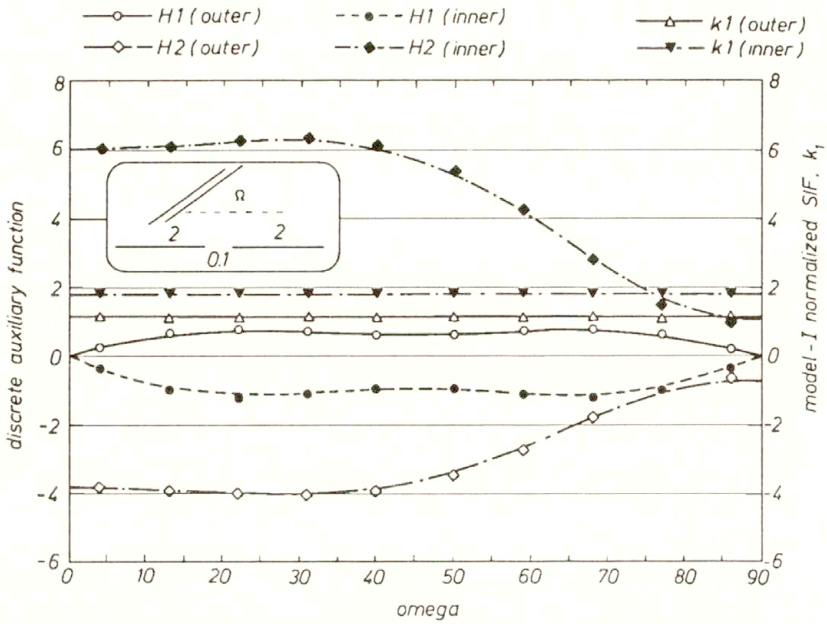


FIG. 6. Discrete auxiliary function and SIF for two collinear cracks versus fiber angle for the ratio of anisotropy = 40.

we can substitute (3.5) and (3.6) into the (6.1) and solve for $b_{22}$ to get:

$$b_{22} = b_{11}\left(a^2 + b^2\right)\left(c^2 + d^2\right), \tag{6.2}$$

or in terms of the roots of the characteristic equation one may show that

$$r_1 r_2 r_3 r_4 = \frac{b_{22}}{b_{11}}. \tag{6.3}$$

In case of the orthotopic material $b = d = 0$, and (6.3) reduces to well-known mathematical relation in the following form:

$$a^2 c^2 = \frac{E_{LL}}{E_{TT}}. \tag{6.4}$$

Upon substitution (6.2) into (3.7) and using the Eq. (3.4), we can find that

$$E_{xy}^{(1)} = E_{yy}^{(2)} \frac{c(a^2 + b^2) + a(c^2 + d^2)}{(a + c)}. \tag{6.5}$$

Equation (6.5) can be reduced to orthotopic case for $b = d = 0$. Further, using (6.4) together with the orthotopic form of (6.5), it may be shown that:

$$\left[\frac{E_{xy}^{(1)}}{E_{yy}^{(2)}}\right]_{b=d=0} = ac = \sqrt{\frac{E_{LL}}{E_{TT}}}. \tag{6.6}$$

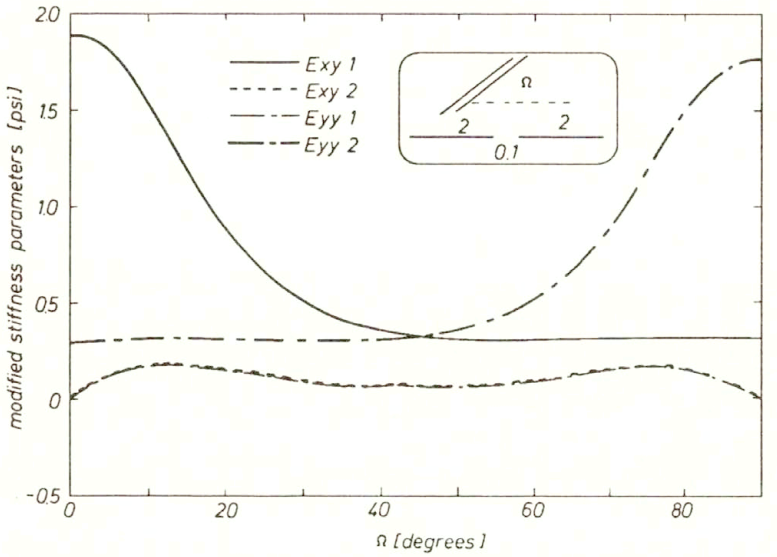


FIG. 7. Modified stiffness parameters for two collinear cracks versus fiber angle for the ratio of anisotropy = 40.

Finally, using the Eq. (6.6) and the observation of Fig. 7, we may conclude that for the general anisotropic case $E_{xy}^{(1)}$ is proportional to the square root of the effective Young's modulus in the local $x$-direction, and $E_{yy}^{(2)}$ is proportional to the square root of the effective Young's modulus in the local $y$-direction.

Total SERR in terms of the fiber angle $\Omega$ is shown in Fig. 8. SERR are maximum at $\Omega = 0°$, and minimum at $\Omega = 90°$ for both the inner and outer crack tips. The other two important angles are $\Omega = 12°$, where the SERR arrive at their local minimum, and $\Omega = 42°$, where the SERR reach their local maximum.

Figure 9 shows the variation of the SIF and opening of displacements for two cracks that are not collinear. The convenient parameter that can be controlled is the angle between the horizontal axis and the line connecting inner crack tips, i.e., the angle $\alpha$, (see insert in Fig. 9). When $\alpha = 0°$, the previous case of collinear cracks is obtained. The constant parameters are: the distance between inner crack tips, $0.1 \cdot a_1$, the ratio of anisotropy $E_{LL}/E_{TT} = 40$, and the fiber angle $\Omega = 45°$. As a result of the change of the crack configuration, SIF are not constant anymore for the inner crack tips. Mode-II SIF is zero only for $\alpha = 0°$ and 90°, and it becomes maximum at $\alpha = \Omega = 45°$. Mode-I of SIF monotonically increases with the angle $\alpha$ for the inner crack tip. SIF for the outer crack tips are not significantly influenced and they are the same as the collinear crack configuration.

It is also interesting to analyze the Discrete Auxiliary Functions, $H_1$ and $H_2$. The shear term of the inner crack tip is zero only for $\alpha = 40°$, and it is larger for the case of $\alpha = 90°$ than for the collinear crack configuration. Normal crack

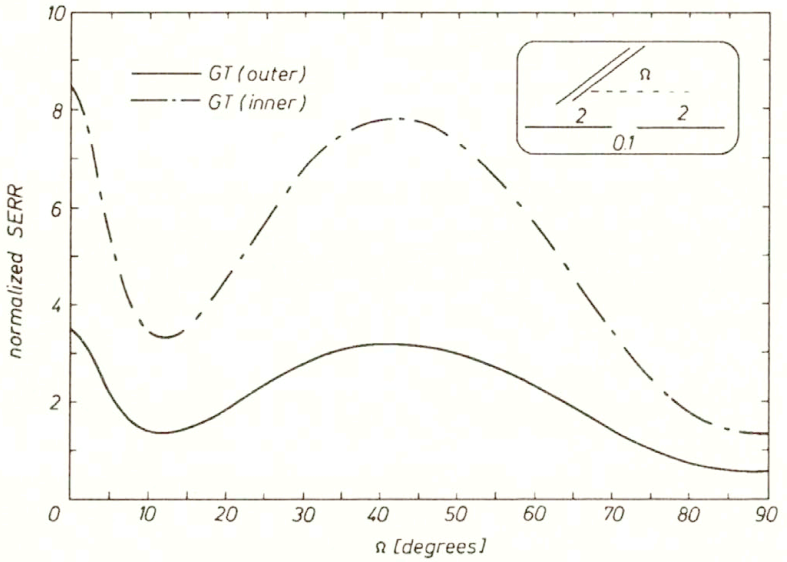


FIG. 8. Total SERR for two collinear cracks versus fiber angle for the ratio of anisotropy = 40.

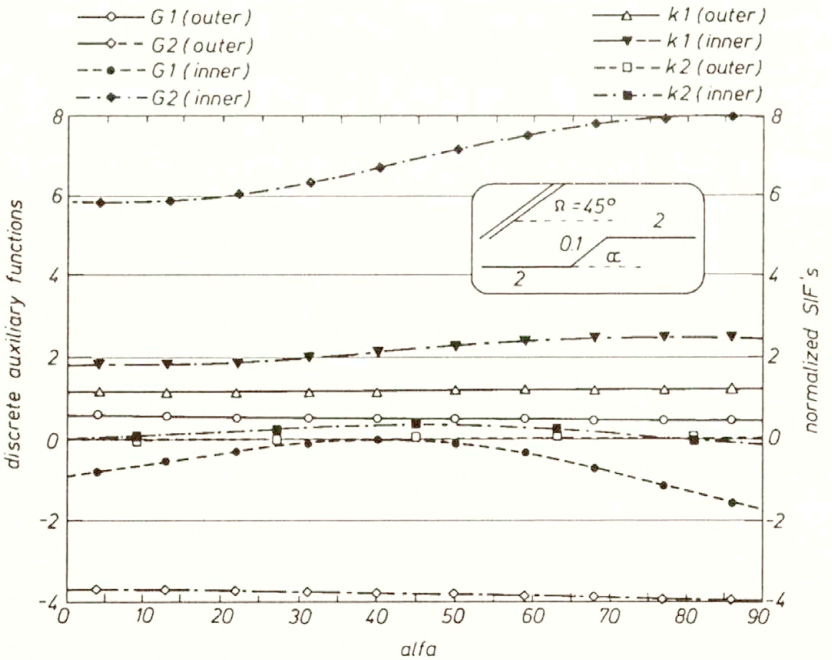


FIG. 9. Discrete auxiliary functions and SIF for two parallel cracks versus crack tip angle alfa. Fiber angle is 45 degrees and ratio of anisotropy is 40.

opening displacements are the largest also for $\alpha = 90°$. Since change of the angle $\alpha$ does not change the material properties in the local coordinate system, therefore MPD can be found in Fig. 7 for the fiber orientation $\Omega = 45°$.

The combined effect of the SIF and local displacement is captured by SERR, shown in the Fig. 10. The shape of the $G_T$ resembles in parts the shapes of $k_1$ and $H_2$, for the inner crack tips. The maximum of SERR is, however, reached for $\alpha = 70°$, at the inner crack tips. The outer crack tip SERR is slightly affected by change of the angle $\alpha$, and reaches its maximum for $\alpha = 90°$.

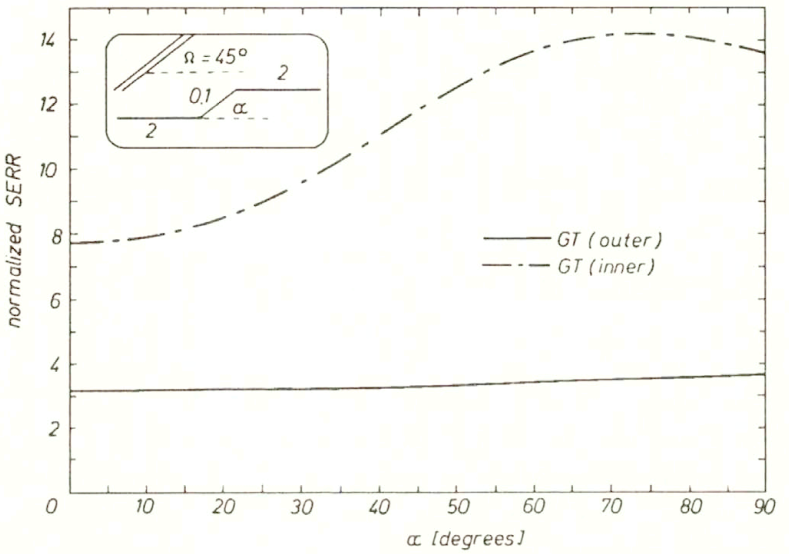


FIG. 10. Total SERR for two parallel cracks versus crack tip angle. Fiber angle is 45 degrees and ratio of anisotropy is 40.

**(ii) Three crack interaction**

Consider anisotropic plate with ratio of anisotropy $E_{LL}/E_{TT} = 40$ and three parallel cracks, as shown in the insert of Fig. 11. Two cracks on the right are always symmetric to each other with respect to the horizontal line, that coincides with the crack $ab$. The distance between the inner crack tips $bc$ and $be$ are always identical and for the first study it is kept constant $bc = be = 0.1a_1$. As a parameter for the first study, consider the change of the fiber angle $\Omega$. Mode-I SIF for the tips $b$, $c$ and $e$ are shown in Fig. 11. As one may note, $k_1(b)$ curve resembles inverted parabola with the maximum for $\Omega = 45°$. SIF at the tip $b$ is the largest for the whole range of $\Omega$, because of the magnification influence of the remaining two crack that are situated in front of the crack $ab$. The SIF for the cracks $cd$ and $ef$ are smaller because of the shielding effect of the cracks above or below. SIF at the tips $c$ and $e$ are identical within the first part of the range of the fiber angle, i.e., $0 < \Omega < 25$, while they start to differ from each other in a symmetrical manner within the remaining part of the range of the fiber angle.

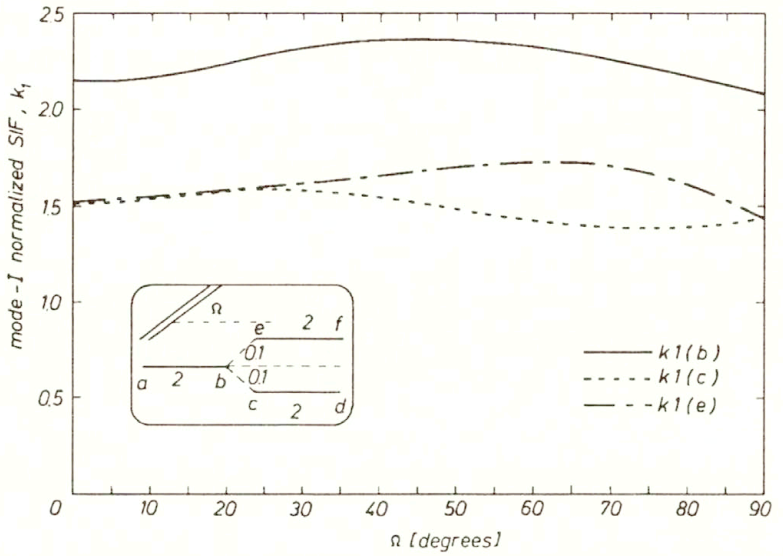


FIG. 11. Mode-I normalized SIF for the three parallel cracks versus fiber angle for ratio of anisotropy 40.

Evidently, the singular stresses are stronger transmitted along the fibers than in any other direction, because $k_1(e)$ is larger than $k_1(c)$.

Mode-II of SIF are shown in Fig. 12. Here, the absolute value of $k_2(b)$ is always close to zero and exactly zero for the orthotopic conditions, i.e., $\Omega = 0$, 90 degrees. The absolute value of Mode-II SIF at tip $e$ is the largest with the local

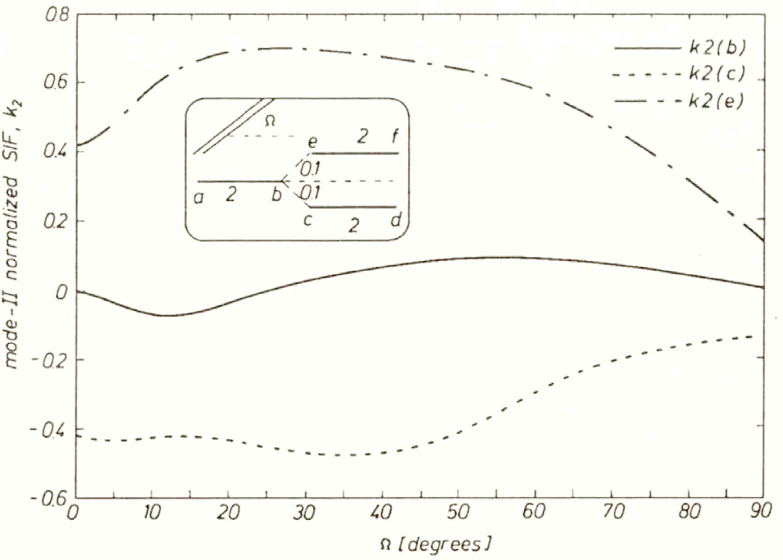


FIG. 12. Mode-II normalized SIF for the three parallel cracks versus fiber angle for ratio of anisotropy 40.

maximum for $\Omega = 25°$, because of the directional stress tunneling effect. It is also interesting to note, that the absolute values if $k_2$ are identical for crack tips $c$ and $e$ under orthotopic conditions, but the values for $\Omega = 0$ are more than twice as large as for $\Omega = 90$.

We can also analyze the crack opening displacements at the inner crack tips using Fig. 13. It may be noted that shear opening displacement is zero for crack tip $b$ and very close to zero for crack tips $c$ and $e$. The only other case of zero $\Delta u$ is for the crack tip $e$ at $\Omega = 22°$. All crack opening displacements reach their local maxima within the middle range of the fiber angle. Normal opening displacements are almost constant for the $0° < \Omega < 45°$, and they become much smaller for $45° < \Omega < 90°$.

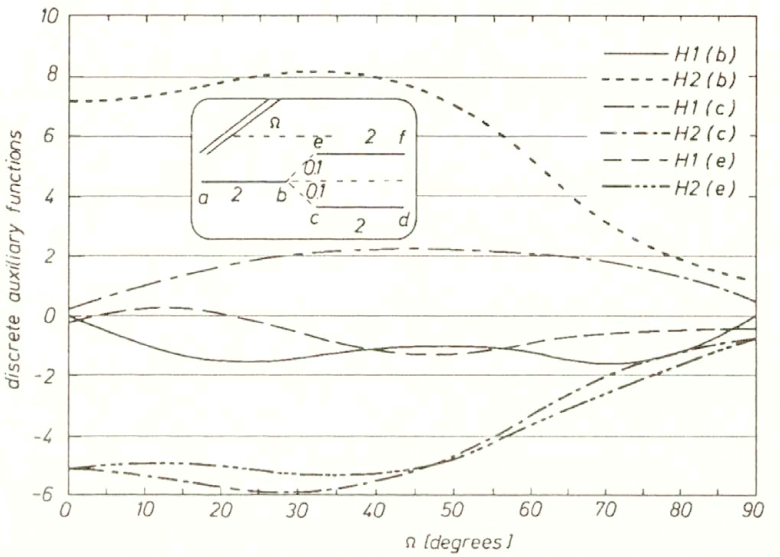


FIG. 13. Discrete auxiliary functions for the three parallel cracks versus fiber angle for ratio of anisotropy 40.

Variation of the SERR for this study is shown in Fig. 14. SERR combines all the above characteristics for each crack tip in one convenient parameter, that shows strong dependence on the fiber angle $\Omega$. Local maxima for each curve are located at $\Omega \approx 45°$ where SERR for crack tip $b$ is the largest and followed by the maximum for SERR of the crack tip $e$. It may be concluded that the easiest crack propagation can take place for the fiber angle $\Omega = 45°$, for which fibers connect crack tips $b$ and $e$. Henceforth, as a result of a physical crack propagation, one may anticipate the connection between crack $ab$ and $ef$ and, consequently, the zigzag crack development.

In Figure 15 the variations of the SERR are shown for the case of $\Omega = 45°$, when the middle left crack slides between two parallel cracks. When the parameters DIST are zero, tip $b$ is on the same vertical line which connects

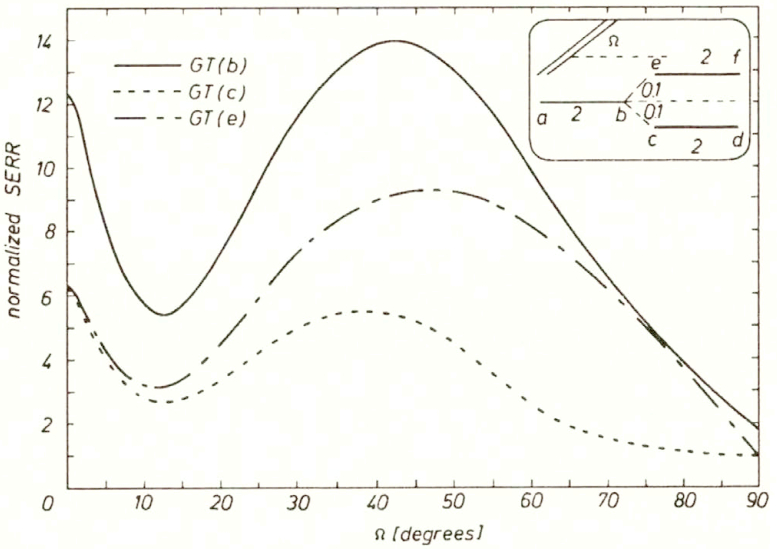


FIG. 14. Total SERR for the three parallel cracks versus fiber angle for ratio of anisotropy 40.

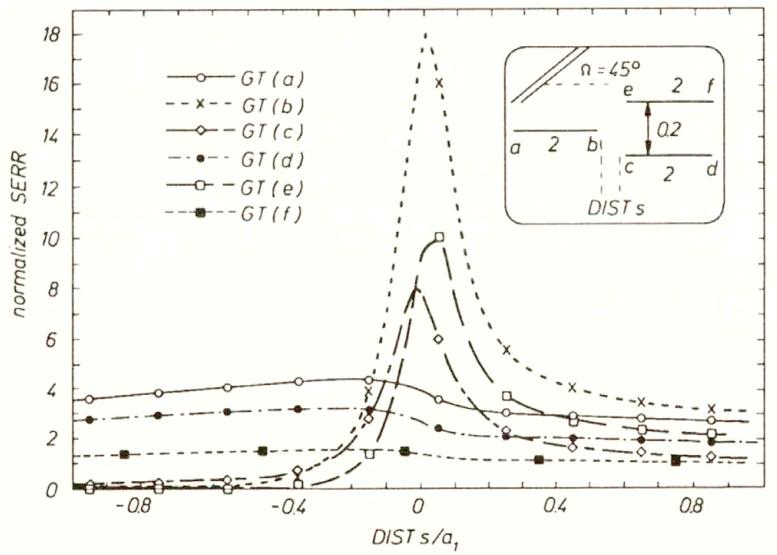


FIG. 15. Total SERR for the three parallel cracks versus crack shift distance DIST for ratio of anisotropy 40 and fiber angle 45 degrees.

tips $c$ and $e$. When the crack $ab$ is away from the parallel cracks, the parameter DIST $> 0$, and when tip $b$ is between cracks $cd$ and $ef$, the parameter DIST $< 0$. It can be noticed, that the magnifying trend for SERR takes place, when crack tip $b$ come closer to the vertical line connecting tips $c$ and $e$. When DIST becomes negative, all inner tips become strongly shielded, so that SERR sharply drops to almost zero.

**(iii) Horizontal notch interaction with three microcracks**

Consider now the plate with ratio of anisotropy $E_{LL}/E_{TT} = 40$, that contains large horizontal notch of the length $2a_1$ and three radially oriented microcracks of the length $a_2 = a_3 = a_4 = 0.1a_1$, as shown in the insert of the Fig. 16. Let us constrain the fiber angle to be $\Omega = 15°$, and vary the inner tip distance between the notch tip $b$ and the microcracks tips $c$, $e$ and $g$. Figure 16 shows the amplifying effect of the cloud of microcracks interaction, that becomes noticeable for the tip distance less than $0.1a_1$. The SERR is the largest for the notch tip $b$ until the tip distance is about $0.04a_1$, when SERR for the microcrack inclined at 45° drastically increase exceeding all other curves.

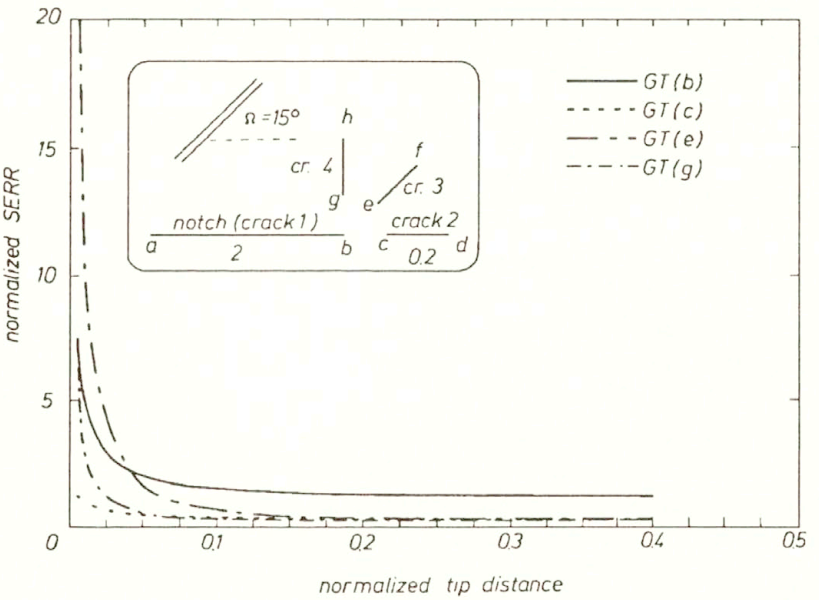


FIG. 16. Total SERR for the horizontal notch and three microcracks versus the normalized crack tip distance for the fiber angle = 15 degrees and for the ratio of anisotropy 40.

Finally, the rate of anisotropy can be studied, as shown in the Fig. 17. It is assumed that the fiber angle and tip distance are constant, i.e., $\Omega = 15°$, and the tip distance $0.005a_1$, while the rate of anisotropy $E_{LL}/E_{TT}$ is changed. When the material is isotropic, i.e., $E_{LL}/E_{TT} = 1$, the SERR at the notch tip $b$ is much larger than for the remaining microcrack inner tips. Even small change of the anisotropy rate significantly influences the value of SERR for all the cracks. When $E_{LL}/E_{TT} > 18$, the SERR for the inclined microcrack tip becomes the largest. Since the crack having the highest SERR propagates first, the kink crack will be generated after 45 degrees crack connects with the notch.

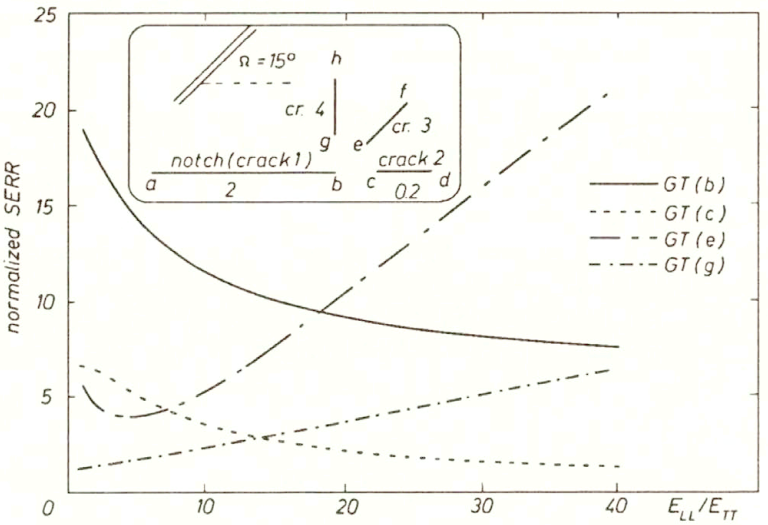


FIG. 17. Total SERR for the horizontal notch and three microcracks versus the ratio of anisotropy for the fiber angle = 15 degrees.

## 7. Concluding remarks

A rigorous formulation has been presented and validated for calculating the SIF and SERR of a multi-cracked anisotropic medium. The size, orientation, and distribution of all cracks were considered to be independent parameters of the solution. With this capability, numerous parametric studies could easily be performed to analyze the contribution of each parameter to the local stress field as well as the characteristics of the damage progression in a material.

The accuracy of the results was examined and parametric studies were conducted. The problem of two interacting cracks for various cases of anisotropy shown that off-axis reinforcement can produce highly mixed-mode crack propagation, even for the Mode-I type of crack geometry. The small change of the ratio of anisotropy, i.e. $0 < E_{LL}/E_{TT} < 5$, can highly influence SERR and the crack opening displacements that reach a plateau for $E_{LL}/E_{TT} > 15$. Therefore, even slightly anisotropic materials should be analyzed using full anisotropic approach.

Variation of MSP has been presented for various ratios of anisotropy and various fiber directions. It was concluded that $E_{xy}^{(1)}$ and $E_{yy}^{(2)}$ are proportional to square roots of the effective Young's modulus in $x$ and $y$-directions, respectively. The other two MSP are identical, i.e., $E_{xy}^{(2)}$ and $E_{yy}^{(1)}$, and related to $b_{16}$ and $b_{26}$, so they vanish for the orthotropic and isotropic cases.

The discrete auxiliary functions were shown to be related to the crack opening displacements $\Delta u$ and $\Delta v$. It was shown, that there are cases, found for the off-axis fiber orientation, when Mode-I local stress field is produced by Mixed-Mode local deformations, and Mode-I normal deformation produces Mixed-Mode local stress field.

Total SERR was shown to be the most complete fracture parameter, that can be used for crack propagation and crack path predictions. The interaction effects were demonstrated for all fracture parameters. The amplification of SERR and/or SIF takes place when cracks are located in front of the main crack, and reduction of SERR or SIF takes place upon shielding of crack by other cracks located above and/or below.

The stress tunneling effect was discovered to play a significant role in the crack interaction mechanisms. Stresses are channeled along the fiber direction, and may cause non-symmetric interaction even for symmetric crack configuration. The model was shown to be capable of solving various crack problems with high computational speed and accuracy.

## References


1. R. BADALIANCE and G.G. GUPTA, *Growth characteristics of two interacting cracks*, Eng. Fract. Mech., **8**, 2, pp. 341–353, 1976.
2. W.K. BINIENDA, S.M. ARNOLD, H.Q. TAN and M.H. XU, *Stress intensity factors in a fully interacting, multi-cracked, isotropic plate*, Comp. Mech., **12**, 5, pp. 297–314, 1993.
3. G.P. CHEREPANOV, *Mechanics of brittle fracture*, McGraw-Hill, N.Y. 1979.
4. F. DELALE and F. ERDOGAN, *The problem of internal and edge cracks in an orthotropic strip*, J. Appl. Mech., **44**, 6, pp. 237–242, 1977.
5. F. DELALE and F. ERDOGAN, *Bonded orthotropic strips with cracks*, Int. J. Fract., **15**, 8, pp. 343–364, 1979.
6. F. DELALE, I. BAKIRTAS and F. ERDOGAN, *The problem of an inclined crack in an orthotropic strip*, J. Appl. Mech., **46**, 3, pp. 90–96, 1979.
7. F. ERDOGAN, *On the stress distribution in plates with collinear cuts under arbitrary loads*, Proc. Fourth U.S. National Congress of Applied Mechanics, Vol 1, ASME, New York, pp. 547–553, 1962.
8. F. ERDOGAN, *Mixed boundary-value problems in mechanics*, Mechanics Today, S. NEMAT-NASSER [Ed.], Vol. 4, Pergamon Press, New York, pp. 1–32, 1978.
9. H. HORII and S. NEMAT-NASSER, *Elastic fields of interacting inhomogeneities*, Int. J. Solids Struct., **21**, 7, pp. 731–745, 1985.
10. S. TIMOSHENKO and J.N. GOODIER, *Theory of elasticity*, Third Ed., McGraw-Hill, New York 1969.


DEPARTMENT OF CIVIL ENGINEERING
UNIVERSITY OF AKRON, AKRON, USA.

*Received September* 16, 1994.

Arch. Mech., 47, 1, pp. 69–80, Warszawa 1995

# Reflection of a moving shock wave; boundary conditions for Monte-Carlo and continuum descriptions

K. KANTIEM, A. KOZŁOWSKI
and Z.A. WALENTA (WARSZAWA)

THE PAPER contains the results of the shock tube experiments, Direct Simulation Monte-Carlo calculations, and continuum model calculations based on Navier–Stokes equations for the problem of reflection of a moving shock wave from a wedge. Comparison of these results makes it possible to draw some conclusions concerning the conditions at the reflecting surface.

## 1. Introduction

REFLECTIONS OF shock waves have been investigated by the scientists for more than a hundred years. The first paper on that subject was presented by ERNST MACH in 1878 [1]. Still, not all aspects of the phenomenon seem to be fully understood even now.

There are two basic types of the shock reflection. During the "regular" one the incident and reflected shocks meet at the reflecting surface. During the "irregular" reflection, the shocks meet at some distance above the surface, and from this point the third shock emerges. This shock is commonly called the "Mach stem" and the point where the three shocks meet – the "triple point".

The shock waves are usually produced in supersonic wind tunnels (stationary shocks) and in shock tubes (moving shocks). In the present paper we will deal with reflections of the moving shocks from stationary wedges, placed inside a shock tube.

Very roughly speaking, if the wedge angle is sufficiently large, the moving shock wave reflects from it regularly. For small wedge angles the irregular reflection occurs (Fig. 1a, b).

Irregular reflection of a moving, plane shock wave at a wedge was initially considered to be a self-similar phenomenon. The picture was supposed to be always the same, provided that it was scaled with the distance between the leading edge and the incident shock. The triple point was supposed to move along a straight line, starting at the wedge tip.

The first suggestion on the possible lack of self-similarity in the neighbourhood of the leading edge was given in 1980 by HENDERSON and SIEGENTHALER [2]. It was confirmed later by a number of experimentalists (WALENTA 1980 [3], 1983 [4], SCHMIDT 1985 [5], DEWEY *et al.* 1991 [6]). Presently it seems to have been

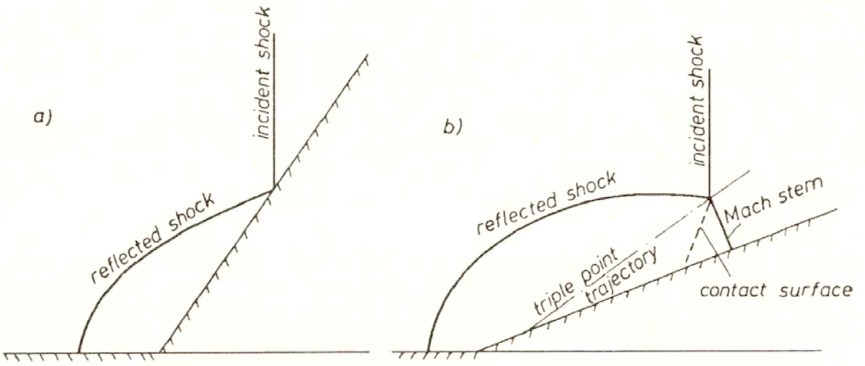


FIG. 1. Reflection of a moving shock wave: a) regular, b) irregular.

established, that the triple point is generated very close to the leading edge, and begins to move along the line nearly parallel to the reflecting surface. This line then gradually steepens, tending asymptotically to a straight line, inclined at a certain angle to the wedge surface [7].

The length of the curved part of the triple point trajectory is of the order of some hundreds mean free paths of the gas particles. It is therefore invisible with the usual optical methods (shadowgraph, schlieren). That was the reason why lack of self-similarity in this area was recognized so late.

In the present study we show some experimentally obtained flow pictures for reflection of the shock wave from a wedge in the area, where the phenomenon is non-self-similar. These pictures are then compared with the computational results obtained by Direct Simulation Monte-Carlo (DSMC) technique and with the use of the Navier–Stokes equations (continuum model calculations). Adjusting conditions at the reflecting wall, we were able to produce flow pictures very close to the experimental ones. This method provided us with some insight into the phenomena occurring at the wall surface.

## 2. Experiment

### 2.1. Experimental setup

The results presented here were obtained in a low-density shock tube (250 mm I. D., 17 meters long) at the Institute of Fundamental Technological Research in Warsaw. The primary shock wave was reflected from a wedge, placed inside the test section of the tube. To maintain the planarity of the flow, the wedge was placed between two plates, extending 75 centimeters upstream of the test section (Fig. 2).

The measurements were performed with the standard, electron beam attenuation technique. The beam was parallel to the wedge surface and perpendicular to the tube axis. Its position with respect to the wedge could be varied. In a single

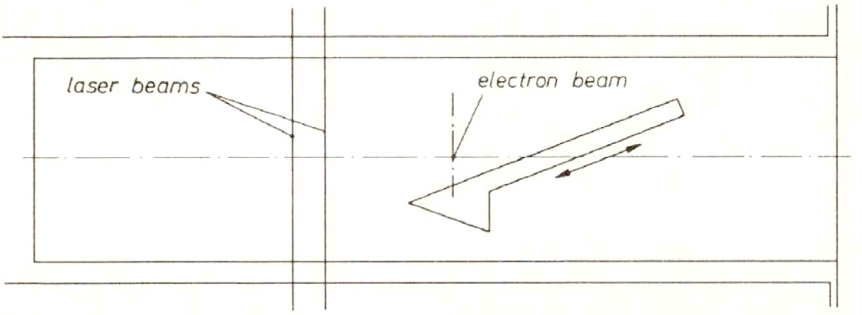


FIG. 2. Test section of the shock tube (with shock reflecting wedge).

run the density history at one point above the wedge was registered. To obtain the picture of the whole density field, a number of runs at the same flow conditions and different positions of the beam had to be done. The reference time instant, necessary for superposition of the results, was obtained in each run from a laser differential interferometer, placed at a fixed position in front of the wedge.

The scatter of the shock speeds, $\pm 2.5$ percent of the mean value, seemed sufficiently small to produce meaningful results with the described method.

### 2.2. Conditions of experiment

Conditions of experiment were chosen to match the specific requirements of the problem:

- The noble gas – Argon – was used for all the tests.
- The shock Mach number Ms was equal to $2.80 \pm 0.08$.
- The initial pressure was equal to 7.33 Pa.
- The initial temperature, equal to the room temperature, was $298 \pm 3$ K.

For such conditions the mean free path of the gas atoms was equal to about 0.95 mm and the maximum slope shock thickness 3.75 mm.

The wedges used for the experiments were made of aluminum. The one for the irregular reflection was symmetric, with half-angle 25 degrees. Fig. 3 shows the details of positioning the electron beam with respect to the wedge.

The wedge for regular reflection was asymmetric, with angle 60 degrees (Fig. 4). In this case it was sufficient to place the electron beam at three distances behind the leading edge only.

It should be pointed out here, that the smallest possible distance between the beam and the solid surface was about 2.4 mm. Therefore no information on gas density closer to the wedge could be obtained from the experiment (as indicated in Figs. 7 and 11, where the constant density lines end somewhere above the wedge surface).

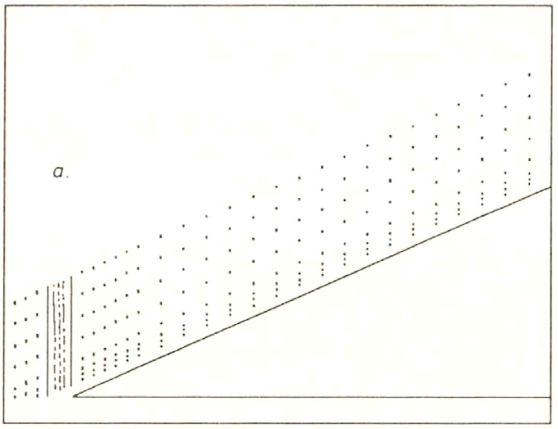


FIG. 3. Positions of the electron beam with respect to the wedge in the case of irregular reflection.

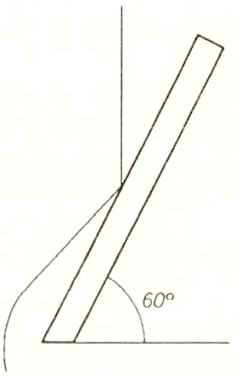


FIG. 4. Shock reflecting wedge in the case of regular reflection.

### 2.3. Accuracy

The possible inaccuracy of the position of the electron beam with respect to the wedge was estimated to be about 0.1 mm in both directions. The inaccuracy of the measurement of density was about ±5 percent of the current value. The resulting inaccuracies of the positions of the constant density lines in the pictures of the flow field (Figs. 7, 11) were equal to about one half of the distances between the neighbouring lines shown in the pictures.

## 3. Direct simulation Monte-Carlo calculations

For the DSMC calculations the standard procedure according to BIRD [8] was employed. Simulations of the particle collisions were performed using the ballot-box scheme, as proposed by YANITSKIĬ [9]. Interactions of the particles

with physical boundaries were simulated utilizing the concept of accommodation coefficient according to MAXWELL [10]. For gas particles the Bird's Variable Hard Sphere (VHS) model [11] was employed.

The calculations were done for both the regular and irregular reflections. The physical space was divided into a matrix of rectangular cells (Fig. 5) containing, in the case of the regular reflection, 80 columns and 50 rows. All cells had the same dimensions: $0.5\lambda$ in the direction of the wave propagation and $\lambda$ in the direction perpendicular to it ($\lambda$ is the mean free path in the undisturbed gas). The total number of the model particles was equal to 9000.

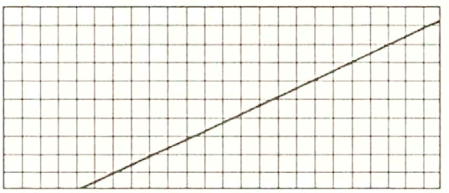

FIG. 5. Cell pattern for DSMC calculations.

For the irregular reflection the numbers of columns and rows were equal to 110 and 36, respectively. The dimensions of the cells were $0.5\lambda$ and $0.8333\lambda$, respectively. The total number of the model particles was equal to 10000([1]).

The results were averaged over 500 to 1500 calculation runs. They were subsequently smoothed following the procedure suggested by HONMA *et al.* [13].

## 4. Continuum model calculations

For continuum model calculations the two-dimensional, time-dependent Navier-Stokes equations [14] were employed. The gas (Argon) was assumed to be perfect, with constant adiabatic exponent and coefficients of viscosity and thermal conductivity proportional to temperature.

The calculations were carried out with the two-step, second order MACCORMACK difference scheme [15]. The scheme was considered on a rectangular mesh in the $(\overline{x}, \overline{y})$ plane. The $\overline{x}$, $\overline{y}$ coordinates were nondimensionalized with the mean free path of the gas particles. The computational domain was bounded by the wall (positioned on the $x$-axis) and three artificial boundaries, creating a rectangle, as shown in Fig. 6. The position of the incident shock wave, before encountering the wall, is shown in the same figure. The initial structure of the incident shock was assumed to be identical with Taylor's solution for weak shocks [16].

Three kinds of boundary conditions at the reflecting wall were considered:

1) adiabatic, slip wall (no energy and tangential momentum exchange between the gas and the wall),

([1]) The authors are indebted to Prof. V.V. SERIKOV for allowing them to make use of his original computer program [12].

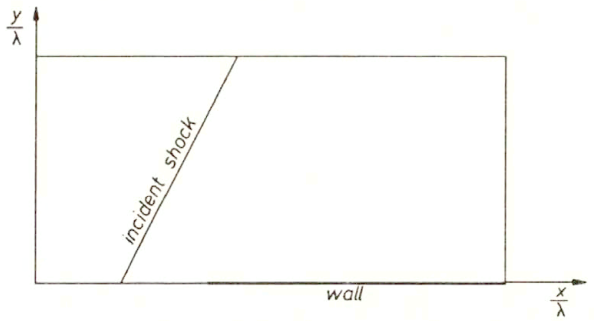


FIG. 6. Computational domain for continuum model.

2) isothermal, no-slip wall (gas temperature and velocity at the wall equal to those of the wall),

3) "intermediate" conditions:

$$u_{gw} - u_i = \beta(u_w - u_i),$$
$$T_{gw} - T_i = \beta(T_w - T_i),$$

where $u_{gw}$, $T_{gw}$ – tangential velocity and temperature of the gas at the wall, respectively, $u_w$, $T_w$ – velocity and temperature of the wall, $u_i$, $T_i$ – tangential velocity and temperature of the gas inside the flow, near the wall (about one mean free path from the wall).

The values of the coefficient $\beta$ remain in the range between 0 and 1. The case of $\beta = 0$ corresponds to adiabatic, slip wall, $\beta = 1$ – to isothermal, no-slip wall.

## 5. Results

The results presented here consist of the pictures of constant density contours for the region above the wedge and the diagrams of gas temperature and velocity components at the wedge surface.

The non-dimensional density is expressed as

$$\overline{\rho} = \frac{\rho - \rho_1}{\rho_2 - \rho_1},$$

where $\rho$ is the current density value, $\rho_1$ and $\rho_2$ are the values in front and behind the incident shock, respectively.

Similarly, the non-dimensional temperature:

$$\overline{T} = \frac{T - T_1}{T_2 - T_1},$$

the tangential velocity component (parallel to the surface):

$$\overline{u} = \frac{u}{u_2},$$

(as the velocity in front of the incident shock equals zero), and the normal velocity component (perpendicular to the surface):

$$\overline{v} = \frac{v}{u_2}.$$

The values of the non-dimensional density, corresponding to the contours shown for irregular reflection, are equal to: $0.1, 0.3, 0.5, 0.7, 0.9, 1.1, 1.2, 1.3, \ldots$, while for regular reflection the values are: $0.1, 0.3, 0.5, 0.7, 0.9, 1.1, 1.3, 1.5, \ldots$.

**5.1. Irregular reflection**

Figures 7a, b shows two diagrams of the constant density lines, obtained experimentally for the flow conditions specified in the paragraph 2.2. The distances from the leading edge to the centerline of the incident shock, as measured along the shock tube axis, were equal to about 32 and 72 mean free paths, respectively. This corresponds to about 35 and 80 mean free paths along the wedge surface.

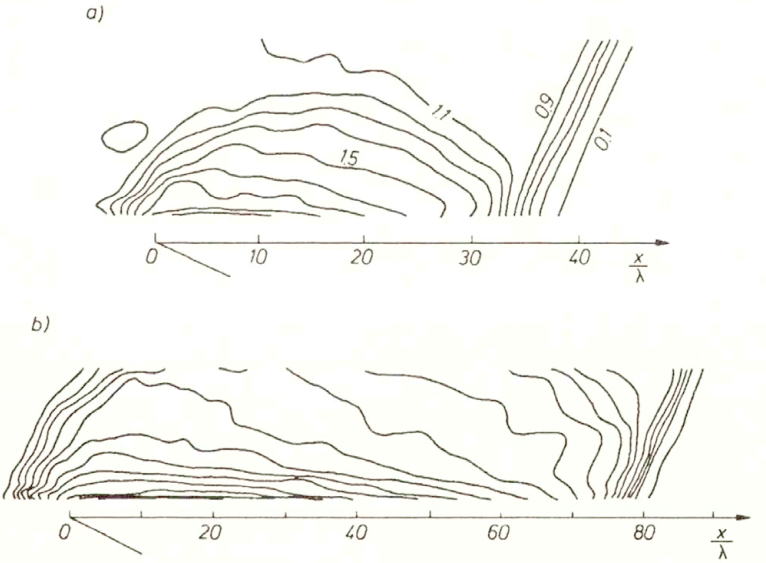


FIG. 7. Constant density contours for irregular reflection, obtained experimentally; a) incident shock 35 mean free paths behind the leading edge, b) incident shock 80 mean free paths behind the leading edge, (note different scales of the pictures).

Figures 8a, b, c shows similar diagrams calculated with the described DSMC procedure for the same flow conditions. The hard sphere model of molecular collisions (the limiting case of the VHS model) was applied. The values of the accommodation coefficient were assumed equal to 0.0, 0.5 and 1.0, respectively. The diagram, calculated for the accommodation coefficient equal to 0.5 seems to be closest to the experiment (Fig. 7a). The visible discrepancies stay within the estimated uncertainty of the results.

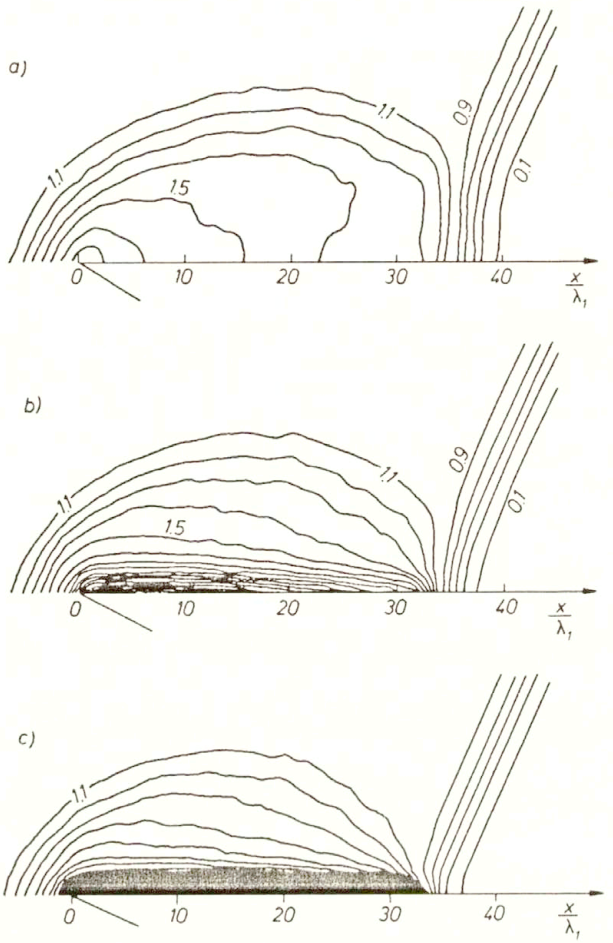


FIG. 8. Constant density contours for irregular reflection, obtained from DSMC calculations (incident shock 35 mean free paths behind the leading edge); a) for accommodation coefficient $\alpha = 0.0$, b) for accommodation coefficient $\alpha = 0.5$, c) for accommodation coefficient $\alpha = 1.0$.

It should be mentioned at this point, that a number of calculations have been performed for various conditions at the wall, including those with different values of the momentum and energy accommodation coefficients, as well as those assuming finite time of resting of the particles at the surface. No better agreement with experiment was achieved.

To see the influence of the intermolecular potential the calculations were repeated for the "softest" limit of the VHS model. The difference was nearly invisible, manifesting itself only with very slight increase of the thickness of the incident shock.

Figure 9 shows the diagrams of the gas temperature, and also tangential and normal velocities at the reflecting surface, as calculated for the accommodation

coefficient 0.5. Appreciable tangential velocity slip and temperature jump at the wall can be seen close to the shock wave, decreasing gradually at larger distances from it. It seems peculiar, that in the area of maximum gradients inside the shock wave even the normal velocity has some finite value, being directed towards the wall.

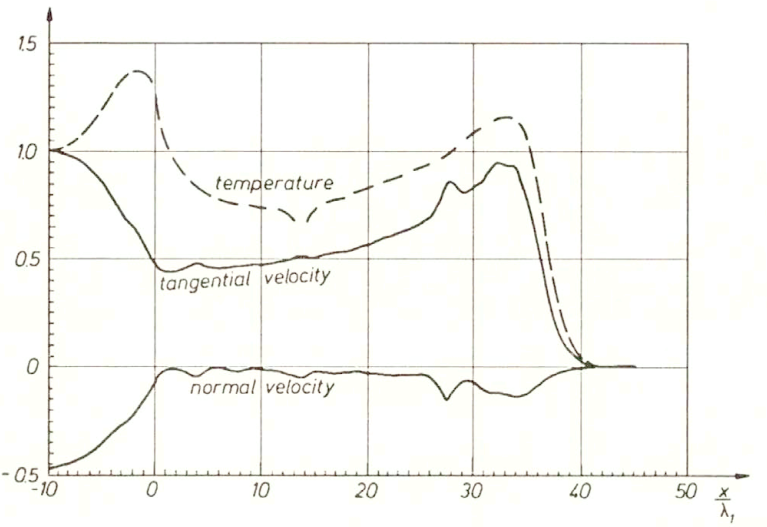


FIG. 9. Gas temperature and velocity components at the surface from DSMC calculations for irregular reflection and accommodation coefficient $\alpha = 0.5$ (incident shock 35 mean free paths behind the leading edge).

The continuum calculations of the problem were performed for several values of the coefficient $\beta$ (see Sec. 4). Figure 10 shows the constant density lines for $\beta = 0.2$ and the distance of about 80 mean free paths from the leading edge to

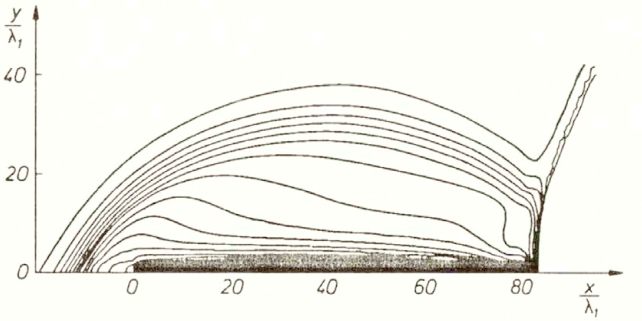


FIG. 10. Constant density contours for irregular reflection, obtained from continuum calculations (incident shock 80 mean free paths behind the leading edge).

the centerline of the incident shock, as measured along the wedge surface. The agreement between Fig. 10 and the experimentally obtained Fig. 7b seems to be at least satisfactory. The difference between the line patterns in the vicinity of

the reflecting wall may be due to constant value of the coefficient $\beta$ assumed for calculation. It seems conceivable that $\beta$ should probably vary along the reflecting surface, as might be concluded when inspecting Fig. 9, based on DSMC calculations.

### 5.2. Regular reflection

Figure 11 shows the diagram of the constant density lines, obtained experimentally for the same set of the flow conditions. The distance from the leading edge to the centerline of the incident shock, measured this time along the wedge surface, was equal to about 84 mean free paths. It should be pointed out, however, that the measurements performed at three distances from the leading edge, equal to 51, 84 and 178 mean free paths, respectively, gave (within experimental accuracy) the same picture of the neighbourhood of the reflection point. It was therefore safe to assume, that this picture did not change appreciably with increasing distance from the leading edge, and comparison could be done with calculations made for distances selected arbitrarily.

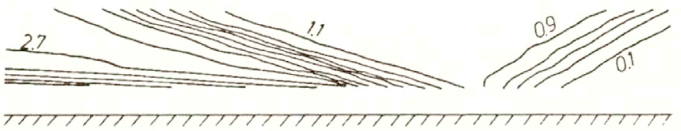


FIG. 11. Constant density contours for regular reflection, obtained experimentally.

Figure 12 shows the diagram of constant density lines, calculated with the DSMC procedure for the accommodation coefficient equal to 0.3 and the distance from the leading edge to the centerline of the incident shock about 40 mean free paths. This result is closest to the experimental one, shown in Fig. 11. For the regular reflection, however, the discrepancy between the results for different accommodation coefficients is much less pronounced than for the previously described irregular case.

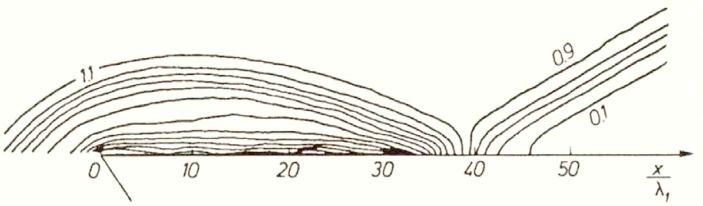


FIG. 12. Constant density contours for regular reflection, obtained from DSMC calculations for accommodation coefficient $\alpha = 0.3$.

Figure 13 shows the calculated diagrams of the gas temperature, and tangential and normal velocities at the surface, corresponding to the conditions of Fig. 12. It is quite similar to the Fig. 9, made for the irregular reflection.

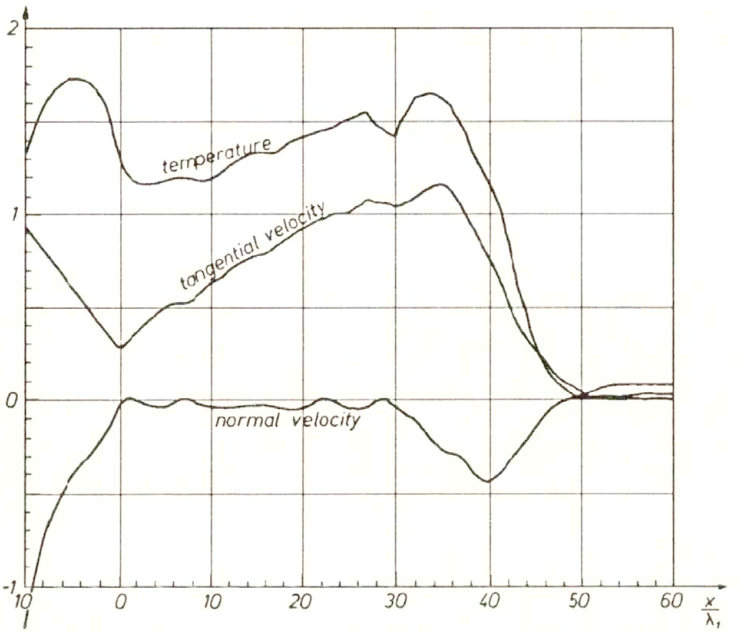


FIG. 13. Gas temperature and velocity components at the surface from DSMC calculations, for regular reflection and accommodation coefficient $\alpha = 0.3$.

The continuum calculations were performed, as before, for several values of the coefficient $\beta$. Figure 14 shows the result for $\beta = 0.3$. Its agreement with experiment is indeed very good. This time the value of the coefficient $\beta$ may be safely assumed to be constant, as only relatively small part of the wall, just behind the shock, can influence the flow pattern visible in Fig. 14. This follows from the fact that the flow behind the reflected shock is supersonic with respect to the reflection point, and therefore no signals from the wall can travel "upstream".

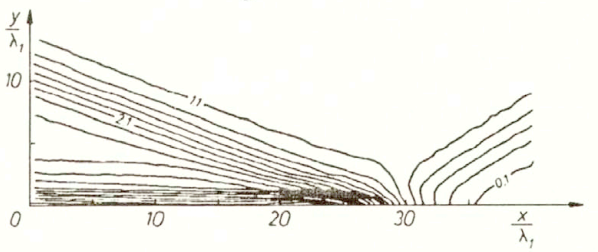


FIG. 14. Constant density contours for regular reflection, obtained from continuum calculations.

## 6. Conclusions

1. The Direct Simulation Monte-Carlo technique seems to be adequate for calculation of the shock reflection process in its initial stage, when the incident shock is close to the leading wedge and the whole problem is far from self-similarity.

2. The hard-sphere model of intermolecular potential seems to be sufficient for moderately strong shocks.

3. One, single accommodation coefficient, according to Maxwell, seems to be sufficient to describe the interactions of the particles with the reflecting surface. The optimum value of this coefficient, in the described experiments, stayed within range from 0.3 to 0.5.

4. Continuum model calculations can produce meaningful results, even in relatively close neighbourhood of the leading edge, provided that suitable velocity slip and temperature jump at the wall are assumed.

**Acknowledgments**

One of the authors (A. KOZŁOWSKI) of this paper was supported in part by the KBN grant No. 2-P301-027-06.

## References

1. E. MACH, Akad. Wiss., Wien, 77, II, 1228, 1878.
2. L.F. HENDERSON and A. SIEGENTHALER, *Experiments on the diffraction of weak blast waves: the von Neumann paradox*, Proc. Roy. Soc., London, **A369**, 537–555, 1980.
3. Z.A. WALENTA, *Microscopic structure of the Mach-type reflexion of the shock wave*, Arch. Mech., **32**, 819–825, 1980.
4. Z.A. WALENTA, *Formation of the Mach-type reflection of shock waves*, Arch. Mech., **35**, 187–196, 1983.
5. B. SCHMIDT, *Stosswellenuebergang von regulaerer Reflektion zur Mach Reflektion auf der Flanke eines Keils*, ZAMM, **65**, 234–236, 1985.
6. J.M. DEWEY, A.A. VAN NETTEN, *Observations of the initial stages of the Mach reflection process*, Proc. 18th Int.Symp. on Shock Waves, Sendai, 227–232, 1991.
7. Z.A. WALENTA, *Formation of the Mach reflection in vibrationally relaxing gases*, Proc.19th Int. Symp. on Shock Waves, Marseille 1993.
8. G.A. BIRD, *Molecular gas dynamics*, Clarendon Press, Oxford, 1976.
9. V.E. YANITSKII and O.M. BELOCERKOVSKII, *The statistical method of particles in cells for the solution of problems of the dynamics of a rarefied gas, Part I*, Zh. Vychisl. Mat. Mat. Fiz., **15**, 1195–1208; *Part II*, Zh. Vychisl. Mat. Mat. Fiz., **15**, 1553–1567, 1975.
10. J.C. MAXWELL, *The scientific papers of James Clark Maxwell*, W.D. NIVEN [Ed.], New York, Dover, **2**, 706, 1952.
11. G.A. BIRD, *Definition of mean free path for real gases*, Physics of Fluids, **26**, (11), 3222–3223, 1983.
12. V.V. SERIKOV, Private communication.
13. H. HONMA, D.Q. XU and T. ABE, *DSMC approach to nonstationary Mach reflection of strong incoming shock waves using a smoothing technique*, Shock Waves, **3**, 67–72, 1993.
14. K. KANTIEM, *Numerical investigation of the two-dimensional shock wave reflection*, Arch. Mech., **46**, 5, 1994.
15. R.W. MACCORMACK, *Numerical solution of the interaction of a shock wave with a laminar boundary layer*, Proc. of the 2nd International Conference on Numerical Methods in Fluid Dynamics, Berkeley, 1970, Lecture Notes in Physics, 8, 151–163, 1970.
16. G.I. TAYLOR, *The conditions necessary for discontinuous motion in gases*, Proc. Roy. Soc. A, **84**, 371–377, 1910.

DEPARTMENT OF MATHEMATICS, WARSAW UNIVERSITY
and
POLISH ACADEMY OF SCIENCES
INSTITUTE OF FUNDAMENTAL TECHNOLOGICAL RESEARCH, WARSZAWA.

*Received September* 30, 1994.

Arch. Mech., 47, 1, pp. 81–99, Warszawa 1995

# Dissipation of configurational forces in defective elastic solids (*)

G.A. MAUGIN (PARIS) and C. TRIMARCO (PISA)

THE NOTION of material force originating from Eshelby's mechanics provides an expression for the configurational forces which drive several types of "defects" in otherwise homogeneous nonlinear elastic bodies. The classes of defects examined include straight cracks, cavities, dislocations, disclinations, and coherent interfaces. The latter represent progressing phase-transition fronts. The method consists in evaluating the elementary dissipation in an irreversible progress of the defects, "en block" on the material manifold. This is compared to a recent energetic approach of Dascalu and Maugin who based on the use of generalized functions.

## 1. Introduction

CONFIGURATIONAL forces are those fictitious forces which act on the defects and thus radically differ from physical (Newtonian) forces which act on the mass elements. In d'Alembert's vision of virtual work, they are the "forces" that are associated with virtual displacements of defects (one could say, *lattice sites* in a crystal) rather than of physical points. As such, it makes no sense *a priori* to speak of their possible *dissipation* as they are conceptually related to the notion of *material inhomogeneity* (lack of invariance of material properties under rigid displacement of the lattice sites) and, outside a set of singular points (in effect, the points of extension of defects) we assume a *thermodynamically recoverable* behaviour. In other words, *material inhomogeneities* (the fact that physical properties change with material point) may have no relation to dissipation (see MAUGIN [21]). But the material bodies of interest may present singularities in the field solution. These singularities, in elasticity, account for *elastic defects* among which we can identify notches, (macro) cracks, dislocations (microcracks), cavities, disclinations, and elastic-phase transition fronts (the latter being the fact that one phase is viewed as a defect by the other phase). These singularities are related to the singular solutions in an otherwise nondissipative medium (as a matter of fact, a dissipative medium would have a natural tendency to make the solution less singular). But with a movement or progress of the "defect", the problem may present a *global irreversibility*, or *dissipation*, as energy is expended in this movement or progress. If the said defect progresses with uniform (we later say, "en bloc") rate of expansion, then the resulting *global dissipation* can be expressed in the traditional *bilinear form* of a product of a "force" (here a global

(*) This paper of a somewhat review nature was intended to celebrate Paul M. NAGHDI's seventieth anniversary. It is dedicated to the memory of Paul.

configurational one) and a generalized "velocity". This can be exploited, just as for viscosity, plasticity and fracture, to devise criteria of progress of the defect, the Griffith criterion being for macrocracks an example of such popular criteria.

In this work, by computing the elementary global dissipation in the possible irreversible progress of a variety of *elastic defects*, directly on the *material manifold* of finite-strain solid mechanics (and not in physical space), we deduce straightforwardly the corresponding expression of the rate of global dissipation in terms of the Eshelby stress or its "moments". The necessary (brief) elements of kinematics and deformation theory of solids are recalled in Sec. 2. The notion of *elastic defect* is made more precise in Sec. 3. Section 4 presents as the first and most classical example the quasi-static progress of a straight-through crack. Section 5 indicates how an essentially similar derivation applies to dislocations, expanding spherical cavities, and disclinations. In Sec. 6, we consider the quasi-static steady progress of a coherent phase-transition front in an elastic body. The expanding cavity may be considered anew as a special case of this. The general *irreversible thermodynamics* of global configurational forces is outlined in Sec. 7. Brief indications to treat the fully dynamical cases are provided in Sec. 8. Conclusions and prospects are listed in Sec. 9.

The work essentially builds on original ideas of ESHELBY [9, 10], ROGULA [27], HILL [14] and CHEREPANOV [4], and previous work by MAUGIN and TRIMARCO [24, 25] – also the synthesis by MAUGIN [21]. Wherever this applies, comparisons are made with the work of BUDIANSKY and RICE [3], GÜNTHER [12], KNOWLES and STERNBERG [16], FREUND (1972), HERRMANN [13], for fracture and conservation laws, with ESHELBY [10], HILL [14] and others for phase-transiton fronts (MALOMED and RUMANOV [17]; TRUSKINOVSKY [32,33]), and DASCALU and MAUGIN [6, 7] for another type of approach to the same problem. Most of the proofs given are only sketchy in order to keep the paper within reasonable bounds.

## 2. Elements of kinematics

In what follows we need very few elements of kinematics and deformation theory. We consider two essentially equivalent descriptions, at least when all fields are smooth enough. These we call the *direct-motion* and *inverse-motion descriptions* (e.g., in MAUGIN [21]). Let $\mathcal{K}_t$ be the *actual* (or current) *configuration* of the solid body $\mathcal{B}$. The latter is made of material points $X$ which are referred to a position $\mathbf{X}$ of components $X^K$, $K = 1, 2, 3$, in a *reference configuration* $\mathcal{K}_R$. The *direct motion* of $\mathcal{B}$ is the *time*-parametrized mapping of $\mathbf{X} \in \mathcal{M}^3$, where $\mathcal{M}^3$ is called the *material manifold*, onto $\mathbb{E}^3$, the physical Euclidean space of Newtonian physics, such that

$$\mathbf{x} = \chi(\mathbf{X}, t), \qquad \mathbf{F} := \left.\frac{\partial \chi}{\partial \mathbf{X}}\right|_t \equiv \nabla_R \chi, \qquad \mathbf{v} := \left.\frac{\partial \chi}{\partial t}\right|_{\mathbf{X}}, \tag{2.1}$$

with the invertibility condition

$$J_F \equiv \det \mathbf{F} > 0 \quad \text{always} \quad (\text{i.e., } \forall t). \tag{2.2}$$

Thus we can also define the *inverse motion*

$$\mathbf{X} = \chi^{-1}(\mathbf{x}, t), \qquad \mathbf{F}^{-1} := \left.\frac{\partial \chi^{-1}}{\partial \mathbf{x}}\right|_t \equiv \nabla \chi^{-1}, \qquad \mathbf{V} := \left.\frac{\partial \chi^{-1}}{\partial t}\right|_{\mathbf{x}}. \tag{2.3}$$

We let the reader check by use of the chain rule of differentiation that $\mathbf{F}$ and $\mathbf{F}^{-1}$ on the one hand, and $\mathbf{v}$ and $\mathbf{V}$ on the other hand, are related by

$$\mathbf{F}\mathbf{F}^{-1} = \mathbf{1}, \qquad \mathbf{F}^{-1}\mathbf{F} = \mathbf{1}_R, \tag{2.4}$$

and

$$\mathbf{v} = -\mathbf{F} \cdot \mathbf{V}, \qquad \mathbf{V} = -\mathbf{F}^{-1} \cdot \mathbf{v}. \tag{2.5}$$

Thus $\mathbf{F}$ is the *direct-motion* gradient, and $\mathbf{F}^{-1}$ is the *inverse-motion* gradient – which is none other than the inverse of $\mathbf{F}$. We call $\mathbf{v}$ and $\mathbf{V}$ the *physical* and *material* velocity fields, respectively. More generally, a tensorial field with components in $\mathbb{E}^3$ is called *physical*, while a tensorial field with components on $\mathcal{M}^3$ is called *material*. $\mathbb{E}^3$, by its very structure, does not distinguish between covariant and contravariant quantities (in other words, the natural inner product is effected with the Kronecker symbol), but $\mathcal{M}^3$ *does*.

We also need the relation ($T$ = transposition)

$$\mathbf{F} = \mathbf{1}_s + (\nabla_R \mathbf{u})^T, \tag{2.6}$$

where $\mathbf{u}(\mathbf{X}, t)$ is the displacement field and $\mathbf{1}_s$ is the so-called shifter, and the definitions of finite strains

$$\mathbf{C} = \mathbf{F}^T \cdot \mathbf{F}, \qquad \mathbf{C}^{-1} = \mathbf{F}^{-1} \cdot (\mathbf{F}^{-1})^T \equiv (\mathbf{C})^{-1}, \tag{2.7}$$

and

$$\mathbb{E} := \frac{1}{2}(\mathbf{C} - \mathbf{1}_R), \qquad \mathbb{E}^* := \frac{1}{2}(\mathbf{1}_R - \mathbf{C}^{-1}). \tag{2.8}$$

The matter density $\rho(\mathbf{x}, t)$ at time $t$ at the image point $\mathbf{x}$ of $X$ is related, at all regular points, to the matter density $\rho_0$ in $\mathcal{K}_R$ by the *continuity equation*

$$\rho(\mathbf{x}, t) = \rho_0(\mathbf{X}) J_F^{-1}. \tag{2.9}$$

By this we mean that $\rho_0$ is at most a function of $\mathbf{X}$. More generally, we say that the body is *materially inhomogeneous* when its properties depend *explicitly* on the material point $X$ through $\mathbf{X}$. The usual formulation of *nonlinear* continuum mechanics makes use of fields which are functions of space-time variables $(\mathbf{X}, t)$. But these fields may be expressed in, or "projected" on, or "convected to" (else, "pulled back" or "pushed forward", to) $\mathbb{E}^3$ or $\mathcal{M}^3$. In the present case a strict *material representation* with fields canonically projected onto $\mathcal{M}^3$, but still functions of $(\mathbf{X}, t)$ is the most appropriate one (notice that *no fields* are called *Lagrangian*). This is all we need in so far as kinematics is concerned.

## 3. Elastic defects

To start with we consider the case of a nonlinear (hyper) elastic solid body $\mathcal{B}$ in the material description. It occupies the regular domain $\Omega$ of $\mathcal{M}^3$ with boundary $\partial\Omega$. We denote by $C$ a subset of $\mathbb{R}^3\backslash\Omega$ (note that $\mathbb{E}^3 \cong \mathbb{R}^3$), that is the set of *points* occupied by the *elastic defect*. We call $\mathcal{S}$ the set of *extension points* of the elastic defect when the latter progresses. To fix ideas, for a straight-through crack such as in Fig. 1, $C$ is made of the cut $\Sigma$ occupying the surface $[0, l] \times \mathbb{R}$

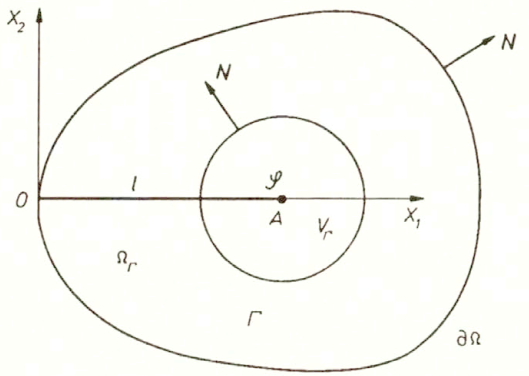


FIG. 1. Straight-through crack.

(considering the body as infinite in the direction orthogonal to the figure's plane), while $\mathcal{S}$ is made of only *one point*, the *tip of the crack* (in fact a line, as both the body and $\mathcal{S}$ extend to infinity in the orthogonal direction). The situation would be the same for a *dislocation* or *disclination*. For a spherical cavity such as in Fig. 2, $C$ is the whole spherical volume of radius $l$ while $\mathcal{S}$ is the spherical surface of radius $l$. Finally, in the case of a phase-transition front in Fig. 3, the set $C$ is the whole material on one side of $\Sigma$ and $\mathcal{S}$ is $\Sigma$ itself. In the last case the *defect*

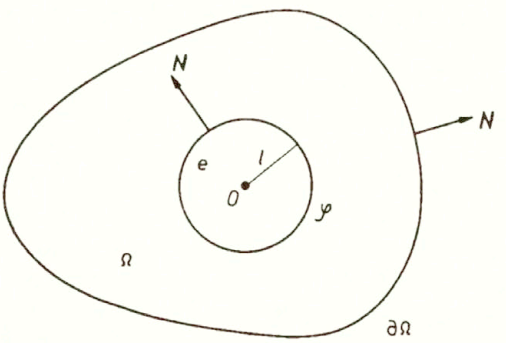


FIG. 2. Spherical cavity.

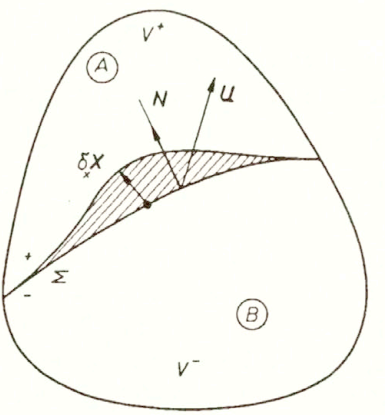


FIG. 3. Coherent phase-transition front.

is nothing but the growth of one *phase* at the expense of the other *phase*. It is important to notice that *defects* may have the *same dimension* as the body (this is the case of the cavity and the phase-transition) or a dimension less than that of the body (case of the crack, case of *dislocations* and *disclinations*). In fact, in $\mathbb{E}^3$, we may have only *points, lines*, and *walls* as defects from the topological point of view (KLÉMAN [15]). From the classical analytical point of view, *elastic defects* are defined by the fact that smooth solutions of elasticity fail at the set of *extension points of such defects*, while the elastic solution behaves regularly outside (even though the "outside" may be void of matter). This definition is checked by all *elastic defects* introduced so far, but some *defects* are simpler to study than others (the straight-through crack in so-called Mode III in particular – cf. MAUGIN [20], Chapter 7).

The problem on which we want to focus the attention is the *kinetics* of the progress of *elastic defects*. To proceed to these kinetic laws, we must evaluate the *dissipation growth* in the irreversible progress of the said defect. This dissipation will be expressible as the product of a "force" and a "velocity", which are conjugate in the sense of *thermodynamics*, and then we shall almost be done. The "force" in question is, as we know, the so-called *force on an elastic singularity* in the sense of ESHELBY [9]. This is not a force in the Newtonian style (where "forces" act on elements of matter, i.e., mass) but in the *Eshelbian style* (i.e., *fictitious forces* that act on defects). For us, however, they are *true material forces* (cf. MAUGIN [21]), i.e., the mechanical quantities *dual* to infinitesimal changes of position $\mathbf{X}$ *on the material manifold* $\mathcal{M}^3$. But as inhomogeneity properties relate to an explicit dependence on $\mathbf{X}$, they are also conceptually *inhomogeneity forces*, so that *Eshelbian forces, material forces, inhomogeneity forces*, and forces on elastic singularities are used as synonymous.

If the material elastic body was *materially inhomogeneous*, it would have an energy density per unit volume in $\mathcal{K}_R$ of the form $W(\mathbf{F}; \mathbf{X})$, where the explicit dependence upon $\mathbf{X}$ is emphasized. Here we consider only intrinsically *homogeneous elastic solids* for which this, in one phase of the material, reduces to

$$W = \overline{W}(\mathbf{F}), \tag{3.1}$$

in the absence or neglect of thermal properties. Thus "elastic inhomogeneities" are only of the above-introduced singularity type; they do not appear through the *energy density* (see, however, the generalized-function approach in DASCALU and MAUGIN [6].

## 4. Quasi-static progress of a straight-through crack

As the first simple example we consider the problem in Fig. 1, admitting that if the crack progresses at all, the two faces of the crack cannot solder back by themselves so that there occurs a *global dissipation*, although the material itself

does not admit a dissipative behaviour at any regular point. Ignoring inertial effects (so-called *quasi-statics*), we try to evaluate the *increment* of global dissipation in an *elementary progress of the crack*. Dissipation, if it occurs at all, will be the difference between the elementary global work developed by applied tractions (there are no body forces) and the elementary consumption of *elastic energy from the body*. Let $\mathbf{T}^d$ be the applied tractions at $\partial\Omega$. Calling $\Phi$ the dissipation, we have thus the following *variational formulation*

$$\delta\Phi = \int_{\partial\Omega} \mathbf{T}^d \cdot \delta_{\mathbf{X}} \chi \, dA - \delta_{\mathbf{X}} \int_{\Omega} W(\mathbf{F}) \, dV, \tag{4.1}$$

where we emphasize that $\Omega = \Omega(l)$ and $l = l(t)$, where $l$ is the length of the crack at time $t$. The variation introduced in the right-hand side in (4.1) must be understood as a *material variation* (cf. MAUGIN and TRIMARCO [24]), i.e., a variation at fixed $\mathbf{X}$, defined by

$$\delta_{\mathbf{X}} \chi = \left. \frac{\partial \chi(\mathbf{X}, t, \varepsilon)}{\partial \varepsilon} \right|_{\varepsilon = 0}, \tag{4.2}$$

which presents the convenience to commute with both $\nabla_R$ (and material-volume integration), and $\partial/\partial t$ (the latter is unimportant in our quasi-static approximation). Notice that with *dead loading*, Eq. (4.1) can also be written as

$$\delta\Phi = -\delta P, \tag{4.3}$$

where $P$ is the *total potential energy* of the body. Thus, formally at least,

$$\delta\Phi = -\frac{\delta P}{\delta l} \delta l = \mathcal{F} \delta l, \qquad \mathcal{F} \equiv -\delta P / \delta l, \tag{4.4}$$

where $\delta P/\delta l$ denotes the *functional derivative* of the *potential energy*, since $P$ depends on $l$ through the domain of integration $\Omega$.

With $\mathbf{N}$ the unit outward normal to $\partial\Omega$ in $K_R$, Eq. (4.1) reads

$$\delta\Phi = \int_{\partial\Omega} (\mathbf{N} \cdot \mathbf{T}) \cdot \delta_{\mathbf{X}} \chi \, dA - \delta_{\mathbf{X}} \int_{\Omega(l)} W(\mathbf{F}) \, dV, \tag{4.5}$$

where $\mathbf{T}$ is the first Piola–Kirchhoff stress.

One must pay special attention to the evaluation to the second contribution in Eq. (4.5) as the domain of integration evolves with the quasi-static extension of the crack. Taking account of the fact that no tractions are acting along the "lips" of the crack, $\Sigma^+$ and $\Sigma^-$, and isolating the region $V_\Gamma$ around the crack tip (line), we in fact have directly

$$\delta_{\mathbf{X}} \int_{\Omega} W \, dv = \delta_{\mathbf{X}} \int_{\Omega - V_\Gamma} W \, dV + \int_{\Gamma} W (\mathbf{N} \cdot \delta_{\mathbf{x}} \chi^{-1}) \, d\Gamma, \tag{4.6}$$

and

$$\delta_{\mathbf{X}} \int_{V_\Gamma, \Omega - V_\Gamma} W \, dV = \int_{V_\Gamma, \Omega - V_\Gamma} (\delta_{\mathbf{X}} W) \, dV, \qquad \delta_{\mathbf{X}}(dV) \equiv 0, \tag{4.7}$$

with

$$\delta_{\mathbf{X}} W = (\partial W / \partial \mathbf{F}) \cdot \delta_{\mathbf{X}}(\nabla_R \chi) = \mathbf{T} \cdot \nabla_R (\delta_{\mathbf{X}} \chi), \tag{4.8}$$

where we have introduced the first Piola–Kirchhoff stress $\mathbf{T}$ by its constitutive equation

$$T = \partial W / \partial \mathbf{F}, \tag{4.9}$$

and accounted for the fact that there is a *flux through the boundary* $\Gamma$ of $V_\Gamma$ as $V_\Gamma$ moves with the crack tip *into the material*. The variation $\delta_{\mathbf{x}} \chi^{-1}$ is defined from Eq. (2.3) by [compare to (4.2)]

$$\delta_{\mathbf{x}} \chi^{-1} = \left. \frac{\partial \chi^{-1}(\mathbf{x}, t, \varepsilon)}{\partial \varepsilon} \right|_{\varepsilon = 0}, \tag{4.10}$$

and it is checked that it is related to $\delta_{\mathbf{X}} \chi$ by [cf. MAUGIN and TRIMARCO [25]; compare to Eq. (2.5)]

$$\delta_{\mathbf{X}} \chi + \mathbf{F} \cdot \delta_{\mathbf{x}} \chi^{-1} = \mathbf{0}. \tag{4.11}$$

Accounting now for the equilibrium equations (the symbolism [..] denotes the jump of its enclosure)

$$\operatorname{div}_R \mathbf{T} = \mathbf{0}, \qquad \mathbf{N} \cdot [\mathbf{T}] = \mathbf{0}, \tag{4.12}$$

at all regular points in $\Omega$, and across $\Gamma$, respectively, we find that Eq. (4.1), up to an integrated term that goes to zero with $V_\Gamma$, takes on the form

$$\delta \Phi = \int_\Gamma (\delta_{\mathbf{x}} \chi^{-1} \cdot \mathbf{b} \cdot \mathbf{N}) \, d\Gamma, \tag{4.13}$$

where $\mathbf{b}$ is the mixed (fully material) stress tensor defined by

$$\mathbf{b} := W \mathbf{1}_R - \mathbf{F}^T \cdot \mathbf{T}. \tag{4.14}$$

This is the *quasi-static* version of the so-called *Eshelby* "energy-momentum" tensor (ESHELBY [10]). By the way, if we do multiply Eq. $(4.12)_1$ to the left by $\mathbf{F}^T$, and integrate the result by parts, while accounting for (4.9), we do find that, at all, *regular* points in $\Omega$, there holds the additional equilibrium law:

$$\operatorname{div}_R \mathbf{b} = \mathbf{0}. \tag{4.15}$$

As we know from our general study, this is but the *quasi-static version* of the balance law of *pseudomomentum*, which is the expression of the balance of linear momentum after *canonical projection onto* $\mathcal{M}^3$ (MAUGIN and TRIMARCO [24]). There is thus an intimate relationship between Eq. (4.15) valid at all regular points in $\Omega$ and expression (4.13) which gives the "*dynamical flux*" of $\mathbf{b}$ through the cylinder-like surface encircling the tip (line) of the crack. In particular, as $\delta_{\mathbf{x}}\chi^{-1}$ is a *virtual variation*, we can take it as an "*en bloc*" (i.e., rigid-body-motion like) virtual (inverse) motion of the region $V_\Gamma$ around the tip, e.g., since the eventual progress of the crack is supposed to take place in the direction of the crack itself,

$$\delta_{\mathbf{x}}\chi^{-1} = \mathbf{E}_I \delta l, \tag{4.16}$$

where $\mathbf{E}_I$ is a unit material vector along the crack direction (here $X_I$). The elementary dissipation (4.13) then takes on the sought form

$$\delta\Phi = \mathcal{F}_{(I)}\delta l, \qquad \mathcal{F}_{(I)} := \int_\Gamma \mathbf{E}_I \cdot \mathbf{b} \cdot \mathbf{N}\, d\Gamma, \tag{4.17}$$

where $\mathcal{F}_{(I)}$ is a *global material force*. Per unit time, this result can also be written as

$$\dot{\Phi} = G\dot{l}, \qquad G = \mathcal{F}_{(I)}, \tag{4.18}$$

where $G$ is traditionally called the *energy-release rate* (cf. MAUGIN [20], Chapter 7). Obviously, the $\mathcal{F}$ of Eq. (4.4) is none other than $\mathcal{F}_{(I)}$. The reader will have noticed that we did not make $\Gamma$ shrink to the crack tip $A$, for there is no need to do that. This follows from the fact that the obtained integral is *contour-independent* (as easily checked) about $A$. As a matter of fact, Eq. $(4.17)_2$ is none other than the *J-integral* of Eshelby, Cherepanov and Rice; in particular, in small strains where the behaviour of the stress is $O(1/\sqrt{r})$ about $A$ in the plane of Fig. 1, we have

$$\lim_{\Gamma\to 0} \int_\Gamma \mathbf{N} \cdot \mathbf{T} \cdot \mathbf{E}_I \, d\Gamma = 0, \tag{4.19}$$

so that with Eq. (2.6) and $N_1 = \mathbf{N} \cdot \mathbf{E}_1$, we obtain

$$\lim_{\Gamma\to 0} \mathcal{F}_{(I)} = \lim_{\Gamma\to 0} J_\Gamma, \qquad J_\Gamma := \int_\Gamma \left( W N_1 - \mathbf{N} \cdot \mathbf{T} \cdot \frac{\partial \mathbf{u}}{\partial X_1} \right) d\Gamma, \tag{4.20}$$

from the definition of $\mathbf{b}$.

## 5. The case of cavities and disclinations

We shall not examine the case of (translation) *dislocations* which, conceptually, is very much similar to that of straight-through cracks. The reason for this is that if in Fig. 1 the tip $A$ of the crack is viewed as the point where the dislocation line pierces the plane of the figure, the cut $\Sigma$ may be considered as being introduced to make the displacement field of the elastic dislocation solution single-valued. The essential difference, however, is that the *singularity order* of the elastic solution in the neighbourhood of $A$ is different from that of the crack solution and the resulting analysis is a little bit more involved as shown by DASCALU and MAUGIN [6].

Of particular interest is the case of the *spherical cavity* in Fig. 2. Formula (4.13) which does not specify the type of defect is still valid. Then the Art of the Matter resides in the selection of the virtual increment $\delta_{\mathbf{x}}\chi^{-1}$. For a spherical cavity in *uniform expansion*, centered at $\mathbf{X}_0$, we select

$$\delta_{\mathbf{x}}\chi^{-1} = \eta(\mathbf{X} - \mathbf{X}_0), \tag{5.1}$$

where $\eta$ is an infinitesimally small ($\eta \ll 1$) constant independent of point $\mathbf{X}$. We can also center the coordinate system at the cavity so that $\mathbf{X}_0$ disappears from the formulation. Considering this case and passing to time derivatives by replacing $\eta$ (which becomes homogeneous to a reciprocal time) by the rate of expansion $\dot{l}/l$, we find that Eq. (4.13) provides the following result:

$$\dot{\Phi} = \mathcal{M}(\dot{l}/l), \tag{5.2}$$

where

$$\mathcal{M} := \int_{\mathcal{S}} (\mathbf{X} \cdot \mathbf{b} \cdot \mathbf{N})\, dA. \tag{5.3}$$

It is readily checked in two dimensions (where $\mathcal{C}$ becomes the inside of the circle of radius $l(t)$ and $\mathcal{S}$ the circle of radius $l(t)$), that $\mathcal{M}$ is none other than the path-independent integral of KNOWLES and STERNBERG [16]. If we return to the original meaning of $\dot{\Phi}$, i.e.,

$$\dot{\Phi} = \int_{\partial\Omega} \mathbf{T}^d \cdot \mathbf{v}\, dA - \frac{d}{dt}\int_{\Omega} W(\mathbf{F})\, dV, \tag{5.4}$$

we see that we have somewhat parodied in a different language the proof presented by BUDIANSKY and RICE [3].

As we have already considered *rigid translations* and *uniform expansions* for $\delta_{\mathbf{x}}\chi^{-1}$, it remains to examine the case of a *rigid-body rotation*, still in material space. To that purpose, we envisage a virtual inverse-motion variation such as

$$\delta_{\mathbf{x}}\chi^{-1} = \varepsilon(\mathbf{X} - \mathbf{X}_0) \times \omega, \tag{5.5}$$

where $\varepsilon$ is an infinitesimally small ($\varepsilon \ll 1$) parameter, and the axial (material) vector $\omega$ represents a *finite uniform* ($\nabla_R \omega \equiv 0$) *rotation* that is centered at $\mathbf{X}_0$. Formula (4.13) then delivers the expression

$$\delta\Phi = \varepsilon\omega \cdot \left\{ \int_\Gamma (\mathbf{b} \cdot \mathbf{N}) \times (\mathbf{X} - \mathbf{X}_0)\, d\Gamma \right\}. \tag{5.6}$$

In the limit as we pass to time derivatives and $\varepsilon\omega$ is replaced by $\mathbf{E}_\omega \dot{\alpha}$, where $\mathbf{E}_\omega$ is a unit vector along the rotation axis and $\dot{\alpha}$ is the rate of rotation, we obtain a rate of dissipation given by

$$\dot{\Phi} = L_\omega \dot{\alpha}, \tag{5.7}$$

where

$$L_\omega := \int_\Gamma \{(\mathbf{b} \cdot \mathbf{N}) \times (\mathbf{X} - \mathbf{X}_0)\} \cdot \mathbf{E}_\omega\, d\Gamma. \tag{5.8}$$

In general $L_\omega$ depends on time through $\mathbf{E}_\omega(t)$. However, we easily verify in two dimensions, with $\mathbf{E}_\omega$ orthogonal to the plane of the figure, that $L_\omega$ is constant and that it is none other than the $L$-integral of GÜNTHER [12]. We have thus exhausted the apparent possibilities of choice for $\delta_{\mathbf{x}}\chi^{-1}$. Note that *uniform expansion* has no equivalent in *physical space*. It remains to identify the class of *material defects* to which Eq. (5.7) applies. If in Fig. 1 we consider $A$ as the point at which a straight *disclination* line (disclinations are "rotation" dislocations which present a defect of closure in the *rotation angle* of a triad transported in a circuit around the line) pierces the plane, and the cut $\Sigma$ is introduced to render the solution single-valued, then we see that our result (5.7) is applicable to such *disclinations*.

## 6. Coherent phase-transition front

We consider now the case illustrated in Fig. 3, where, as mentioned before, the set of defect points is the matter on one side of the regular surface $\Sigma$, say in the material region $V^-$, and this grows in the region $V^+$, the set of *extension points* being $\Sigma$. Obviously then, the *elastic* material may not even be the same on both sides of $\Sigma$ (it is the *same* but up to a *material symmetry* which respects some matching conditions at $\Sigma$ (cf. GRINFELD [11]), hence the name of *coherent* phase-transition fronts). Let $V = V^+ \cup V^-$. We envisage the possibility that the growth of $V^-$ at the expense of $V^+$ occurs with a *dissipation* (but not necessarily). Thus, again, we have to consider the infinitesimal variation

$$\delta\Phi = \int_{\partial V} (\mathbf{N} \cdot \mathbf{T}) \cdot \delta_{\mathbf{X}} \chi\, dA - \delta_{\mathbf{X}} \int_V W(\mathbf{F})\, dV, \tag{6.1}$$

where, indeed,

$$\int_V W(\mathbf{F})\,dV = \int_{V^+} W^+(\mathbf{F})\,dV + \int_{V^-} W^-(\mathbf{F})\,dV, \tag{6.2}$$

as the two elastic *phases* may be regarded as essentially different materials. We can borrow some results from the analysis of Sec. 4. In particular, assuming that it is $V^-$ that progresses *into* $V^+$, applying a transport theorem such as in Eq. (4.6), we can write

$$\delta_{\mathbf{X}} \int_{V^\pm} W^\pm(\mathbf{F})\,dV = \int_{V^\pm(\text{fixed})} \delta_{\mathbf{X}} W^\pm\,dV - \int_{\Sigma^\pm} W^\pm(\mathbf{N}^\pm \cdot \delta_{\mathbf{x}}\mathbf{X}^\pm)\,d\Sigma, \tag{6.3}$$

where we note that $\mathbf{N}_\Sigma \equiv \mathbf{N}^- = -\mathbf{N}^+$, so we can write the second contribution to Eq. (6.1) as

$$\delta_{\mathbf{X}} \int_V W(\mathbf{F})\,dV = \int_{V^+\cup V^-} \delta_{\mathbf{X}} W(\mathbf{F})\,dV + \int_\Sigma \mathbf{N}_\Sigma \cdot \left[W\delta_{\mathbf{x}}\chi^{-1}\right] d\Sigma, \tag{6.4}$$

where $[A] := A^+ - A^-$ if $A^\pm$ are the uniform limits of $A$ in approaching $\Sigma$ along it normal on both sides of $\Sigma$ (i.e., $[A]$ is the classical *jump* of continuum physics). The last term in Eqs. (6.3) and (6.4) is akin to that found in some variational formulations (MAUGIN and TRIMARCO [25]). Now in computing the first contribution to Eq. (6.4) we have

$$\int_{V^+\cup V^-} \delta_{\mathbf{X}} W^\pm(\mathbf{F})\,dV = -\int_{V-\Sigma} (\operatorname{div}_R \mathbf{T}) \cdot \delta_{\mathbf{X}}\chi + \int_{\partial V-\Sigma} (\mathbf{N}\cdot\mathbf{T})\cdot\delta_{\mathbf{X}}\chi\,dA + \int_\Sigma \mathbf{N}_\Sigma \cdot [\mathbf{T}\cdot\delta_{\mathbf{X}}\chi]\,d\Sigma, \tag{6.5}$$

where the *jump* term comes from the application of the divergence theorem in both $V^+$ and $V^-$ and the gluing back of the two resulting terms. Now we have the equilibrium equations

$$\begin{aligned} &\operatorname{div}_R \mathbf{T}^\pm = \mathbf{0} \quad \text{in} \quad V^\pm, \qquad \mathbf{T}^\pm = \partial W^\pm/\partial \mathbf{F}, \\ &\mathbf{N}\cdot\mathbf{T} = \mathbf{T}^d \quad \text{at} \quad \partial V - \Sigma \end{aligned} \tag{6.6}$$

and

$$\mathbf{N}\cdot[\mathbf{T}] = \mathbf{0} \quad \text{across} \quad \Sigma. \tag{6.7}$$

Therefore, collecting nonvanishing contributions from Eqs. (6.4) and (6.5), we obtain that

$$\delta\Phi = -\int_\Sigma N_\Sigma \cdot \left[W\delta_{\mathbf{x}}\chi^{-1} + \mathbf{T}\cdot\delta_{\mathbf{X}}\chi\right] d\Sigma. \tag{6.8}$$

At this point we follow HILL [14] – although this author does not use the same language and formalism (see also ROITBURD [28]) – by selecting the virtual variations in *direct* and *inverse* motions in the most realistic way. We cannot control the *direct motion* which, therefore, can suffer a jump in its first variation. But the situation is different for the inverse motion as, for a *coherent phase transformation*, we have continuity in the displacement of lattice sites, or, in continuous terms, continuity of the *material* displacement velocity, i.e. **V**. In variational terms this translates to the continuity of the variation $\delta_{\mathbf{x}}\chi^{-1}$. Consequently, in taking the jump of the general relation (4.11) at $\Sigma$, for a *coherent* interface, we obtain

$$[\delta_{\mathbf{X}}\chi] = -[\mathbf{F}]\cdot\delta_{\mathbf{x}}\chi^{-1}. \tag{6.9}$$

On account of the fact that

$$\begin{aligned}[\mathbf{N}_\Sigma\cdot\mathbf{T}\cdot\delta_{\mathbf{X}}\chi] &= -[\mathbf{N}_\Sigma\cdot\mathbf{T}\cdot\mathbf{F}\cdot\delta_{\mathbf{x}}\chi^{-1}] \\ &= -[\mathbf{N}_\Sigma\cdot\mathbf{T}\cdot\mathbf{F}]\cdot\delta_{\mathbf{x}}\chi^{-1} = -\langle\mathbf{N}_\Sigma\cdot\mathbf{T}\rangle\cdot[\mathbf{F}]\cdot\delta_{\mathbf{x}}\chi^{-1}\end{aligned} \tag{6.10}$$

since $\left(\langle A\rangle := \frac{1}{2}(A^+ + A^-)\right)$

$$[AB] = \langle A\rangle[B] + [A]\langle B\rangle \equiv \langle A\rangle[B] \tag{6.11}$$

for $A$ continuous across $\Sigma$, we can rewrite our final result as

$$\delta\Phi = \int_\Sigma \mathbf{f}_\Sigma\cdot\delta_{\mathbf{x}}\chi^{-1}\,d\Sigma, \tag{6.12}$$

where the *material force* $\mathbf{f}_\Sigma$, with support $\Sigma$, is defined as

$$\mathbf{f}_\Sigma := -\mathbf{N}_\Sigma\cdot[\mathbf{W}(\mathbf{F})\,\mathbf{1}_R - \langle\mathbf{T}\rangle\cdot\mathbf{F}] \equiv -\mathbf{N}_\Sigma\cdot[\mathbf{b}], \tag{6.13}$$

where the last relation is easily verified on account of (6.7). Obviously, **F**, just like **v** (*direct motion*), is discontinuous at a *coherent front*. The Maxwell–Hadamard representation of the jump of **F** is given by

$$[\mathbf{F}] = \mathbf{f}\otimes\mathbf{N}_\Sigma, \qquad \mathbf{f} \equiv [\mathbf{F}]\cdot\mathbf{N}_\Sigma, \tag{6.14}$$

where **f** is a vector field in $\mathbb{E}^3$. Obviously, then, $[\mathbf{F}]\cdot\delta_{\mathbf{x}}\chi^{-1} = \mathbf{f}(\mathbf{N}\cdot\delta_{\mathbf{x}}\chi^{-1})$. Passing to time derivatives instead of infinitesimal variations, we can rewrite Eq. (6.12) as

$$\dot{\Phi} = \int_\Sigma f_\Sigma \mathcal{V}_\Sigma\,d\Sigma, \tag{6.15}$$

where $\mathcal{V}_\Sigma$ is the scalar normal speed of the front (this is equal to the normal (material) speed of each phase), and

$$f_\Sigma = -\mathbf{N}_\Sigma\cdot[\mathbf{b}]\cdot\mathbf{N}_\Sigma = -[W(\mathbf{F})] + \langle\mathbf{N}_\Sigma\cdot\mathbf{T}\rangle\cdot\mathbf{f}. \tag{6.16}$$

We let the reader check that this is also equivalent to the formula (tr = trace)

$$f_\Sigma = -\mathcal{H}, \qquad \mathcal{H} := [\mathbf{W}(\mathbf{F}) - \mathrm{tr}\,(\langle \mathbf{T} \rangle \cdot \mathbf{F})] \tag{6.16'}$$

which suggests a resemblance of the function within square brackets to the Gibbs enthalpy at fluid phase transitions (compare, BOWEN [2]). Expressions such as (6.16) have been proposed by other authors with a view to treating the progress of *damaged zones* and the property of *delamination* (DEMS and MRÓZ [8]; PRADEILLES–DUVAL and STOLZ [26]). The first of Eqs. (6.16') may be viewed as a *surface balance equation* between the *Hugoniot–Gibbs* (our coinage) field quantity $\mathcal{H}$ – a *configurational force*, per se – which is known once we know the fields on both faces of $\Sigma$, and the *constitutive material force* $f_\Sigma$ which is responsible for the dissipation at $\Sigma$. The elementary rate of dissipation *per unit area* of $\Sigma$ is

$$\dot{\varphi} = f_\Sigma \mathcal{V}_\Sigma, \tag{6.17}$$

which is again in the traditional *bilinear form* of conventional *irreversible thermodynamics*.

**Particular case.** Obviously, we may also verify that an expanding spherical cavity centered at the origin of $\mathbf{X}$ coordinates, is also a special type of *coherent phase transition front*, as in that case there is no matter on the side $V^-$ (vacuum), and so with $\mathcal{V}_\Sigma = \mathbf{X} \cdot \mathbf{N}_\Sigma(\dot{l}/l)$, we recover the result of Sec. 5. As a matter of fact, with an internal surface $\mathcal{S}$ free of tractions, the *dissipation* then reduces to

$$\dot{\Phi} = \mathcal{M}(\dot{l}/l), \qquad \mathcal{M} = \int_{\mathcal{S}} W^+(\mathbf{X} \cdot \mathbf{N}_\mathcal{S})\, dA, \tag{6.18}$$

so that we can also write ($\mathbf{X} \cdot \mathbf{N}_\mathcal{S} = r$ the radius).

$$\dot{\Phi}(\mathcal{S}(t)) = f(3\dot{l}/l), \qquad f := \mathcal{V}(\mathcal{C}(l))W(\mathbf{F}(l(t))), \tag{6.19}$$

where $\mathcal{V}(\mathcal{C}) = 4\pi l^3/3$ is the volume of the spherical cavity. We see that $f$ is none other than the *energy of the* sphere of radius $l$ (which is actually a vacuum) equipped with a density equal to that of the elastic material. It is as if the expansion of the cavity swallowed an *elastic energy rate*. This is indeed *dissipation*. In other words, the expense of energy, although apparently distributed at the set of extension points $\mathcal{S}$ (integral over $\mathcal{S}$), is in fact distributed over the *whole set of points of the defect* $\mathcal{C}$, the cavity itself. This is the same result as in the recent analysis of DASCALU and MAUGIN [6] based on local balance equations expressed by means of generalized functions.

## 7. Irreversible thermodynamics

All expressions so far obtained for the *dissipation*, i.e,. Eqs. (4.18), (5.2), (5.7) and (6.17), during the *quasi-static* progress of the relevant *elastic defects*, are *per force, non-negative*. They are all in the traditional *bilinear form*. Three essential types of behaviours can be envisaged depending on whether: (i) the thermodynamical force involved is *bounded* (i.e., is constrained to remain in a closed set which here is a *closed convex* one, because all thermodynamic forces met here are scalars – and a segment of $\mathbb{R}$ is obviously convex) or not, and (ii) the dissipative phenomenon studied exhibits a *characteristic time* or not. As we know from *plasticity* and *fracture* (cf. MAUGIN [20], to whom we refer the reader for details), if the "force" is restrained to a convex set and no characteristic time is exhibited, the corresponding *dissipation* is only *homogeneous of degree one* in the corresponding "velocity", and the behaviour is said to be of the *"plastic" type*; if the "force" is not restrained and there is a characteristic time, the behaviour is said to be of the *"viscous"* type (or *"relaxation"* type) and the dissipation potential is homogeneous of degree *two* in the velocity; finally, if there exist simultaneously a closed convex set for the "force" and a characteristic time, then we say that the behaviour is of the *"viscoplastic"* type.

For instance, in the case of the straight-through crack, *Griffith's criterion of progress* is such that (cf. MAUGIN [20], Chapter 7):

$$\dot{l} \in N_c(G), \qquad \mathcal{D}^* = \mathrm{Ind}\, C(G), \qquad C(G) = [0, G_c] \in \mathbb{R}, \tag{7.1}$$

for *materials that fracture in the brittle regime*. Here $\mathcal{D}^*$ is the *pseudo-potential of dissipation*, which happens to be the so-called *indicator function of the convex set* $C$. The latter is just a segment of the real line with maximum energy release rate $G_c$. $N_c$ indicates the "cone" of outward unit normals to $C$. The first of Eq. (7.1) tells that there is possible *dissipation* and *progress of the crack* (but not necessarily) only when $G$ has reached the critical value $G_c$, which is indeed a *surface energy* of cohesion type in Griffith's original proposal. Similar criteria of progress can be devised for the *expanding cavity*, or for dislocations of the "displacement type" (dislocations *per se*), and of the "rotation type" (then called *disclinations*) on the basis of (4.18) or (5.7). The critical force then is the Peach–Koehler force.

Of greater originality is the case of the coherent phase-transition front. First, it is possible that no *dissipation* occurs at all in the present purely mechanical approach when, for $\mathcal{V}_\Sigma$ nonzero, the "force" vanishes identically, i.e.,

$$f_\Sigma := -[W(\mathbf{F}) - \langle \mathbf{N}_\Sigma \cdot \mathbf{T} \rangle \cdot \mathbf{F} \cdot \mathbf{N}_\Sigma] = -[W(\mathbf{F}) - \mathrm{tr}\,(\langle \mathbf{T} \rangle \cdot \mathbf{F})] = 0. \tag{7.2}$$

One can show that such a relation exactly corresponds to the *Hugoniot relation* that shock waves have to satisfy in elastic solids (cf. MAUGIN, POUGET *et al*, [23], p. 171), when thermal effects are discarded. For phase transitions, Eq. (7.2) accounts for the classical *Maxwell rule* (cf. GRINDFELD [11], TRUSKINOVSKY [33]). If

$f_\Sigma$ does not vanish, then we have *dissipation*, and the force $f_\Sigma$ may be called the *thermodynamical driving force* (compare to ABEYARATNE and KNOWLES [1]), of the front, as to have nonzero dissipation we have to write a relationship between $f_\Sigma$ and $\mathcal{V}_\Sigma$. The relationship may be of the "viscous", "plastic", or "viscoplastic" type. The most relevant case is the "plastic" type, for which there exists a critical $f_\Sigma^c$ such that $|f_\Sigma| < f_\Sigma^c$, no progress, while for $|f_\Sigma| = f_\Sigma^c$ there is a possible progress, and by analogy with Eq. (7.1) we can write the relationship

$$\mathcal{V}_\Sigma \in N_c(f_\Sigma), \qquad \mathcal{D}^* = \mathrm{Ind}\, C(f_\Sigma), \qquad C(F_\Sigma) = [0, f_\Sigma^c]. \tag{7.3}$$

The very interesting study of TRUSKINOWSKY [32] is an attempt at sustaining (7.3) on the basis of a smooth but sharp transition between the two phases – when viscosity, dispersion and temperature effects are taken into account. In general we can write the first of (7.3) as

$$\mathcal{V}_\Sigma = \frac{\partial \mathcal{D}^*}{\partial f_\Sigma}, \tag{7.3'}$$

where the degree of homogeneity of the pseudo-potential of dissipation $\mathcal{D}^*$ depends on the behaviour. The first work to try to give the *velocity* of a transition front was by MALOMED and RUMANOV [17]. The same idea transpires in CHEREPANOV [4]. Note that the critical $f_\Sigma$ is in fact an *energy* per unit volume (see the definition of $f_\Sigma$) and $f_\Sigma^c$ is a critical *volume* energy $W_c$.

Using the last remark it is salient to return to the case of a *cavity* if the latter progresses according to a criterion "à la Griffith", but with a critical *volume energy* (and *not* a critical surface energy, contrary to some authors, e.g., SIH and LIEBOWITZ [30]). If there is expansion of the cavity in these conditions, it means that the criterion is reached at the set of extension points $\mathcal{S}$ (Fig. 2). DASCALU and MAUGIN [6] were then able to formulate a *distributional* (i.e., in the sense of *generalized functions* or *distributions*) balance law of energy for the system "elastic body *plus* elastic defect". In the quasi-static regime and a steady progress of the defect, they have for the case of a cavity

$$D_t\{W + W_c H(l - r)\} = \mathrm{Div}_R(\mathbf{T} \cdot \mathbf{v}) + \mathbf{T}^d \cdot \mathbf{v}\delta(\partial\Omega), \tag{7.4}$$

where $D_t$ and $\mathrm{Div}_R$ are *distributional derivatives* with respect to time and the $\mathbf{X}s$, $\delta(\partial\Omega)$ is the delta generalized function with support $\delta\Omega$, and $H$ is the *radial* Heaviside function (of the spherical cavity, indeed). Equation (7.4) valid at all points of $\mathbb{E}^3$ includes the natural boundary condition at $\partial\Omega$, and the *criterion of expansion* at $\mathcal{S}$. It is a *conservation equation* which tells that the *energy of the system "solid* plus *defect"* is conserved. But the "energy rate" of the defect is none other than the *dissipation* in total agreement with the present derivation.

## 8. Accounting for inertia. Remark

In the absence of distributed material inhomogeneities, at all regular points in the body, the fully dynamical balances of *physical momentum* Eq. $(4.12)_1$ *and pseudomomentum* (4.15) are given by (cf. MAUGIN [19])

$$\frac{\partial}{\partial t}\mathbf{p}\Big|_{\mathbf{X}} - \mathrm{div}_R\mathbf{T} = \mathbf{0}, \tag{8.1}$$

and

$$\frac{\partial}{\partial t}\mathcal{P}\Big|_{\mathbf{X}} - \mathrm{div}_R\mathbf{b} = \mathbf{0}, \tag{8.2}$$

where $\mathbf{p} = \rho_0\mathbf{v}(\mathbf{X}, t)$, while the pseudo-momentum *covariant, material* vector $\mathcal{P}$ is defined by

$$\mathcal{P} := -\mathbf{F}^T \cdot \mathbf{p} = -\rho_0\mathbf{F}^T \cdot \mathbf{v} = \rho_0\mathbf{C} \cdot \mathbf{V}, \tag{8.3}$$

and the *dynamical Eshelby stress* is given by

$$\mathbf{b} = -(\mathcal{L}\mathbf{1}_R + \mathbf{F}^T \cdot \mathbf{T}), \tag{8.4}$$

where $\mathcal{L}$ is none other than the Lagrangian density per unit volume of $\mathcal{K}_R$:

$$\mathcal{L} = \frac{1}{2}\rho_0\mathbf{v}^2 - W(\mathbf{F}) = \frac{1}{2}\rho_0\mathbf{V} \cdot \mathbf{C} \cdot \mathbf{V} - W(\mathbf{F}). \tag{8.5}$$

In Eqs. (8.3) and (8.5), $\mathbf{V}$ is the *material velocity* defined in Eq. $(2.3)_3$ and $\mathbf{C}$ is the *Green finite-strain tensor* defined in (2.7). The latter acts as *deformed metric* on $\mathcal{M}^3$ (as shown by the last of (8.3)). Applying the *objectivity* requirement, we can also introduce an energy $\overline{W}(\mathbb{E})$; and (8.4) takes on the following *explicit form*:

$$\mathbf{b} = \left(\overline{W}(\mathbb{E}) - \frac{1}{2}\rho_0\mathbf{V} \cdot \mathbf{C} \cdot \mathbf{V}\right)\mathbf{1}_R - \mathbf{C} \cdot \mathbb{S}, \qquad \mathbb{S} = \partial\overline{W}/\partial\mathbb{E}, \tag{8.6}$$

where $\mathbb{S}$ is the second Piola–Kirchhoff stress tensor (a *material contravariant symmetric tensor* on $\mathcal{M}^3$).

As $\mathbf{b}$ already intervened as a flux in all computations of the elementary dissipation in Secs. 4 through 6, it is sensible to imagine, on the basis of standard *theorems of transport of continuum mechanics* (Reynolds), that in the fully dynamical case the role of $\mathbf{b}$ is replaced by that of an *effective Eshelby stress*

$$\mathbf{b}^{\mathrm{dyn}} := \mathbf{b} + \mathcal{P} \otimes \overline{\mathbf{V}}, \tag{8.7}$$

where $\overline{\mathbf{V}}$ is the *material velocity* of the *extension points of the defect*. This was indeed proved by MAUGIN [22] in the case of cracks in *dynamical fracture* in both elasticity

and electroelasticity (where $\mathcal{P}$ has a non-mechanical component as well). The last term in (8.7) is important because it provides the necessary term which, at the set of defect points $\mathcal{S}$, where $\mathbf{V} = \overline{\mathbf{V}}$ in the first order of approximation (DASCALU and MAUGIN [5]), helps either to pass from the *Lagrangian* density present in **b** to the *Hamiltonian* density to be found in the expression of the energy-release rate in dynamical brittle fracture, or to show that inertia disappears altogether from the driving force acting on a coherent phase-transition front (cf. TRIMARCO and MAUGIN [31]), even in the full dynamics of thermoelastic conductors.

## 9. Conclusions and prospects

The general philosophy to be extracted from the present type of approach is that the *material manifold* is the true arena of all phenomena related to distributed or abrupt *material inhomogeneities, elastic singularities* being material inhomogeneities in their own right as they do exhibit "forces" (*configurational forces*) and "dissipation" (of these "forces") in displacement fields, or velocities, or progress rates which are true *material fields, per se*. The approach is quite general and suited to all types of *elastic defects* with various "dimensions". We have at hand all the basic equations to establish the corresponding generalizations to *electroelasticity* (see already DASCALU and MAUGIN [7]) and *magnetoelasticity*. The general expressions of Eshelby stresses in these cases were given by one of the author (MAUGIN [19] – also [21], Chapter 8) and all what is required for these extensions is to be found in existing volumes (MAUGIN [18], MAUGIN, POUGET *et al.* [23]). In some works, especially those involving jumps such as with interfaces at equilibrium, what we called the *Eshelby stress*, is sometimes referred to the "chemical potential" tensor, without attributing it to Eshelby (BOWEN [2], ROITBURD [28]; GRINFELD [11]). But it must be emphasized that the Eshelby stress or, more generally, the *canonical* stress tensor is a general concept of *field theory* (cf. MAUGIN [21]) whose field of application cannot be reduced to mixtures and interfaces only.

What is perhaps more original is that for *ferroelectrics* and *ferromagnetics*, some of the results can also be applied in the case of *rigid* bodies. For instance, a *magnetic domain wall* is a defect([1]) in the spatial arrangement of magnetic spins. In a quasi-static movement it may generate a *dissipation* (this is what happens during magnetic hysteresis at a microscopic scale where the wall moves in a landscape of energy barriers due to lattice defects) in agreement with standard formulas such as (6.15)–(6.17) on the condition to replace the direct-motion gradient by the *magnetization gradient*. The criterion of progress of the wall may be of the *viscoplastic type* or of the more *singular*, plastic type, the magnetic field

([1]) Traditionally this is considered as a *two-dimensional* (or planar) *defect* by *physicis* (cf. KLÉMAN [15]). But in the above-exposed view it is truly a three-dimensional defect (it is similar to the phase-transition front, which is what it is!) and it is its *set of extension points* which is planar and constitutes the (in some mathematical limit) zero-thickness wall.

playing the role previously played by stress; such behaviours were indeed exhibited from a microscopic model in SABIR and MAUGIN [29] in relation with Néel's model of irreversible magnetization processes. We leave such fruitful developments to future works. These works will also include thermal effects, especially for the phase-transition case where they cannot be ignored.

## 10. Acknowledgements

This work was started in the friendly atmosphere of the Institute of Applied Mathematics at Università di Pisa, when G.A.M was a visiting Professor of the C.N.R. (April 1993). C.T. acknowledges the support of G.N.F.M. of C.N.R. and M.U.R.S.T.

## References

1. R. ABEYARATNE and J.K. KNOWLES, *On the driving traction acting on a surface of strain discontinuity in a continuum*, J. Mech. Phys. Sol., **38**, 345–360, 1990.
2. R.M. BOWEN, *Toward a thermodynamics and mechanics of mixtures*, Arch. Rat. Mech. Anal., **24**, 370–403, 1967.
3. B. BUDIANSKY and J.R. RICE, *Conservation laws and energy release rates*, J. Appl. Mech., **40**, 201–203, 1973.
4. G.P. CHEREPANOV, *Configurational forces in the mechanics of a solid deformable body*, P.M.M. (J. Appl. Math. Mech.), **49**, 456–464, 1985.
5. C. DASCALU and G.A. MAUGIN, *Material forces and energy-release rates in homogeneous elastic bodies with defects* [in French], C.R. Acad. Sci. Paris, **II-317**, 1135–1140, 1993.
6. C. DASCALU and G.A. MAUGIN, *The energy of elastic defects*, Proc. Roy. Soc. Lond., **A.445**, 23–37, 1994.
7. C. DASCALU and G.A. MAUGIN, *Energy-release rates and path-independent integrals in electroelastic crack propagation*, Int. J. Engng. Sci., **32**, 755–765, 1994.
8. K. DEMS and Z. MRÓZ, *Stability condtions for brittle-plastic structures with propagating damage surfaces*, J. Struct. Mech., **13**, 95–122, 1985.
9. J.D. ESHELBY, *The force on an elastic singularity*, Phil. Trans. Roy. Soc. Lond., **A244**, 87–112, 1951.
10. J.D. ESHELBY, *Energy relations and the energy-momentum tensor in continuum mechanics*, [in:] Inelastic Behaviour of Solids, M.F. KANNINEN, E.F. ADLER, A.R. ROSENFELD and R.I. JAFFE [Eds.], pp. 7–115, McGraw Hill, New York 1970.
11. M.A. GRINFELD, *Thermodynamic methods in the theory of heterogeneous systems*, Longman, Harlow 1991.
12. W. GÜNTHER, *Über einige Randintegrale der Elastodynamik*, Abh. Braunschw. Wiss. Ges., **14**, 54–72, 1962.
13. G. HERRMANN, *Material momentum tensor and path-independent integrals of fracture mechanics*, Int. J. Solids Structures, **18**, 319–326, 1982.
14. R. HILL, *Energy-momentum tensors in elastostatics: some reflections on the general theory*, J. Mech. Phys. Sol., **34**, 305–317, 1986.
15. M. KLEMAN, *Points, lines and walls*, J. Wiley, Chichester, U.K. 1989.
16. J.K. KNOWLES and E. STERNBERG, *On a class of conservation laws in linearized and finite elastostatics*, Arch. Rat. Mech. Anal., **44**, 187–211, 1972.
17. B.A. MALOMED and E.I. RUMANOV, *Intrinsic velocity of the interphasal boundary*, Dokl. Akad. Nauk. SSSR., **284**, 6, 1984.
18. G.A. MAUGIN, *Continuum mechanics of electromagnetic solids*, North-Holland, Amsterdam 1988.
19. G.A. MAUGIN, *Sur la conservation de la pseudo-quantité de mouvement en mécanique et électrodynamique des milieux continus*, C.R. Acad. Sci. Paris, **II-311**, 763–768, 1990.
20. G.A. MAUGIN, *The thermomechanics of plasticity and fracture*, Cambridge University Press, U.K. 1992.
21. G.A. MAUGIN, *Material inhomogeneities in elasticity*, Chapman and Hall, London 1993.

22. G.A. MAUGIN, *On the J-integral and energy-release rates in dynamical fracture*, Acta Mech., **105**, 33–47, 1994.

23. G.A. MAUGIN, J. POUGET, R. DROUOT and B. COLLET, *Nonlinear electromechanical couplings*, J. Wiley, New York 1992.

24. G.A. MAUGIN and C. TRIMARCO, *Pseudo-momentum and material forces in nonlinear elasticity: variational formulations and application to brittle fracture*, Acta Mech., **94**, 1–28, 1992.

25. G.A. MAUGIN and C. TRIMARCO, *Note on a mixed variational principle in finite elasticity*, Rend. Mat. Acc. Lincei, **9**, 69–74, 1992.

26. R.M. PRADEIL-DUVAL and C. STOLZ, *Sur le problème d'évolution des solides avec changement de phase irréversible*, C.R. Acad. Sci. Paris, **II-313**, 297–302, 1991.

27. D. ROGULA, *Forces in material space*, Arch. Mech., **29**, 705–715, 1977.

28. A.L. ROITBURD, *Martensitic transformation as a typical phase transition in solids*, [in:] Solid State Physics, Vol. 33, pp. 317–407, Academic Press, New York 1978.

29. M. SABIR and G.A. MAUGIN, *Microscopic foundations of the Barkhausen effect*, Arch. Mech., **40**, 829–841, 1988.

30. G.C. SIH and H. LIEBOWITZ, *On the Griffith energy criterion for brittle fracture*, Int. J. Solids Struct., **3**, 1–22, 1967.

31. C. TRIMARCO and G.A. MAUGIN, *Configurational forces and coherent phase transitions in thermoelastic solids*, [in:] IUTAM-ISIMM Symp. on Anisotropy, Inhomogeneity and Nonlinearity in Solids (Nottingham 1994) D.F. PARKER and A.H. ENGLAND [Eds.], Kluwer, Amsterdam 1995.

32. L.M. TRUSKINOWSKY, *Dynamics of non-equilibrium phase boundaries in a heat-conducting nonlinearly elastic medium*, P.M.M., **51**, 777–784, 1987.

33. L. TRUSKINOWSKY, *Kinks versus shocks*, [in:] Shock-Induced Transitions in General Media, R. FOSDICK, E. DUNN and M. SLEMROD [Eds.], Springer-Verlag, Berlin 1992.

UNIVERSITÉ PIERRE ET MARIE CURIE,
LABORATOIRE DE MODÉLISATION EN MÉCANIQUE, PARIS, FRANCE
and
UNIVERSITÀ DI PISA,
INTITUTO DI MATEMATICHE APPLICATE "U. DINI", PISA, ITALY.

*Received October* 3, 1994.

Arch. Mech., 47, 1, pp. 101–116, Warszawa 1995

# Propagation of an effective shear stress as a solitary wave and possibility of non-crystallographic slip in polycrystals

A. PAWEŁEK (KRAKÓW), S. PILECKI (WARSZAWA)
and Z. JASIEŃSKI (KRAKÓW)

THE NONLINEAR solitary waves in a system of a moving dislocation group are reported. It is shown that the propagation of the mobile dislocations can be described by the solitary wave solution of the nonlinear partial differential equation which is a well-known one in hydrodynamics, heat conductivity or diffusion. In this way the shape of the nonlinear dislocation density wave has the Taylor shock wave profile which propagates as a step front. Some experimental data on the formation of the dislocation patterns during plastic deformation (especially shear bands) are also briefly analysed in terms of self-organization processes. The results obtained in this paper are discussed in the context of the concept of the so-called "plaston" which is applied to the proposed explanation of the nature of the shear band formation and propagation through grain boundaries in polycrystalline metals.

## 1. Introduction

DESCRIPTION OF the dynamic equilibrium between the process of dislocation diffusion, multiplication and annihilation, as well as of the formation of dislocation structure during various kinds of plastic deformation of crystals in terms of self-organization, bifurcation and/or dislocation cooperative processes, becomes more and more attractive for physicists and mechanicians [e.g. 1–7]. On the other hand, it has been pointed out [6, 7] that also the soliton processes – being, in general, the consequence of the equilibrium between the nonlinearity and energy dissipation or medium dispersion – may also play a very important role leading to the formation of well-organized dislocation patterns.

The soliton nature of a single dislocation is quite well reported [e.g. 8–18]. However, to our knowledge, no attempt has been made to describe the behaviour of a moving group of coplanar dislocations in terms of soliton processes. The dynamics of a coplanar group of dislocations resulting in a formation of a single slip line at a microscopic level is the first basic element in a hierarchy of the organization processes responsible for the formation of macroscopic Lüders bands (LB), Portevin–LeChatelier bands (PLB) and shear (slip) bands (SB) in deformed crystals. It also creates a skeleton for the formation of a dislocation substructure (patterning). Therefore, the soliton-like behaviour of a moving dislocation group deduced in other papers [6, 7] on the basis of nonlinear *ordinary* differential equation, as well as some experimental arguments, which we present briefly in Sec. 2, justify the aim of this paper. It is to search the nonlinear *partial* differential

equation which would describe the space-time evolution of the shear stress or dislocation density exactly in terms of soliton processes.

## 2. Experimental background

The space-time organization of dislocations within the slip bands during LB and PLB propagation or into shear bands, observed at high strains, is the very first requirement for strain localization resulting in a macroscopic instability of plastic flow [e.g. 19–22]. The organization processes originate at the microscopic level, where dislocations form single slip lines. At the mesoscopic level the slip lines cluster into slip bands, and finally, at the macroscopic level, the latter form well-organized bands of LB or PLB type. A similar organization of dislocations occurs during secondary straining (change of deformation path) characteristic of coarse slip, or during formation of microshear bands at high strains, e.g. in channel-die testing. In this case shear bands observed at a macroscopic level represent organized objects composed of a family of microshear bands, Fig. 1.

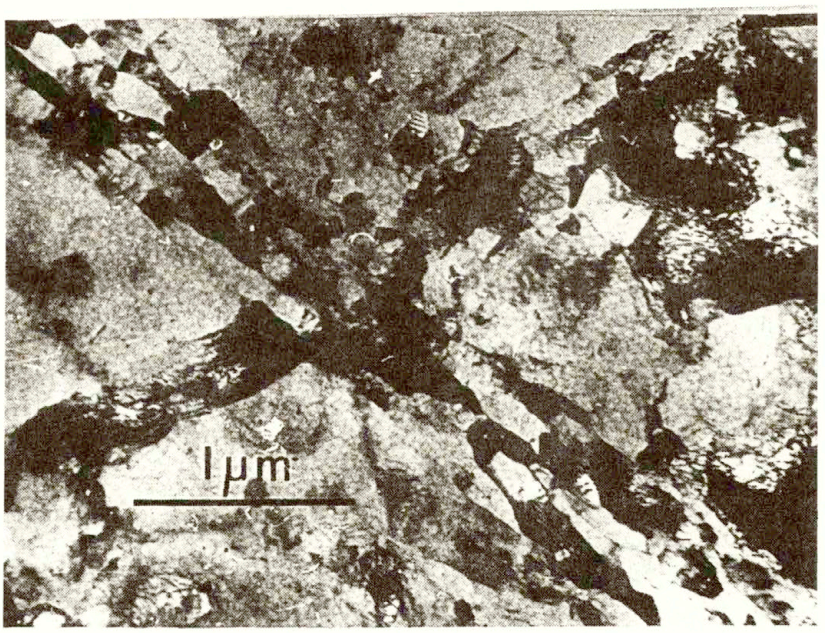


FIG. 1. The structure of macroshear band built up of a family of microshear bands [24].

On the other hand, one intriguing dynamic behaviour of a moving dislocation group is the formation of a macroshear band, which often corresponds to the early stage of the necking, e.g. as in the case of deformed polycrystalline stainless steel, Fig. 2 [24]. One can see that the micro-necking is a consequence of the localization of strain along the long and very thick zone propagating, perhaps,

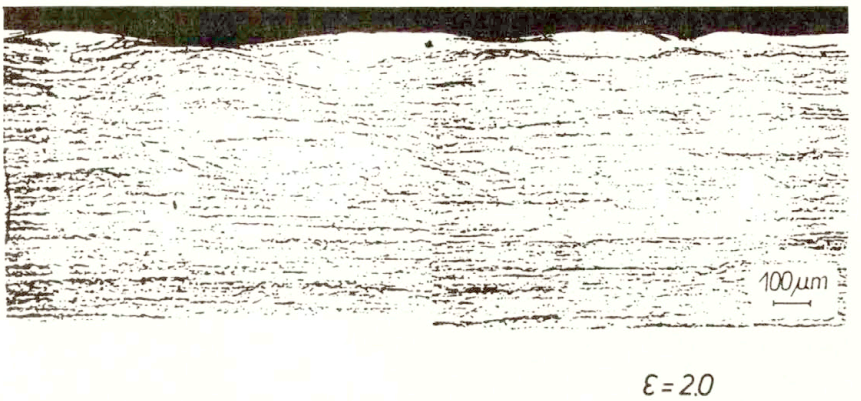


FIG. 2. Transcrystalline propagation of the shear bands (seen within the neck) through many grains in stainless steel [24].

in a transcrystalline way through many grains (here the grain size is equal to about 30 μm). This experimental observation suggests that in this case there is no essential change in the direction of the passage of plastic zone from one grain to the other. Many other experimental observations [5, 23, 26] also suggest the possibility of a transcrystalline passage of the plastic zone through grain boundaries. If it is so, then we suppose that the dynamic and nonlinear processes involved in the space-time organization of the shear band, would be explained on the basis of the solitary wave behaviour of a system of moving dislocations.

## 3. Theory

Starting up from the equation of continuity for a coplanar array of moving dislocations (generated e.g. by the Frank–Read source and distributed continuously), let us consider the dynamics of a group of moving dislocations emitted from a source in terms of a, recently very popular, concept of the dislocation flux which would obey the equation formally similar to the diffusion or heat transfer. In a one-dimensional space we may define the dislocation flux

$$J(x,t) = \rho(x,t)\, v(x,t) \tag{3.1}$$

which satisfies the equation of continuity

$$\frac{\partial \rho(x,t)}{\partial t} = -\frac{\partial J(x,t)}{\partial x}, \tag{3.2}$$

where $\rho(x,t)$ is the linear density and $v(x,t)$ is the dislocation velocity [see e.g. 27, 28]. The general problem to be solved is the determination of the dislocation flux $J(x,t)$ during plastic flow and especially during its localization. However, we restrict our treatment to the one-dimensional case, i.e. we consider a dislocation flux only in one direction corresponding to the one active slip system.

It is well-known from diffusion theory (e.g. [29]) that the most common factor giving rise to directed movements (i.e. diffusion flux of matter) is the gradient of chemical potential $\partial\mu/\partial x$. Chemical potential of $i$-th component is [29]

$$\mu_i = \left(\frac{\partial G}{\partial n_i}\right)_{p,T,n_k,\ i\neq k} \tag{3.3}$$

or

$$G = \sum \mu_i n_i, \tag{3.4}$$

where $G$ is a free enthalpy of a system consisting of $k$ components and $n_i$ is a number of elements of $i$-th component of a system. For example, chemical potential of vacancies is therefore equal to the free enthalpy per one vacancy. One can also use the so-called macroscopic chemical potential [e.g. 30]

$$\mu_a = \left(\frac{\partial G}{\partial n_a}\right)_{p,T} \tag{3.5}$$

taking for $G$ free enthalpy of the whole system, and for $n_a$ – total number of atoms in the system. Macroscopic potential has a phenomenological character and has nothing to do with the real microscopic structure of a solid. In the case of external load acting on a solid, the chemical potential is modified [30, 31]

$$\mu_i = \left(\frac{\partial F}{\partial n_i}\right)_{\sigma,T,n_k} \pm W, \tag{3.6}$$

where $F$ is a free energy, $W = \sigma V_A$ is a work per component element, $\sigma$ is stress and $V_A$ is an activation volume.

Equations (3.3), (3.5) or (3.6) cannot describe the chemical potential of dislocations in the usual thermodynamic sense as it is possible in the case of vacancies, since the dislocations are not thermodynamically stable, i.e. there is no equilibrium state for total dislocation density in any crystal.

The essence of our approach consists in the fact that these equations may be applied only to the mobile dislocations, because the motion of dislocations through the crystal is a thermally activated process in a wide range of temperatures and strain rates. In the case of fcc-crystals, the velocity of dislocations is controlled by the process of the intersection of gliding dislocations in active slip planes with the forest dislocations from inactive slip systems. The process is by nature thermally activated. In this way Eqs. (3.3), (3.5) or (3.6) are of physical meaning when quantity $G$ is just the free enthalpy of activation for this process (commonly called the activation energy; see Fig. 3). Figure 3 illustrates a process of thermally activated motion of dislocation through the crystal. The parameters

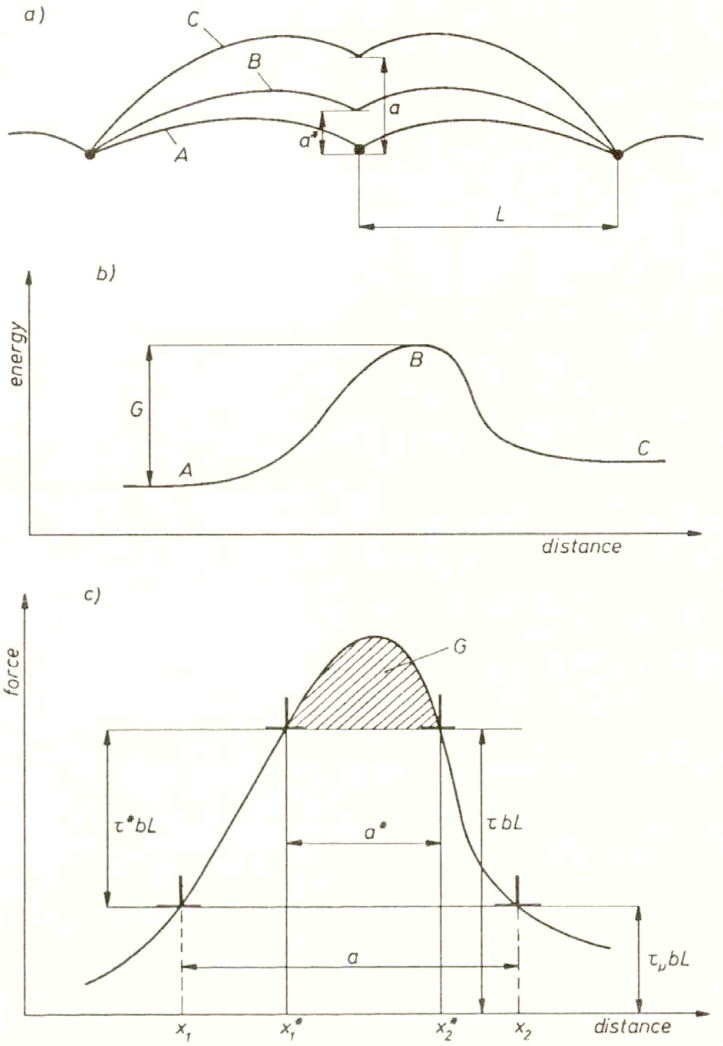


FIG. 3. A schematic illustration of the mechanism of thermally controlled dislocation motion in fcc-crystals.

describing this process are the quantities involved in the Arrhenius type of equation for strain rate $\dot{\varepsilon} = b\rho v$

$$\dot{\varepsilon} = \dot{\varepsilon}_0 \exp\left(-\frac{G}{kT}\right) \tag{3.7}$$

or dislocation velocity

$$v = v_0 \exp\left(-\frac{G}{kT}\right), \tag{3.7'}$$

where $G = G^* - (\tau - \tau_\mu)V$ or $G = G_0 - \tau V$ and $G^*$ is the free enthalpy of activation for zero applied stress ($\tau = 0$), $\tau_\mu$ is the internal stress, $\tau^* = \tau - \tau_\mu$ is the effective stress, $V = bLa^*$ is the activation volume, $a^*$ is the activation length, $G_0 = G^* + \tau_\mu bLa$, where $a$ is the activation length at zero stress ($0 \leq a^* \leq a$), $L$ is the distance between the obstacles (forest dislocations), $b$ is the magnitude of the Burgers vector and $v_0$ and $\dot{\varepsilon}_0 = b\rho v_0$ are the constants (for more details see also [13–16, 22, 39]).

Moreover, the Eq. (3.7)′ involves implicitly the space-time dependent flow stress $\tau(x,t)$, [or effective shear stress $\tau^*(x,t)$], and thus it is equivalent to the commonly accepted power relationship between the stress and dislocation velocity, $v(x,t)$, which may be written in the following form

$$v(x,t) = v_0 \left[\frac{\tau(x,t)}{\tau_0}\right]^m, \tag{3.8}$$

where $v_0, \tau_0, m$ are the constants ($v = v_0$ at $\tau = \tau_0$), and $m \equiv \partial \ln v / \partial \ln \tau^* = \tau^* V / kT$. Furthermore, from Fig. 3 it follows that the displacement of dislocation over the very short distance $\Delta x \leq a^* = x_2^* - x_1^*$ (in comparison to the distance passed by dislocation during running time, i.e. when $\Delta x \gg a$) is of a diffusion character, and the chemical potential $\mu$ for dislocation activation may be expressed by the free enthalpy of activation per dislocation unit length if this unit is assumed to be equal to the average distance $L$ between the forest dislocations

$$\mu = \frac{G}{L} = \frac{G_0}{L} - \tau b a^*, \tag{3.9}$$

or simply ($L \equiv 1$)

$$\mu = \mu_0 - \tau b a^*, \tag{3.10}$$

where $\mu_0 = G_0/L = G^*/L + \tau_\mu ba =$ constant at a given strain rate $\dot{\varepsilon}$, temperature $T$ and structure (influencing $\tau_\mu$).

The role of thermal activation in a dislocation motion is very important from the macroscopic point of view. Namely, poor gliding of dislocations in a slip plane, i.e. the motion of dislocations between the obstacles, is of a very non-diffusive character (a possible thermal activation of very small Peierls barriers in fcc-crystals may be completely neglected), and occurs due to only mechanical applied force $b\tau(x,t)$. However, the time of this motion (running time) is considerably less than the time during which the dislocation must wait for thermal activation (waiting time). The velocity of dislocations and thus the motion of all active dislocations through the crystal, understood as a macroscopic process, is so essentially controlled by thermal activation processes that this movement is indeed of diffusion character from a macroscopic point of view. This is not a paradoxical statement with regard to the relation between the running and waiting time.

Besides, from Fig. 3 it follows that for $\tau = 0$ (i.e. when diffusive displacement of dislocation, $\Delta x \leq a$, is potentially equal to a maximum value $a = x_2 - x_1$)

$$G(x \leq x_1) = G^* + \tau_\mu b L a \equiv G_0 \tag{3.11}$$

whereas, for a given particular process, when $\tau \neq 0$ and $0 \leq a^* < a$, the mechanical force increases up to its maximum value $F = \tau b$ (per unit length of dislocation). Thus the diffusion displacement of the dislocation from the distance $x$, $(x_1^* \leq x \leq x_2^*)$, to the distance $x + \Delta x$, $(x_1^* \leq x + \Delta x \leq x_2^*$ and $\Delta x \leq a^*)$, requires the energy

$$\Delta G = G(x + \Delta x) - G(x) = -\Delta\tau b L x - \tau b L \Delta x, \tag{3.12}$$

or the change of chemical potential of activated dislocation

$$\Delta\mu = \mu(x + \Delta x) - \mu(x) \cong -\Delta\tau b x - \tau b \Delta x. \tag{3.13}$$

In this way we may relate the generalized thermodynamic force, understood as a gradient of chemical potential of dislocation activation, $\operatorname{grad}\mu$, to the mechanical force, $\tau b$, acting on a dislocation unit length $L$ in a given process

$$\operatorname{grad}\mu = \frac{\partial\mu}{\partial x} = -\tau b\left[1 + \frac{\partial \ln\tau}{\partial \ln x}\right]. \tag{3.14}$$

In further consideration we apply other analogies to the diffusion theory. Making use of the macroscopic chemical potential (e.g. Eq. (3.5)), we get for the flux of activated dislocations the formulae of the form proposed by ONSAGER (see e.g. [32])

$$J = M\frac{\partial\mu}{\partial x}, \tag{3.15}$$

where $M = -B\rho$ is the dislocation mobility in the range of diffusion displacement, $0 < \Delta x < a^*$, and $B = D/kT$ is the mobility according to Einstein (see e.g. [33]) where the quantity $D$ plays the role of the diffusion coefficient for the thermally activated process of the "diffusion" motion of dislocations through the forest dislocations. Consequently, we may relate the gradient of chemical potential $\mu$ to the gradient of concentration, i.e. the density of mobile dislocations which are undergoing thermal activation

$$-\operatorname{grad}\mu = -\frac{\partial}{\partial x}\left[kT \ln\frac{\rho}{\rho_0}\right] = -\frac{kT}{\rho}\frac{\partial\rho}{\partial x}, \tag{3.16}$$

where $\rho_0$ is a constant for a given deformation process, and constitutes the characteristic value of the density of mobile dislocations to which the mobile dislocation density $\rho(x, t)$ tends in any process of plastic flow. We should like to emphasize

here again, using the Eqs. (3.14), (3.15) and (3.16), that the basic conclusion from our diffusion-like approach to the macroscopic motion of dislocations in a real crystal, is that the maximal mechanical force required for this motion is closely related to the gradient of chemical potential for dislocation activation which, in turn, is proportional to the gradient of mobile dislocation density. In other words, the gradient of chemical potential for dislocation activation, determined by the formulae (3.14), decides on the macroscopic motion of dislocation through the real crystal.

Using Eqs. (3.15) and (3.16) we get for thermally activated motion of dislocations the following formulae analogous to that for heat conduction or diffusion processes

$$J(x,t) = -D\frac{\partial \rho(x,t)}{\partial x} \tag{3.17}$$

and finally, using Eq. (3.2), we get the evolution equation for density of activated dislocations which is analogous to the Fourier law of heat transfer or to the second Fick law of diffusion

$$\frac{\partial \rho(x,t)}{\partial t} = D\frac{\partial^2 \rho(x,t)}{\partial t^2}. \tag{3.18}$$

This equation is the simplest version of the equation discussed earlier by PILECKI [1, 34–38], and later also by AIFANTIS with co-workers [2–4, 40–42], i.e the Eq. (3.18) is related to the "poor extracted" case of dislocation motion where the terms responsible for both the multiplication ($\sim$ to $\rho$) and annihilation ($\sim$ to $\rho^2$ or $\rho^3$) of dislocations are here neglected.

In order to determine the flux of activated dislocations, $J(x,t) = \rho(x,t)v(x,t)$, it is necessary to find the evolution equation for dislocation velocity $v(x,t)$, or evolution equation for stress $\tau(x,t)$, since the relation between these quantities is known (Eq. (3.8)). For this purpose we use the Eqs. (3.1) and (3.17); however, in view of the fact that for any deformation process we have a spectrum of activation energies, we should replace therefore the dislocation flux, $J = \rho v$, by the average value which may be assumed simply as $J = \rho v/2$. Thus, Eq. (3.17) may be written in the new form

$$\frac{1}{2}\rho(x,t)v(x,t) = -D\frac{\partial \rho(x,t)}{\partial x}. \tag{3.19}$$

The most important consequence of our basic conclusion is that the Eq. (3.19) has a form of the Cole–Hopf transformation known in mathematical theory of soliton (see e.g. [43]),

$$v(x,t) = -2D\frac{\rho_x}{\rho}, \tag{3.20}$$

where it is assumed that $\rho_x \equiv \partial\rho/\partial x$. This transformation maps solutions of the heat transfer type equation (3.18) onto solutions of the Burgers equation which may be written in the following form:

$$\frac{\partial v(x,t)}{\partial t} + v(x,t)\frac{\partial v(x,t)}{\partial x} - D\frac{\partial^2 v(x,t)}{\partial x^2} = 0 \tag{3.21}$$

or simply in the form

$$v_t + vv_x - Dv_{xx} = 0, \tag{3.22}$$

where (and hereafter) $v_t \equiv \partial v/\partial t$, $v_x \equiv \partial v/\partial x$ and $v_{xx} \equiv \partial^2 v/\partial x^2$. (One can see that the assumption on the average dislocation flux (Eq. (3.19)) is not necessary since without this assumption we get also Eq. (3.22) in which the coefficient $D$ will be replaced by $D/2$). In this way the Eq. (3.20) represents, at the same time, one of the possible physical interpretations of the pure mathematical Cole–Hopf transformation.

Using Eqs. (3.8) and (3.18) we get the general evolution equation for effective shear stress (for simplicity we write $\tau$ instead of $\tau^*$)

$$\tau_t + C\tau^m\tau_x - D(m-1)\tau^{-1}\tau_x^2 - D\tau_{xx} = 0, \tag{3.23}$$

where constant $C = v_0/\tau_0^{-m}$. The general solutions to Eq. (3.23) are not known as yet. At present the problem is open and too difficult to be solved generally since this equation – in spite of being the nonlinear partial differential equation having, maybe, the solitary wave solutions – is not known in the mathematical theory of soliton. However, it will be considered in further works. Here we restrict ourselves to the simple case where $m = 1$, i.e. to the case of linear stress-velocity relation which is also often experimentally observed, for instance in copper, silver or aluminum. In this case Eq. (3.23) is also the BURGERS equation [44]

$$\tau_t + \tau\tau_x - D^*\tau_{xx} = 0, \tag{3.24}$$

if we replace in Eq. (3.24) $x$ by $Cx$, where now $C = bB$ and new coefficient $D^* = D/b^2B^2$. It should be emphasized here that the case $m = 1$ is equivalent to the assumption that the second term in the right-hand side of Eq. (3.14) may be neglected, i.e. the case in which the generalized thermodynamic force, $-\text{grad}\,\mu$, is just almost equal to the average maximal mechanical force, $b\tau/2$ (here we replace $\tau$ by $\tau/2$ since the spectrum of activation energy implies the similar spectrum of maximal mechanical forces for the same deformation process at a given temperature and strain rate). It is so because the Eq. (3.24) may then be obtained directly from Eqs. (3.14), (3.16) and (3.22) by using the new Cole–Hopf transformation $\tau = (-2kT/b)\rho_x/\rho$ which is equivalent to the transformation (3.20) just if $v = bB\tau$.

One of the analytical, well-known solutions to the Eq. (3.24) or (3.22) is of the solitary wave-type, the form of which is the Taylor shock profile given by (see e.g [10, 44]

$$\tau(x,t) = \alpha D\left[1 - \tanh\frac{1}{2}(x - D\alpha t)\right], \tag{3.25}$$

where $2\alpha D = \tau_\infty$ is the shear stress at $x \to -\infty$, and $\alpha\tau_\infty/2 \equiv w$ is the velocity of propagation of the step-like front of localized shear stress within a narrow region of the $x$-space (Fig. 4). It is very interesting and necessary to emphasize here that the equation similar to Eq. (3.8) has been derived in a completely different way by WEERTMAN and FALLANSBEE [48]. The solution of their equation, again quite similar to that given by (3.9), describes the propagation of the shock-type profile of the elastic-plastic wave of steady-state finite amplitude.

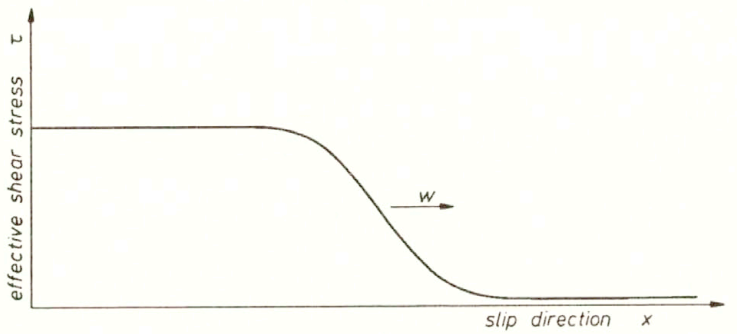


FIG. 4. Step-like front of the solitary wave impulse of effective shear stress.

In agreement with the above considerations, we can now treat the motion of a group of dislocations as a nonlinear wave process, i.e each local propagation of the dislocation group inside the crystal (induced e.g. due to the Frank-Read source operation in the simplest case, or in a more general case – related to the slip and/or shear band propagation) may be treated as a shear stress wave impulse (hereafter called simply SSW impulse) being, at the same time, of the solitary wave character, very similar to the propagation of the Taylor shock profile described analytically by the formulae (3.9). Therefore, below in Sec. 4, we would like to discuss (qualitatively) the formation and propagation of the shear bands in terms of the solitary wave processes as a specific interaction of the SSW impulse with a grain boundary.

## 4. Discussion

The motion of the dislocation group has been considered in terms of both shear stress and mobile dislocation density wave representations, and the soiton-like behaviour of this motion has been deduced from the numerical solutions of

the nonlinear *ordinary* differential equation [6, 7]. Now we shall use the analytical solution of the nonlinear *partial* differential equation, obtained in the previous section, to show that the classical pile-up formation may be graphically shown also in terms of the propagation of SSW which swells against an obstacle (like the back-water), producing high-amplitude shear stress gradient at the head of dislocation group, as schematically shown in Fig. 5. Thus we may say that in this classical case the transition of a slip through the grain boundary occurs usually in the crystalographic way by the generation of a new SSW impulse corresponding to the long-range slip (Fig. 6). However, we try here to modify a simple model of the transcrystalline shear band propagation through grain boundaries, formulated originally in [47], i.e. we discuss this model in terms of solitary wave processes as a specific interaction of the nonlinear SSW with the grain boundary.

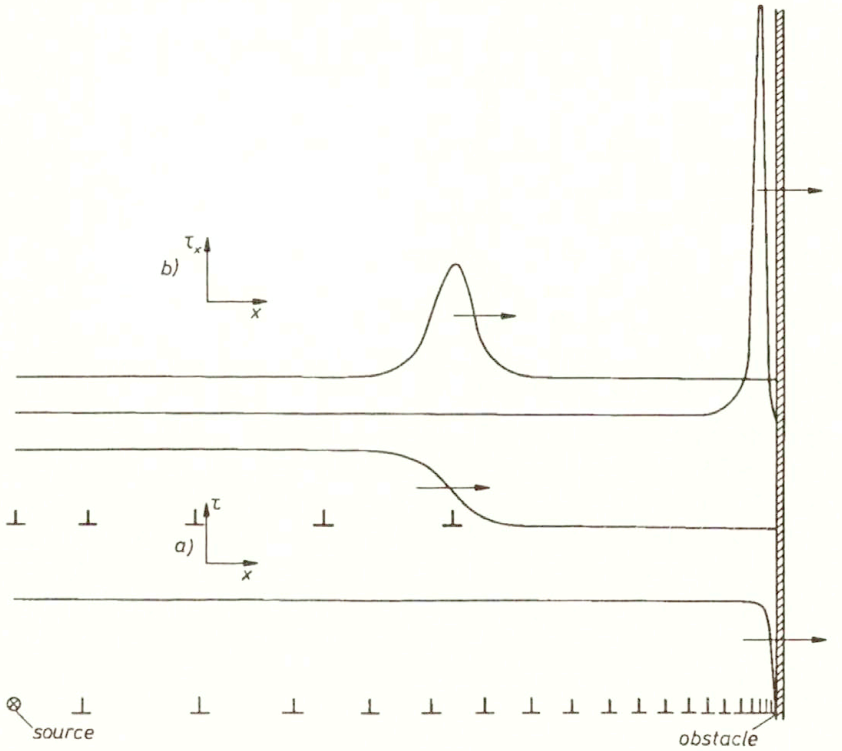


FIG. 5. Dislocation pile-up formation as a process of the interaction of the solitary wave with an obstacle, illustrated schematically: a) in terms of shear stress wave (SSW) impulse, and b) in terms of shear stress gradient

A modified model, proposed below (Fig. 7), is based on three important elements.

**The first** is related to the fact that during the very short time, dynamic impact of the SSW onto the grain boundary (corresponding to the early stage of the shear band formation), the very sharp-step Taylor shock wave is formed leading to the

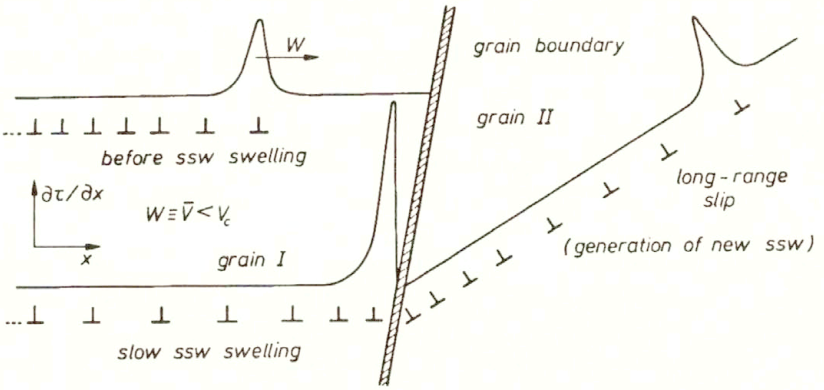


FIG. 6. Transition of the slip through a grain boundary in the usual crystallographic way.

creation of a new step at the grain boundary surface. In the case of edge-oriented dislocations, the nature of this step (Fig. 7a) is such, that it may be considered as a region of highly enhanced atom density similar to a "crowdion-like" object. Consequently, a region of enhanced atom density followed by a region of reduced atom density, i.e. the region of submicrocrack (perhaps like an "anti-crowdion" object in a one-dimensional approximation), is formed in an adjacent grain (Fig. 7a). Hence the creation and the propagation of both these regions may constitute the second stage of formation of the shear band (Fig. 7b). (In a one-dimensional approximation this propagation is, perhaps, like the propagation of bound "crowdion-anticrowdion" pair, which may be able to transport the energy and momentum without the change in primary direction.)

**The second** important element of the model is a criterion for the formation and propagation of the shear band (including both stages of its formation). This criterion should decide on the critical velocity, $v_c$, (mean velocity of the moving dislocation group is assumed here as equal to the velocity, $w$, of the propagation of SSW) above which the creation of the "crowdion-like" objects is possible. The critical velocity, $v_c$, in the first simple approximation [47] may be written in the following form

$$\frac{v_c}{c} \cong \frac{\mu}{d} \Big/ \frac{\partial \tau}{\partial x}, \tag{4.1}$$

where $c$ is the sound velocity, $\mu$ is the shear modulus, $d$ is the thickness of the shear band and $\partial\tau/\partial x$ is the shear stress gradient at the head of the dislocation group.

**The third** element of the model is related to the possible changes in crystallographic orientations of the grains due to the deformation process. Recently it has been suggested that the texture softening effect is one of the important factors determining the angle of shear band propagation. The texture changes are also

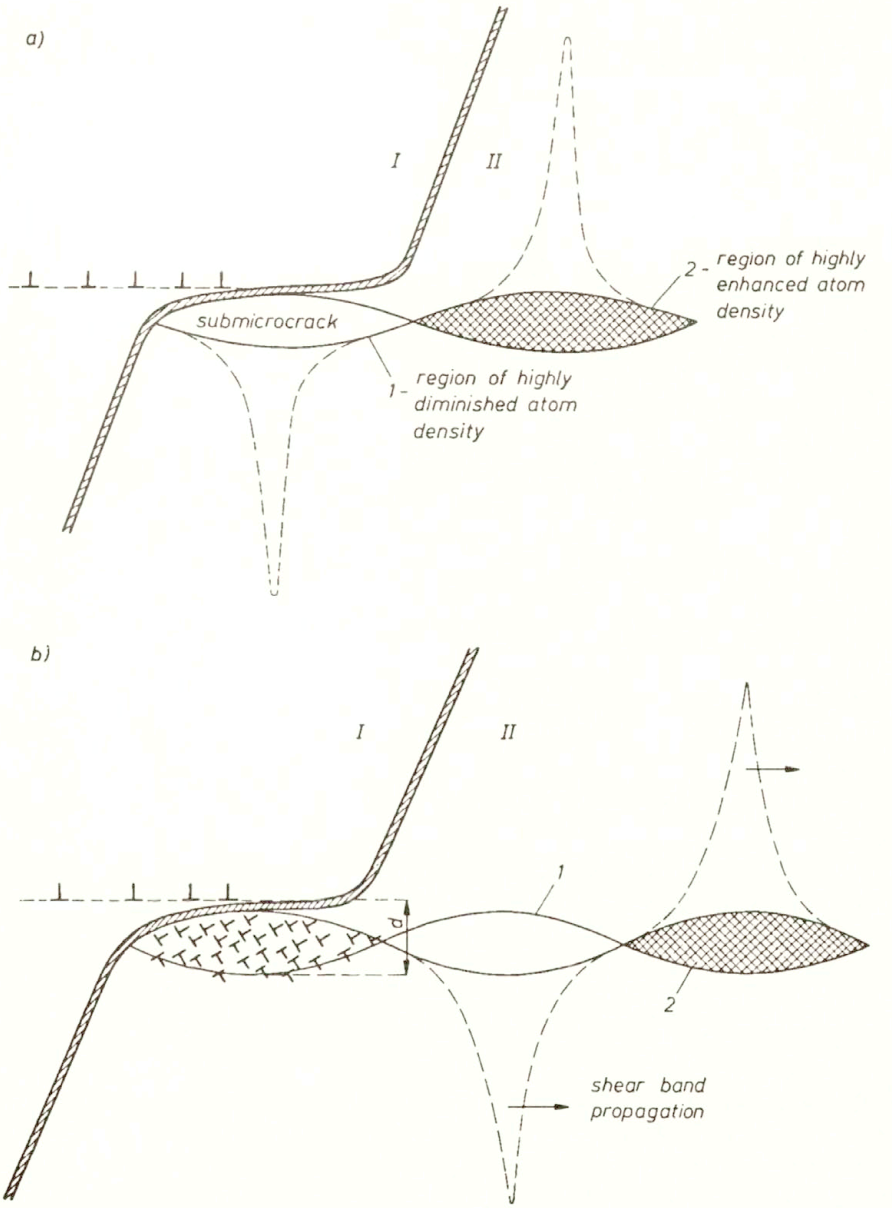


FIG. 7. A simple soliton model of the transcrystallographic transition of the plastic zone (shear band) through the grain boundary: a) creation of the regions of both highly diminished (submicrocrack) and enhanced atom density, and b) propagation of these regions results mainly in a homogeneous nucleation of dislocations.

visibly correlated with the macroscopic localization of strain at the onset of shear band formation, and not only in polycrystalline materials (e.g. [45]) but also in single crystals (e.g. [46]). Hence, we suppose that the long-range transcrystalline

propagation of the shear band through many grains is stimulated by this local change in grain orientations what is schematically illustrated in Fig. 8.

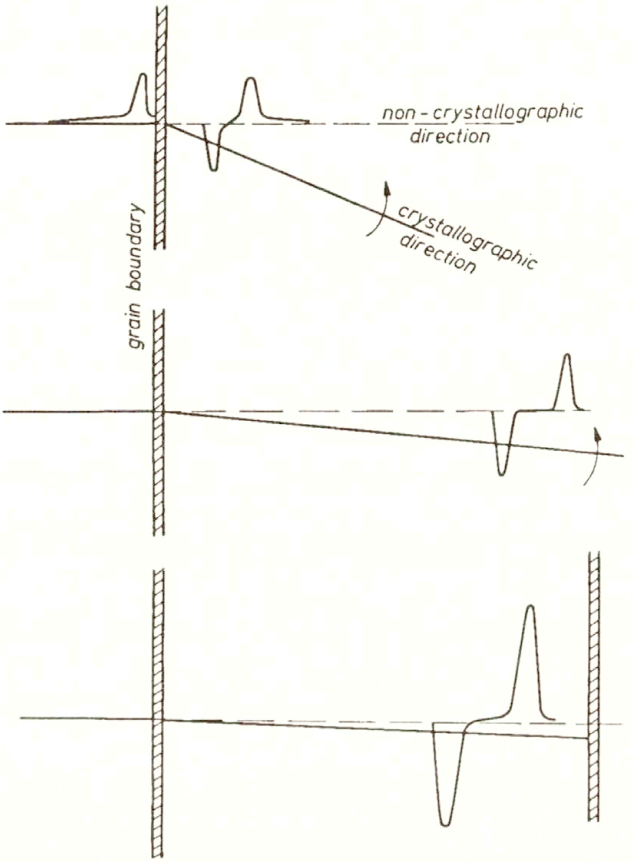


FIG. 8. A schematic illustration of the amplification of the shear stress wave impulse by stimulating effect of the change in grain orientation.

The possibility of creation and transcrystalline propagation of the shear band introduces a quite new physical quality from the point of view of plastic deformation mechanisms, especially in polycrystalline materials. Namely, the crystalographic transfer of the slip (Fig. 6) occurs always when the velocity, $w$, of the SSW propagation is considerably less than the critical value $v_c$, ($w \ll v_c$), and then the "crowdion-like" objects are not created, i.e. the shear band is not formed.

Instead, in the case of shear band formation, the sharpness of the SSW (or amplitude of the shear stress gradient) increases very fast since $w \gg v$, and there is no time for the long-range slip to occur. The "crowdion-like" objects are then formed (Fig. 7a) and the process of plastic zone transition is rather highly nondissipative. Then relaxation processes by long-distance slips are not preferred due to very high velocity (maybe close to the speed of sound) of the "crowdion-like"

objects propagation, and only a homogeneous nucleation of dislocations in a thin zone (of the order of the magnitude of the shear band thickness $d$) of a submicrocrack region is favored (Fig. 7b). However, the possibility of the long-distanced crystallographic slips successively returns due to the stimulating effects of the changes in slip plane orientations in course of the deformation process.

## 5. Conclusions

The simple soliton model of the shear band formation presented in this paper and its transcrystallographic propagation through many grain boundaries may explain two important, experimentally observed facts:

i. The thickness of the shear band is very small ($d \cong 0.1\,\mu m$) due to the homogeneous nucleation of dislocations in the very thin region of the submicrocrack created during formation of the shear band.

ii. The distance of the shear band propagation is very long (running through many grains) due to the highly nondissipative soliton behaviour of the shear stress wave impulse, and due to the stimulation of shearing by the local grain reorientations resulting from the amplification of the amplitude of this impulse.

## References


1. S. PILECKI, Bull. Acad. Polon. Sci., Série Sci. Techn., **17**, 489, 543, 1969.
2. E.C. AIFANTIS, Mat. Sci. Eng., **81**, 563, 1986.
3. E.C. AIFANTIS, Int. J. Plast., **3**, 211, 1987.
4. D. WALGRAEF and E.C. AIFANTIS, J. Appl. Phys., **58**, 688, 1985.
5. A. ZAOUI, A. KORBEL, A. DUBOIS and C. REY, [in:] Non-Linear Phenomena in Materials Science, Proc. Int. Colloque C.N.R.S., Aussois (France), Solid State Phenomena, **3–4**, 433, 1988.
6. A. PAWEŁEK and A. KORBEL, Phil. Mag.(B), **61**, 829–842, 1990.
7. A. PAWEŁEK and A. KORBEL [in press].
8. A. SEEGER, A. DONTH and A. KOCHENDÖRFER, Z. Phys., **134**, 179, 1953.
9. A.S. KOVALEV, Fiz. Tverd. Tela, **21**, 1729, 1979.
10. R.K. DODD, J.C. EILBECK, J.D. GIBBON and H.C. MORRIS, *Solitons and nonlinear wave equations*, Academic Press, Inc. Ltd., London 1984.
11. A. PAWEŁEK, Acta Phys. Polon., **A68**, 815, 1985.
12. A. PAWEŁEK, Arch. Metallurgy, **30**, 296, 1985.
13. A. PAWEŁEK, Scientific Bull. of the Academy of Mining and Metallurgy, Series Metallurgy and Foundry Practice, No. 1109, Bulletin 107, Kraków (Habilitation Thesis), 1987.
14. A. PAWEŁEK, J. Appl. Phys., **62**, 2549, 1987.
15. A. PAWEŁEK, J. Appl. Phys., **63**, 5320, 1988.
16. A. PAWEŁEK, Phys. Lett., **A, 128**, 61, 1988.
17. A. PAWEŁEK and M. JAWORSKI, J. Appl. Phys., **64**, 119, 1988.
18. A. PAWEŁEK, M. JAWORSKI and J. ZAGRODZIŃSKI, J. Phys., **A, 21**, 2727, 1988.
19. H. NEUHAUSER, [in:] Non-Linear Phenomena in Material Science, Colloque Int. du C.N.R.S., Assois (France) 1987, Solid State Phenomena, **3/4**, 407, 1988.
20. A. KORBEL and A. PAWEŁEK, Acta/Scripta Metall. Int. Conf. on Dislocation Modelling of Physical Systems, Gainesville (Florida), p. 332.

21. A. KORBEL and M. SZCZERBA, Scripta Met., **22**, 1725, 1988.
22. A. PAWEŁEK, Z. Metall., **80**, 614, 1989.
23. A. KORBEL and P. MARTIN, Acta Metall., **34**, 1905, 1986.
24. A. KORBEL, Arch. Metallurgy, **32**, 377, 1987.
25. Z. JASIEŃSKI and A. PIĄTKOWSKI, Proc. of the 8th Intern. Conference on the Strength of Metals and Alloys, (ICSMA 8), vol. 1, P.O. KETTUNEN, T.K. LEPISTO and M.E. LEHTONEN [Eds.], Tampere (Finland), Pergamon Press, p. 367, 1988.
26. V.S. ANATHAN and E.O. HALL, Scripta Met., **21**, 519, 1987.
27. A.K. HEAD, Phil. Mag., **26**, 43, 65; **27**, 505, 1972.
28. V. BALAKRISHNAN and C.E. BOTTANI, Phys. Rev., **B33**, 5157, 1986.
29. P.G. SHEWMON, *Diffusion in solids*, McGraw-Hill, New York – London 1963.
30. R.N. STEVENS, R. DUTTON and M.P. PULS, Acta Metall., **22**, 629, 1974.
31. J.C.M. LI, F.V. NOLFI and C.A. JOHNSON, Acta Metall., **19**, 749, 1971.
32. S.R. DE GROT, *Thermodynamics of irreversible processes*, Interscience Publ., New York 1952.
33. J.P. HIRTH and J. LOTHE, *Theory of dislocations*, McGraw-Hill, New York 1972.
34. S. PILECKI, Bull. Acad. Polon. Sci., Série Sci. Techn., **18**, 513, 521, 1970.
35. S. PILECKI, *Introduction to the diffusional theory of metal fatigue*, Reports of the Institute of Fundamental Technological Research, PAS, Warsaw, Rep. No. 8, 1970.
36. S. PILECKI, Proc. 3rd Int. Conf. on Fracture, Munich, vol. 1, p. 241, 1973.
37. S. PILECKI, Arch. Mech., **29**, 505, 1977.
38. S. PILECKI, Proc. 4th Int. Conf. on Fracture, Waterloo (Canada), vol. 2, p. 687, 1977.
39. S. PILECKI, Engng. Trans., **36**, 269, 1988.
40. D.J. BAMMANN and E.C. AIFANTIS, Acta Mech., **45**, 91, 1982.
41. D. WALGRAEF and E.C. AIFANTIS, Int. J. Engng. Sci., **23**, 1351, 1359, 1365, 1985; **24**, 1789, 1986.
42. C. SCHILLER and D. WALGRAEF, Acta Metall., **36**, 3, 563, 1988.
43. M.J. ABLOVITZ and H. SEGUR, *Solitons and the inverse scattering transform*, Studies in Appl. Mathem. (SIAM), Philadelphia 1981.
44. J.M. BURGERS, *The nonlinear diffusion equation. Asymptotic solutions and statistical problems*, D. Reidel Publ. Comp., Dordrecht 1974.
45. Z. JASIEŃSKI, A. PIĄTKOWSKI, A. LITWORA and H. PAUL, IPM PAN Rep., CPBP 02.07, Theme 5.1.13, 1990.
46. Z. JASIEŃSKI and A. LITWORA, IPM PAN Rep., 1988.
47. A. KORBEL, Scripta Metall. Mater., **24**, 1229, 1990.
48. J. WEERTMAN and P.S. FALLANSBEE, Mech. Mater., **7**, 177, 1988.

POLISH ACADEMY OF SCIENCES,
A. KRUPKOWSKI ISTITUTE OF METALLURGY AND MATERIAL SCIENCES, KRAKÓW
and
INSTITUTE OF FUNDAMENTAL TECHNOLOGICAL RESEARCH, WARSZAWA.

*Received October* 3, 1994.

Arch. Mech., 47, 1, pp. 117–124, Warszawa 1995

# Existence theorems for elliptic partial differential equations of reaction-diffusion type

B. KAŹMIERCZAK (WARSZAWA)

WE ANALYZE the relation between "invariant rectangles" theorems and the method of sub- and supersolutions used in existence proofs for reaction-diffusion equations. We prove that these methods are in a sense equivalent.

## 1. Introduction

REACTION-DIFFUSION systems of equations are widely used to describe a variety of phenomena in chemistry, physics, biology, medicine, etc.

One of the methods to prove the existence of solutions to the reaction-diffusion systems of equations is based on invariant rectangles (or generally invariant regions) theorems [1, 2–5]. Another method utilizes the notion of sub- and supersolution pairs [6, 7].

The main objective of this work is to show that these methods are in a sense equivalent. "In a sense" means that we can use one of these theorems in the proof of the other one (see the proof of Theorem 1). To be consise, we will confine ourselves only to elliptic equations, since in the parabolic case a proof can be repeated without significant changes.

## 2. "Invariant" regions theorems

The above notion originates from parabolic initial boundary-value problem theory (see e.g. [2, 3, 5, 8]). It suggests that if certain conditions are satisfied and initial and boundary values lie in a certain convex region in the space of dependent variables, then there exists a solution to the considered problem having its values in this region for all times, for which the solution exists.

In case of elliptic second order quasilinear systems of equations, the corresponding theorems guarantee the existence of a solution if the boundary values can be extended to functions, whose values lie in such a region [4, 6, 9].

Below, we will be considering the following system of elliptic equations:

$$L_i(x,u)u_i = f_i(x,u_1,\ldots,u_m,\partial u_1,\ldots,\partial u_m) \qquad \text{for} \quad x \in \Omega, \tag{2.1}$$

together with the Dirichlet-type boundary conditions:

$$u_i(x) = \phi_i(x) \qquad \text{for} \quad x \in \partial\Omega, \tag{2.2}$$

where $i = 1, \ldots, m \geq 1$ and $u := (u_1, \ldots, u_m)$. For simplicity of notation we have set $\partial u_i := \vec{\nabla} u_i$. We assume that:

H1. $\Omega$ is a bounded open region comprised in $\mathbb{R}^n$, $n \geq 1$, with its boundary of $C^{2+\alpha}$ class. For $i \in \{1, \ldots, m\}$ the function $\phi_i \in C^{2+\alpha}(\overline{\Omega})$, where $\overline{\Omega}$ denotes the closure of $\Omega$. ■

H2. $L_i$ are of the form

$$L_i(x, u) = a^i_{kj}(x, u)\partial_k \partial_j ,$$

where $a^i_{kj}(x, u)$ are symmetric with respect to $k, j$. For all $i = 1, \ldots, m$ and all $u \in \mathbb{R}^m$ the operators are uniformly elliptic in $\overline{\Omega}$, and the coefficients $a_{kj}(x, u)$ are of $C^1$ class. ■

H3. $f := (f_1, \ldots, f_m) : \overline{\Omega} \times \mathbb{R}^m \times \mathbb{R}^{mn} \to \mathbb{R}^m$ are of $C^\alpha$ class (with some $\alpha > 0$) on every compact subset of $\overline{\Omega} \times \mathbb{R}^m \times \mathbb{R}^{mn}$. ■

Let $\Sigma := \prod_{i=1}^{m} (a_i, b_i)$, with $a_i, b_i \in \mathbb{R}^1$, $a_i < b_i$.

H4. $\phi := (\phi_1, \ldots, \phi_m) : \overline{\Omega} \to \overline{\Sigma}$. ■

H5. For any bounded open subset $W \in \mathbb{R}^m$ and any $C^2(\overline{\Omega}, \mathbb{R}^m)$ solution of the problem (2.1), (2.2) with its values lying in the closure of $W$, there exist a real positive number $\eta(\Omega, \phi, W)$ such that $\|\partial u(x)\| \leq \eta$ for all $x \in \overline{\Omega}$. Here $\|\partial u(x)\|$ denotes the norm of $\partial u(x)$ in $\mathbb{R}^{nm}$, $\|u(x)\|$ is the norm of $u(x)$ in $\mathbb{R}^m$. ■

REMARK. There are a lot of papers concerning *a priori* estimates for problems of the type (2.1), (2.2). In [10] H5 is proved, when all $L_i$ are the same, the functions $f_i$ are of $C^1$ class and such that $|f_i(x, u, p)| < c(u)(\|p_i\|^2 + o(\|p\|^2))$, for all $x \in \overline{\Omega}$, where $p \in \mathbb{R}^{nm}$. Also, when $L_i$ are different but $a^i_{kj} = a^i_{kj}(x)$ and $|f_i(x, u, p)| < c(u)b(p)\|p\|^2$ with $b(p) = o\left((\ln | \|p\| |)^{-1}\right)$, one can prove H5 almost straightforwardly only by the use of classical ADN estimates for linear equations [11]. ■

DEFINITION 1. *Let $\mathcal{W}$ denote an open, bounded and convex subset in $\mathbb{R}^m$. Then by an outer normal vector at $u \in \partial\mathcal{W}$ we mean any unit vector $n(u)$ such that*

$$n(u) \cdot (U - u) \leq 0$$

*for all $U \in \overline{\mathcal{W}}$.* ■

The following result may be called an elliptic version of the invariant rectangles theorem.

PROPOSITION 1. Let assumptions H1–H5 be fulfilled. Let $Q = \eta(\Omega, \phi, \Sigma)$. Let us assume that for every $u \in \partial\Sigma$ there exist an outer normal vector $n(u) = (n_1(u), \ldots, n_m(u))$ such that

$$n(u) \cdot f(x, u, p) \geq 0 \tag{2.3}$$

for all $x \in \overline{\Omega}$ and all $p \in \mathbb{R}^{nm}$ such that $\|p\| \leq Q$ and $\sum_{i=1}^{m} p_{ij} n_i(u) = 0$. Then problem (2.1), (2.2) has a solution $u : \overline{\Omega} \to \overline{\Sigma}$ and $u \in C^{2+\tau}(\overline{\Omega})$, $\tau \in (0, \alpha)$. Moreover, if (2.3) is strengthened to $n(u) \cdot f(x, u, p) > 0$, then $\tau = \alpha$. ∎

REMARK. If $L_i = a_{kj}(x, u)$ independently of $i$, then this theorem can be strengthened. Namely $\Sigma$ may be any open, bounded and convex set of $\mathbb{R}^m$. ∎

The proof of Proposition 1 is almost the same as the proof of Theorem 8 p. 270 in [4]. (We have only to be more careful as the coefficients of $L_i$ depend on $u_i$.) However, for convenience of the reader we give it in the Appendix.

## 3. Sub- and supersolution method

For a single second order elliptic differential equation of the form

$$L(x)u = f(x, u) \quad \text{in } \Omega,$$
$$u(x) = \phi(x) \quad \text{on } \partial\Omega,$$

this method simply says that, if we have a pair of functions $y$ and $Y$ such that $y(x) \leq Y(x)$ for $x \in \Omega$, $y(x) \leq \phi(x) \leq Y(x)$ for $x \in \partial\Omega$, $L(x)y \geq f(x, y)$ and $L(x)Y \leq f(x, Y)$ in $\Omega$, then a solution to the above problem exists and it can be constructed by successive approximations (see e.g. [12]).

In case of systems the problem is more complicated. To achieve the same result we have either to change the definition of sub- and supersolution, or to assume certain monotonicity conditions. For example, for the systems of the form:

$$L_i(x)u_i = a^i_{kj}(x)\partial_k\partial_j u_i = f_i(x, u_1, \ldots, u_m) \quad \text{for} \quad x \in \Omega, \tag{3.1}$$
$$u_i(x) = \phi_i(x) \quad \text{for} \quad x \in \partial\Omega, \tag{3.2}$$

the following simple theorem holds.

PROPOSITION 2. Let H 1 and H 2 be fulfilled. Let $y = (y_1, \ldots, y_m) : \overline{\Omega} \to \mathbb{R}^m$ and $Y = (Y_1, \ldots, Y_m) : \overline{\Omega} \to \mathbb{R}^m$ be such that for all $i \in \{1, \ldots, m\}$ the following conditions are satisfied:

a. $y(x) \leq Y(x)$ (componentwise) for $x \in \overline{\Omega}$,

b. $L_i(x)y_i(x) \leq f(x, y(x))$, $L_i(x)Y_i(x) \leq f(x, Y(x))$,

c. $y_i(x) \leq \phi_i(x) \leq Y_i(x)$ for $x \in \partial\Omega$.

Let us also assume that

d. $f_{i,u_j}(x, u) \geq 0$

for all $x \in \Omega$ and all $j \neq i$. Then there exists a solution $u$ to problem (3.1), (3.2) such that $y_i(x) \leq u_i(x) \leq Y_i(x)$ for $x \in \Omega$. ∎

The proof of this theorem may use a sequence of successive approximations (as in the case of one equation) or topological arguments (as in [9]).

In [6] the similar theorem is proved, when $f_i$ depends on $\partial u_i$. Below, we will prove the corresponding theorem for the case of system (2.1), (2.2). Besides, we will show that it is a consequence of Proposition 1. This is the main result of this work.

Now, we will complete the necessary assumptions.

H 6. For $i \in \{1, \ldots, m\}$ let there exist pairs of functions $y_i(x)$ and $Y_i(x)$ of class $C^{2+\alpha}(\Omega)$ such that $y_i(x) < Y_i(x)$ for $x \in \overline{\Omega}$, $y_i(x) < \phi_i(x) < Y_i(x)$ for $x \in \partial\Omega$. Let $W_y = \prod_{i=1}^{m}(c_i, d_i)$, with $c_i, d_i \in \mathbb{R}^1$, $c_i < d_i$ be such that the values of $y_i$ and $Y_i$ are comprised in $(c_i, d_i)$. ■

H 7. Let $\Psi = \eta(\Omega, \phi, W_y)$ and let for all $i \in \{1, \ldots, m\}$

$$L_i(x, u_1, \ldots, y_i(x), \ldots, u_m) y_i(x) \geq f_i(x, u_1, \ldots, y_i(x), \ldots, u_m, p_1, \ldots, \partial y_i(x), \ldots, p_m),$$
$$L_i(x, u_1, \ldots, Y_i(x), \ldots, u_m) Y_i(x) \leq f_i(x, u_1, \ldots, Y_i(x), \ldots, u_m, p_1, \ldots, \partial Y_i(x), \ldots, p_m),$$

for all $x \in \overline{\Omega}$, all $u_\nu$, $\nu \in \{1, \ldots, m\}$, $\nu \neq i$, satisfying the inequalities $y_\nu(x) \leq u_\nu \leq Y_\nu(x)$ and all $\|p\| \leq \Psi$. ■

THEOREM 1. *Let assumptions* H 1 – H 7 *be fulfilled. Then there exists a* $C^{2+\tau}(\overline{\Omega})$, $\tau \in (0, \alpha)$ *solution* $(u_1(x), \ldots, u_m(x))$ *to system* (2.1), (2.2) *such that* $y_i(x) \leq u_i(x) \leq Y_i(x)$ *for* $x \in \overline{\Omega}$. ■

P r o o f. Let us change the dependent variables $u_i \to u_i^*$:

$$u_i = u_i^* Y_i + (1 - u_i^*) y_i. \tag{3.3}$$

Then,

$$L_i(x, u) u_i = L_i^*(x, u) u_i^* + (1 - u_i^*) L_i(x, u) y_i + u_i^* L_i(x, u) Y_i, \tag{3.4}$$

where

$$L_i^*(x, u) = (Y_i - y_i) L_i(x, u) + 2a_{jk}^i(x, u) \{\partial_k (Y_i - y_i)\} \partial_j .$$

Thus, system (2.1), (2.2) can be written as

$$L_i(x, u(u^*)) u_i^* = [(Y_i(x) - y_i(x)]^{-1} f_i^*(x, u^*, \partial u^*) \quad \text{for} \quad x \in \Omega, \tag{3.5}$$
$$u_i * (x) = [\phi(x) - y_i(x)] [(Y_i(x) - y_i(x)]^{-1} := \rho(x) \quad \text{for} \quad x \in \partial\Omega, \tag{3.6}$$

where $i = 1, \ldots, m$,

$$f_i^*(x, u^*, \partial u^*) = -2a_{jk}^i(x, u(u^*)) \{\partial_k (Y_i - y_i)\} \partial_j u_i^* - (1 - u_i^*) L_i(x, u(u^*)) y_i$$
$$- u_i^* L_i(x, u(u^*)) Y_i + f_i(x, u_1(u_1^*), \ldots, u_m(u_m^*), \partial u_1(u_1^*), \ldots, \partial u_m(\partial u_m^*))$$

and, according to (3.3),

$$u_j(u_j^*) = u_j^* Y_j + (1 - u_j^*) y_j ,$$
$$\partial u_j(u_j^*) = Y_j \partial u_j^* + y_j \partial(1 - u_j^*) + u_j^* \partial Y_j + (1 - u_j^*) \partial y_j . \tag{3.7}$$

Let us consider an open rectangle $\Lambda$ in the $u^*$-space, whose vertices have the coordinates equal to 0 or 1.

Now, we can determine a unit (though nonunique) vector field $n^*(u^*)$ on $\partial\Lambda$ satisfying the conditions of Definition 1, and thus being a field of vectors normal to $\partial\Lambda$ at every point of it. Namely, if $u^*$ belongs to an open wall $I_{+1i} := (t_1, \ldots, t_{i-1}, 1, t_{i+1}, \ldots, t_m)$ or $I_{-1i}(t_1, \ldots, t_{i-1}, 0, t_{i+1}, \ldots, t_m)$ with $t_j \in (0,1)$, then let $n^*(u^*) = n_i$ or $n^*(u^*) = -n_i$, where $n_i$ denotes a unit vector directed along the $i$-th axis. For all the other $u^*$ there exists the smallest $i \in \{1, \ldots, m\}$ such that $u^*$ belongs to the intersection of the closures of the walls $I_{\chi i}$ and $I_{\tilde{\chi} j}$, $i \leq j$, $\chi, \tilde{\chi} \in \{-1, +1\}$. Then, let $n(u^*) := \chi n_i(u)$. If we set $\Sigma = \Lambda$, then for such an outer normal vector field and system (3.5), (3.6), assumptions H1–H5 are fulfilled with respect to the variables $u^*$ and $\rho$.

Especially, according to the assumption corresponding to H5, we can find *a priori* estimates for $\partial u^*$, i.e. $\|\partial u^*\| \leq \eta(\Omega, \rho, \Lambda)$.

Now we will check the condition (2.3). We have $n(u^*) = \pm n_i$, where $n_i$ is a unit vector directed along the $i$-th axis. Let us suppose that $n(u^*) = n_i$ for some $u^* \in \partial\Lambda$. Then $u_i^* = 1$ and $n(u^*) \cdot f^*(x, u^*, p^*)$ for $p^* \in \mathbb{R}^{nm}$ such that $\|\partial u^*\| \leq \eta(\Omega, \rho, \Lambda)$ and $p_i^* = 0$ is equal to

$$-u_i^* L_i(x, Y_i(x))Y_i(x) + f_i\Big(x, u_1^* tY_1(x) + (1 - u_1^*)y_1(x), \ldots, Y_i(x), \ldots,$$
$$u_m^* Y_m(x) + (1 - u_m^*)y_m(x), p_1^*, \ldots, \partial Y_i, p_m^*\Big).$$

The *a priori* estimates $\|\partial u^*\| \leq \eta(\Omega, \rho, \Lambda) = Q^*$ are equivalent, according to (3.7), to the estimates $\|\partial u\| \leq \eta(\Omega, \phi, W_\varphi)$ and $\|p^*\| \leq Q^*$ is equivalent to $\|p\| \leq \Psi$.

Thus according to H7, the above expression is nonnegative for all $x \in \overline{\Omega}$, all $u_\nu$, $\nu \in \{1, \ldots, m\}$, $\nu \neq i$, satisfying the inequalities $y_\nu(x) \leq u_\nu \leq Y_\nu(x)$ and all $\|p\| \leq \Psi$. Thus the condition (2.3) is fulfilled. In the same way we can prove that this condition remains valid for $n(u^*) = -n_i$. The theorem is proved. ∎

REMARKS. If the inequalities satisfied by $L_i$ in H7 are strict, then in H6 we can demand only $y_i(x) \leq Y_i(x)$. This follows from the fact that in this case we can change the functions $y_i$ and $Y_i$ to functions $\hat{y}_i$ and $\hat{Y}_i$ (for example by adding constants of sufficiently small absolute value), so that $\hat{y}_i < \hat{Y}_i$ and H7 is fulfilled (for $\hat{y}_i$ and $\hat{Y}_i$).

It is worthwile to note that in principle the methods used in the proofs of Proposition 1 and Theorem 1 can be applied to the systems of the form

$$L_i(x, u, \partial u_i)u_i = f_i(x, u_1, \ldots u_m, \partial u_1, \ldots, \partial u_m),$$

if only an appropriate *a priori* estimate can be given (as in H5). ∎

In the above proof we have used only Proposition 1. On the other hand, by setting $y_i(x) = a_i$ and $Y_i(x) = b_i$ we can obtain Proposition 1 from Theorem 1. In this sense we can say that these two methods are equivalent.

In the case of parabolic system we can prove a theorem analogous to Theorem 1 using the same method. Now, instead of Proposition 1 we can use Theorem 1 in [2]. This theorem concerns systems of the kind

$$\begin{aligned} -u_{it} + L_i(x,u)u_i &= f_i(x,u_1,\dots u_m,\partial u_1,\dots,\partial u_m) && \text{for } x\in\Omega,\\ u_i(x) &= \phi_i(x) && \text{for } x\in\partial\Omega,\\ u_i(x,0) &= u_{i0}(x) && \text{for } x\in\Omega. \end{aligned}$$

This theorem asserts that if the conditions of Proposition 1 are satisfied for all $t\in[0,T]$, $T>0$, the conclusion of Proposition 1 holds also, for at least $t\in[0,T]$.

**Appendix. Proof of Proposition 1**

First we will assume that $n(u)\cdot f(x,u,p)>0$. By fixing $u$ in $a^i_{kj}(x,u)$ we can formally solve the system (2.1), (2.2) to obtain the relation

$$u=\mathcal{N}(u):=\mathcal{R}(u)\circ F(u), \tag{A.1}$$

where $F(u)(x):=[f_1(x,u(x),\partial u(x)),\dots,f_m(x,u(x),\partial u(x))]$. According to the linear theory of elliptic operators, $\mathcal{N}(u)$ is a well-determined operator acting from $C^1(\overline{\Omega})$ to $C^1(\overline{\Omega})$. Moreover, it is completely continuous. Let $\mathcal{E}$ denote the real Banach space of $C^1(\overline{\Omega})$ functions, i.e.

$$\mathcal{E}:=\left\{v:\overline{\Omega}\to\mathbb{R}^m,\quad v\in C^1(\overline{\Omega})\right\}$$

with the natural norm

$$\|v\|_{\mathcal{E}}:=\|v\|_{C^1(\overline{\Omega})}=\sup_{x\in\Omega}\|v(x)\|+\sup_{x\in\Omega}\|\partial v(x)\|.$$

According to H3 for $u$ satisfying (2.1), (2.2) and such that $u(x)\in\Sigma$ for $x\in\overline{\Omega}$, we have $\sup\limits_{x\in\Omega}\|\partial u(x)\|\le Q$. Let us define a bounded open subset of $\mathcal{E}$:

$$\mathcal{O}:=\left\{v\in\mathcal{E}:\quad v\in\overline{\Omega}\to\Sigma,\quad \sup_{x\in\Omega}\|\partial v(x)\|<Q+1\right\}.$$

REMARK. Now, let us note that by a proper translation in the $u$-space we can assume that $\mathbf{0}\in\Sigma$. This translation does not affect the value of constant $Q$. ∎

According to the above Remark we can make use of the following Leray–Schauder's Continuation Theorem (see [4, 13]).

LEMMA. Let $\mathcal{E}$ be a real Banach space and $\mathcal{O}$ its bounded open neighbourhood of $\mathbf{0}$ in $\mathcal{E}$. Let $\mathcal{N}:\overline{\mathcal{O}}\to\mathcal{E}$ be a completely continuous operator such that for all

$\lambda \in (0,1)$ and $u \in \partial\mathcal{O}$, $u \neq \lambda\mathcal{N}(u)$. Then the equation $u = \mathcal{N}(u)$ has a solution $u \in \overline{\mathcal{O}}$. ■

Suppose to the contrary that there exist $\lambda \in (0,1)$ and $u \in \partial\mathcal{O}$ such that

$$u = \lambda\mathcal{N}(u) := \lambda\mathcal{R}(u) \circ F(u). \tag{A.2}$$

Then, $u$ must be a solution of the problem:

$$L_i(x,u)u_i(x,t) = \lambda f_i(x, u_1, \dots u_m, \partial u_1, \dots, \partial u_m) \quad \text{for} \quad x \in \Omega, \tag{A.3}$$

$$u_i(x) = \lambda\phi_i(x) \quad \text{for} \quad x \in \partial\Omega, \tag{A.4}$$

$i = 1, \dots, m$. Let us note that the boundary of $\mathcal{O}$ consists of functions $v : \overline{\Omega} \to \Sigma$ which, at least at one point in $\overline{\Omega}$, achieve a value comprised in $\partial\Sigma$, and of functions $v$ such that $\sup_{x\in\Omega} \|\partial v(x)\| = Q + 1$. However, due to the assumptions of Proposition 1 the second group of functions is empty. Thus, if $u \in \partial\mathcal{O}$ satisfies (A.2), then there exists $\zeta \in \overline{\Omega}$ such that $u(\zeta) \in \partial\Sigma$. On the other hand, as $\Sigma$ is open and convex, $\lambda\phi(x) \in \Sigma$ for $x \in \Omega$ and $\lambda \in (0,1)$. So, $\zeta \in \Omega$. Let us consider the function $r(x) := n(u(\zeta))(u(x) - u(\zeta))$, where $n(u(\zeta))$ is an outer normal at the point $u(\zeta) \in \partial\Sigma$. We have $r(\zeta) = 0$ and $r(x) \leq 0$ for $x \in \overline{\Omega}$ (see Definition 1). Due to assumptions of Proposition 1 it follows that $n(u(\zeta)) \cdot f(\zeta, u(\zeta), \partial u(\zeta)) \geq 0$ and that there exists an index $h \in \{1, \dots, m\}$ such that $n(u(\zeta)) \cdot u(\zeta) = u_h(\zeta)$. Thus we have:

$$\begin{aligned} L_h(\zeta, u(\zeta))r(\zeta) = L_h(\zeta, u(\zeta))u_h(\zeta) &= \lambda f_h(\zeta, u(\zeta), \partial u(\zeta)) \\ &= \lambda n \cdot f(\zeta, u(\zeta), \partial u(\zeta)) > 0. \end{aligned} \tag{A.5}$$

It follows that there exists a ball $B$ with its center at $\zeta$, $\overline{B} \subseteq \overline{\Omega}$, such that

$$L_h(x, u(x))u_h(x) = \lambda f_h(x, u(x), \partial u(x)) \geq 0 \quad \text{for} \quad x \in \overline{B}.$$

From the maximum principle it follows that $u_h(x) \equiv 0$ for $x \in B$. Consequently $L_h(\zeta, u(\zeta))u_h(\zeta) = 0$ which is a contradiction to inequality (A.5). According to the Lemma we obtain a solution to the problem (2.1), (2.2) belonging to the class $C^{2+\alpha}(\overline{\Omega})$.

Now, let us suppose that the inequality $n(u) \cdot f(x,u,p) > 0$ is not fulfilled. Let us replace $f_i$ by $f_{i\varepsilon} = (f_i + \varepsilon u_i)$, $\varepsilon > 0$, at the right-hand sides of the system (2.1). Then, if $\mathbf{0} \in \Sigma$ (see above Remark), assumptions of Proposition 1 will imply that $n(u) \cdot f_\varepsilon(x,u,p) > 0$ everywhere on $\partial\Sigma$. For $\varepsilon_\kappa := (\kappa)^{-1}$, $\kappa \in N_+$, we obtain a sequence of $C^{2+\alpha}(\overline{\Omega})$ solutions to the problems

$$\begin{aligned} L_i(x,u)u_{i\varepsilon}(x,t) &= f_{i\varepsilon}(x, u_{1\varepsilon}, \dots u_{n\varepsilon}, \partial u_{1\varepsilon}, \dots, \partial u_{m\varepsilon}) \quad \text{for} \quad x \in \Omega, \\ u_{i\varepsilon}(x) &= \phi_i(x) \quad \text{for} \quad x \in \partial\Omega. \end{aligned}$$

Due to the compact embedding of $C^{2+\alpha}$ in $C^{2+\tau}$ for any $\tau \in (0,\alpha)$, we can choose a subsequence converging to some function $u$ in $C^{2+\tau}(\overline{\Omega})$ being a solution to the problem (2.1), (2.2). The proof of Proposition 1 is now complete.

## References


1. K. CHUEH, C. CONLEY and J. SMOLLER, *Positively invariant regions for systems of nonlinear diffusion equations*, Indiana Univ. Math. J., **26**, 2, 1977.
2. H. AMANN, *Invariant sets and existence theorems for semilinear parabolic and elliptic systems*, J. Math. Anal. Appl., **65**, pp. 432–467, 1978.
3. M. VALENCIA, *On invariant regions and asymptotic bounds for semilinear p.d.e.*, Nonlinear Analysis TM& A, **14**, 3, pp. 217–230, 1990.
4. K. SCHMITT, *Boundary value problems for quasi-linear second order elliptic equations*, Nonlinear Analysis TM& A, **2**, pp. 263–309, 1978.
5. M. PLUM, *Shape-invariant bounds for reaction-diffusion systems with unequal diffusion coefficients*, J. Diff. Equations, **73**, 82–103, 1988.
6. P. FIFE and M. TANG, *Comparison principles for reaction-diffusion systems: irregular comparison functions and applications to questions of stability and speed of propagation of disturbances*, J. Diff. Equations, **40**, 168–185, 1981.
7. J. BEBERNES, K. CHUEH and W. FULKS, *Some applications of invariance for parabolic systems*, Indiana Univ. Math. J., **28**, pp. 269–277.
8. J. SMOLLER, *Shock waves and reaction-diffusion equations*, Springer-Verlag, 1983.
9. J. HERNANDEZ, *Some existence and stability results for solutions of reaction-diffusion equations with nonlinear boundary conditions*, [in:] Nonlinear Differential Equations: Invariance, Stability and Bifurcation, P. DE MOTTONI and L. SALVADORI [Eds.], Academic Press, New York 1981.
10. O.A. LADYŻENSKAJA and N.N. URALTSEVA, *Linear and quasilinear elliptic equations*, Academic Press, New York 1968.
11. S. AGMON, A. DOUGLIS and L. NIRENBERG, *Estimates near the boundary of elliptic partial differential equations satisfying general boundary conditions*, Comm. Pure Appl. Math., **12**, 623–727, 1959.
12. D. SATTINGER, *Topics in stability and bifurcation theory*, Lecture Notes, **309**, Springer-Verlag, 1973.
13. L. NIRENBERG, *Topics in nonlinear functional analysis*, Courant Inst. Lect. Notes, New York University, New York 1974.


POLISH ACADEMY OF SCIENCES,
INSTITUTE OF FUNDAMENTAL TECHNOLOGICAL RESEARCH, WARSZAWA.

*Received July* 4, 1994; *new version November* 25, 1994.

Arch. Mech., 47, 1, pp. 125–139, Warszawa 1995

# Wave pulses in two-dimensional randomly stratified elastic media

Z. KOTULSKI (WARSZAWA)

IN THE PAPER the propagation of the planar wave pulses in a two-dimensional randomly stratified elastic medium is considered. Two cases: the plane and anti-plane deformations are studied. The problem is described by means of the transition matrix method. In both the cases the transition matrices are obtained and the equations for the wave fields reflected from and transmitted through the randomly stratified elastic slab are derived. Finally, the law of large numbers for the product of random matrices is applied to obtain the effective material constants needed for the description of the elastic wave pulse in the homogenized medium.

## 1. Introduction

ELASTIC WAVE propagation in stratified media has been widely studied in the literature [4, 10, 11] in the context of mechanical and geotechnical applications. Also some elements of structures are segmented in such a way, that they can be considered as stratified waveguides (see e.g. [5]). Among various methods of the analysis of the waves in the stratified media, the transition matrix method is one of the most effective ones. The method, introduced for the investigation of the harmonic surface waves in deterministic stratified media [17, 21, 24] has been applied in the cases of planar volume harmonic waves in elastic media [6, 7], harmonic elastic waves generated by space-distributed sources [8] and waves in stochastic stratified media [2, 25]. The transition matrix method has been also adopted for the investigation of the propagation of wave pulses in segmented elements of structures, both deterministic [1, 18] and stochastic [15, 16].

In this paper we consider the wave pulses in a two-dimensional elastic stratified medium. The results obtained are a generalization of the results obtained in paper [15], where a one-dimensional medium was considered. On the other hand, this paper extends the model of two-dimensional harmonic waves, considered in [12, 13, 14], on the non-stationary phenomenon of wave pulses.

The schedule of the paper is the following. In Sec. 2 the fundamental equations and notation used through the paper are introduced. In the following sections we give the elastic wave equation for the planar elastic wave pulse and derive the expressions for the transition matrices for the anti-plane (Sec. 3) and plane (Sec. 4) state of deformation. Section 5 contains the wave equation in a layered medium written in the transfer matrix language. The main result of the paper is contained in Sec. 6, where, by applying the law of large numbers for the product of random matrices, we obtain the effective material parameters for the homogenized elastic medium. Section 7 summarizes the results of the paper.

## 2. The governing equations in homogeneous medium

Consider a non-harmonic linear elastic wave propagating in the homogeneous isotropic medium. In such a case the equations of motion of the medium constitute the following system of partial differential equations (cf. [19]):

$$\varrho \frac{\partial^2}{\partial t^2} u_i = \sigma_{ij,j}\,, \tag{2.1}$$

$i = 1, 2, 3$, where $\sigma_{ij}$ is the stress tensor, defined as

$$\sigma_{ij} = \mu\,(u_{i,j} + u_{j,i}) + \lambda u_{k,k}\delta_{ij} \tag{2.2}$$

(double indices denote summation from 1 to 3). In the above equations $\lambda$ and $\mu$ are the elastic Lamé constants and $\varrho$ is density of the medium.

Let us assume that the elastic medium has a discontinuity surface (plane). We introduce such a system of independent variables that this plane is perpendicular to the $x$-axis ($x_1$-axis) of coordinates. At the discontinuity plane (being the interface between two homogeneous and isotropic materials) the wave field must satisfy two following continuity conditions (see [9]): continuity of the displacement vector **u** and continuity of the traction vector **t**.

## 3. The anti-plane state of deformation

Consider the simplest two-dimensional problem of elastic wave propagation of the transversal, horizontally polarized plane wave. We assume that the displacement of the medium has the following form:

$$\mathbf{u} = \Big(0, 0, u(x_1, x_2, t)\Big)^T\,, \tag{3.1}$$

that is, it is perpendicular to the plane $x_1$, $x_2$. In such a case the elements of the stress tensor are:

$$\begin{aligned} &\sigma_{11} = \sigma_{12} = \sigma_{21} = \sigma_{22} = \sigma_{33} = 0,\\ &\sigma_{13} = \sigma_{31} = \mu\frac{\partial u}{\partial x_1}\,,\\ &\sigma_{23} = \sigma_{32} = \mu\frac{\partial u}{\partial x_2}\,. \end{aligned} \tag{3.2}$$

Substituting these particular stress tensor components into the system of equations (2.1) we obtain a single non-trivial governing equation:

$$\mu\frac{\partial^2 u}{\partial x_1^2} + \mu\frac{\partial^2 u}{\partial x_2^2} = \varrho\frac{\partial^2 u}{\partial t^2}\,. \tag{3.3}$$

Using the given form of the stress tensor (3.2), we obtain the coordinates of the traction vector in the following form:

$$\tau_1 = \tau_2 = 0, \tag{3.4}$$

$$\tau = \tau_3 = \sigma_{13} = \mu \frac{\partial u}{\partial x_1}. \tag{3.5}$$

From the formulae (3.2) and (3.5) we can obtain the system of equations for two mechanical fields $u$ and $\tau$, remaining continuous at a discontinuity plane:

$$\frac{\partial u}{\partial x_1} = \frac{1}{\mu}\tau, \tag{3.6}$$

$$\frac{\partial \tau}{\partial x_1} = \varrho \frac{\partial^2 u}{\partial t^2} + \mu \frac{\partial^2 u}{\partial x_2^2}. \tag{3.7}$$

To solve the system of Eqs. (3.6)–(3.7) in a non-stationary case, we calculate its Fourier transform with respect to time $t$ and spatial variable $x_2$ (the corresponding transformation variables are $\omega$ and $k$, respectively). We obtain the system of equations for the transformed functions $\hat{u}$ and $\hat{\tau}$ in the following form (we replaced $x_1$ with $x$):

$$\frac{d\hat{u}}{dx} = \frac{1}{\mu}\hat{\tau}, \tag{3.8}$$

$$\frac{d\hat{\tau}}{dx} = \left(\mu k^2 - \varrho\omega^2\right)\hat{u}. \tag{3.9}$$

In the matrix form the system of Eqs. (3.8)–(3.9) can be written as

$$\frac{d}{dx}\hat{\mathbf{u}} = \mathbf{M}\,\hat{\mathbf{u}}, \tag{3.10}$$

where, by definition,

$$\hat{\mathbf{u}} = \begin{bmatrix} \hat{u} \\ \hat{\tau} \end{bmatrix} \quad \text{and} \quad \mathbf{M} = \mathbf{M}(\omega) = \begin{bmatrix} 0 & \frac{1}{\mu} \\ \mu k^2 - \varrho\omega^2 & 0 \end{bmatrix}. \tag{3.11}$$

To solve the wave problem described by Eq. (3.10), we complete it with the following boundary condition:

$$\hat{\mathbf{u}}(0, k, \omega) = \hat{\mathbf{u}}_0(k, \omega) = \begin{bmatrix} \hat{u}_0(k, \omega) \\ \hat{\tau}_0(k, \omega) \end{bmatrix}, \tag{3.12}$$

representing jointly the incident wave pulse reaching the plane $x = 0$ and the pulse reflected from it. Then the value at $x = L$ of the solution of the wave equation (3.10), satisfying boundary condition (3.12), can be represented as

$$\hat{\mathbf{u}}(L, k, \omega) = \mathbf{T}(L)\hat{\mathbf{u}}_0(k, \omega), \tag{3.13}$$

where

$$\mathbf{T}(L) = \exp\{\mathbf{M}(\omega)L\} \tag{3.14}$$

is the transition matrix through the layer of thickness $L$, for the elastic wave in anti-plane state of deformation. Construction of the transition matrix requires the knowledge of the eigenvalues of the system matrix $\mathbf{M}$ of the wave equation (3.10). Solving the characteristic equation

$$\det\{\mathbf{M} - p\mathbf{Id}\} = \det\begin{bmatrix} -p & \frac{1}{\mu} \\ \mu k^2 - \varrho\omega^2 & -p \end{bmatrix} = p^2 - \left(k^2 - \varrho\omega^2/\mu\right) = 0, \tag{3.15}$$

we obtain the following eigenvalues of the system matrix:

$$p_1 = p = \sqrt{k^2 - \varrho\omega^2/\mu}\,, \qquad p_2 = -p = -\sqrt{k^2 - \varrho\omega^2/\mu}\,. \tag{3.16}$$

According to the following Lagrange interpolation formula (see [23]):

$$\exp\{\mathbf{M}L\} = \frac{(\mathbf{M} - p_2\mathbf{Id})}{p_1 - p_2}\exp\{p_1 L\} + \frac{(\mathbf{M} - p_1\mathbf{Id})}{p_2 - p_1}\exp\{p_2 L\}, \tag{3.17}$$

we obtain the explicit expression for the transition matrix $\exp\{\mathbf{M}(\omega)L\}$ in the following form:

$$\mathbf{T}(L) = \exp\{\mathbf{M}L\} = \begin{bmatrix} \operatorname{ch} pL & \frac{\operatorname{sh} pL}{\mu p} \\ \mu p \operatorname{sh} pL & \operatorname{ch} pL \end{bmatrix}, \tag{3.18}$$

where ch and sh are, respectively, the hyperbolic cosine and sine functions.

## 4. The plane state of deformation

In the second possible form of planar wave the displacement vector is

$$\mathbf{u} = \left(u_1(x_1, x_2, t),\, u_2(x_1, x_2, t),\, 0\right)^T. \tag{4.1}$$

Then the stress tensor has the following elements:

$$\sigma_{13} = \sigma_{23} = \sigma_{31} = \sigma_{32} = 0, \tag{4.2}$$

$$\sigma_{11} = (\lambda + 2\mu)\frac{\partial u_1}{\partial x_1} + \lambda\frac{\partial u_2}{\partial x_2}, \tag{4.3}$$

$$\sigma_{12} = \sigma_{21} = \mu\left(\frac{\partial u_1}{\partial x_2} + \frac{\partial u_2}{\partial x_1}\right), \tag{4.4}$$

$$\sigma_{22} = (\lambda + 2\mu)\frac{\partial u_2}{\partial x_2} + \lambda\frac{\partial u_1}{\partial x_1}, \tag{4.5}$$

$$\sigma_{33} = \lambda\left(\frac{\partial u_1}{\partial x_1} + \frac{\partial u_2}{\partial x_2}\right), \tag{4.6}$$

and the traction vector has the following coordinates:

$$\tau_1 = \sigma_{11} = (\lambda + 2\mu)\frac{\partial u_1}{\partial x_1} + \lambda\frac{\partial u_2}{\partial x_2}, \tag{4.7}$$

$$\tau_2 = \sigma_{21} = \mu\left(\frac{\partial u_1}{\partial x_2} + \frac{\partial u_2}{\partial x_1}\right), \tag{4.8}$$

$$\tau_3 = 0. \tag{4.9}$$

In this particular case, the non-trivial governing equations (2.1) can be written as:

$$\frac{\partial \tau_1}{\partial x_1} = \varrho\frac{\partial^2 u_1}{\partial t^2} - \frac{\partial \tau_2}{\partial x_2}, \tag{4.10}$$

$$\frac{\partial \tau_2}{\partial x_1} = \varrho\frac{\partial^2 u_2}{\partial t^2} - \frac{\lambda}{(\lambda + 2\mu)}\frac{\partial \tau_1}{\partial x_2} - \frac{4\mu(\lambda + \mu)}{(\lambda + 2\mu)}\frac{\partial^2 u_2}{\partial x_2^2}. \tag{4.11}$$

From Eqs. (4.7), (4.8) for the traction vector we obtain the pair of equations connecting stresses and displacements,

$$\frac{\partial u_1}{\partial x_1} = \frac{1}{(\lambda + 2\mu)}\tau_1 - \frac{\lambda}{(\lambda + 2\mu)}\frac{\partial u_2}{\partial x_2}, \tag{4.12}$$

$$\frac{\partial u_2}{\partial x_1} = \frac{1}{\mu}\tau_2 - \frac{\partial u_1}{\partial x_2}. \tag{4.13}$$

Equations (4.10)–(4.13) describe completely the wave pulse in elastic media in the plane state of deformation.

After the Fourier transformation with respect to time $t$ and spatial variable $x_2$, the system of equations (4.10)–(4.13) becomes the following system of ordinary differential equations (also in this case $x_1 \equiv x$):

$$\frac{d\hat{u}_1}{dx} = \frac{1}{(\lambda + 2\mu)}\hat{\tau}_1 - ik\frac{\lambda}{(\lambda + 2\mu)}\hat{u}_2, \tag{4.14}$$

$$\frac{d\hat{u}_2}{dx} = \frac{1}{\mu}\hat{\tau}_2 - ik\hat{u}_2, \tag{4.15}$$

$$\frac{d\hat{\tau}_1}{dx} = -\omega^2\varrho\hat{u}_1 - ik\hat{\tau}_2, \tag{4.16}$$

$$\frac{d\hat{\tau}_2}{dx} = -ik\frac{\lambda}{(\lambda + 2\mu)}\hat{\tau}_1 + \left(k^2\frac{4\mu(\lambda + \mu)}{(\lambda + 2\mu)} - \omega^2\varrho\right)\hat{u}_2. \tag{4.17}$$

It is seen that the wave process depends on the following five material parameters (similarly to the stationary harmonic case – see [14]):

$$\alpha = \frac{\lambda}{(\lambda + 2\mu)}, \tag{4.18}$$

$$\beta = \frac{4\mu(\lambda + \mu)}{(\lambda + 2\mu)}, \tag{4.19}$$

$$\kappa = \frac{1}{(\lambda + 2\mu)}, \tag{4.20}$$

$$\eta = \frac{1}{\mu}, \tag{4.21}$$

and density $\varrho$.

Using the above symbols, we can rewrite the system (4.14)–(4.17) in the abstract matrix form analogous to (3.10) where, by definition,

$$\hat{\mathbf{u}} = \begin{bmatrix} \hat{u}_1 \\ \hat{u}_2 \\ \hat{\tau}_1 \\ \hat{\tau}_2 \end{bmatrix}, \qquad \mathbf{M} = \begin{bmatrix} 0 & -ik\alpha & \kappa & 0 \\ -ik & 0 & 0 & \eta \\ -\omega^2\varrho & 0 & 0 & -ik \\ 0 & 4k^2\beta - \omega^2\varrho & -ik\alpha & 0 \end{bmatrix}. \tag{4.22}$$

To find the transition operator (matrix) for the system of equations we must know the eigenvalues of the matrix $\mathbf{M}$. Solving the characteristic equation:

$$\det(\mathbf{M} - p\mathbf{Id}) = p^4 + p^2\left(\omega^2\varrho(\kappa + \eta) + 2k^2(\alpha - 2\beta\eta)\right) + \omega^4\kappa\eta\varrho^2 - \omega^2k^2\varrho\left(\alpha^2\eta + 4\beta\kappa\eta + \kappa\right) + k^4\left(\alpha^2 + 4\beta\kappa\right) = 0 \tag{4.23}$$

and substituting the definitions of the parameters, we obtain

$$p_{1,2,3,4} = \pm\sqrt{2k^2A_1 - \omega^2A_2 \pm \omega^2A_3}/\sqrt{2}, \tag{4.24}$$

where the parameters $A_1$, $A_2$ and $A_3$ are defined by

$$A_1 = 2\beta\eta - \alpha = 1, \tag{4.25}$$

$$A_2 = \varrho(\kappa + \eta) = \varrho\frac{\lambda + 3\mu}{\mu(\lambda + 2\mu)}, \tag{4.26}$$

$$A_3 = \varrho(\kappa - \eta) = \varrho\frac{\lambda + \mu}{\mu(\lambda + 2\mu)}. \tag{4.27}$$

In an explicit form, the eigenvalues are

$$p_{1,2} = \pm\frac{\sqrt{k^2\mu - \omega^2\varrho}}{\sqrt{\mu}}, \tag{4.28}$$

$$p_{3,4} = \pm\frac{\sqrt{k^2(\lambda + 2\mu) - \omega^2\varrho}}{\sqrt{\lambda + 2\mu}}. \tag{4.29}$$

The transition matrix for the wave in the plane state of deformation can be calculated according to the Lagrange interpolation formula, analogous to (3.17), (see [23]). The elements of the transition matrix have the following form:

$$\mathbf{T}_{11}(L) = \frac{2\mu k^2}{\omega^2\varrho}\operatorname{ch} p_1 L + \left(1 - \frac{2\mu k^2}{\omega^2\varrho}\right)\operatorname{ch} p_3 L, \tag{4.30}$$

$$\mathbf{T}_{12}(L) = -\frac{i(\omega^2\varrho - 2\mu k^2)k \operatorname{sh} p_1 L}{\sqrt{k^2 - \omega^2\varrho/\mu}\,\omega^2\varrho} - \frac{2i\sqrt{k^2 - \omega^2\varrho/(\lambda + 2\mu)}\,\mu k \operatorname{sh} p_3 L}{\omega^2\varrho}, \tag{4.31}$$

$$\mathbf{T}_{13}(L) = \frac{k^2 \operatorname{sh} p_1 L}{\sqrt{k^2 - \omega^2\varrho/\mu}\,\omega^2\varrho} - \frac{\sqrt{k^2 - \omega^2\varrho/(\lambda + 2\mu)}\operatorname{sh} p_3 L}{\omega^2\varrho}, \tag{4.32}$$

$$\mathbf{T}_{14}(L) = \frac{ik}{\omega^2\varrho}(\operatorname{ch} p_1 L - \operatorname{ch} p_3 L), \tag{4.33}$$

$$\mathbf{T}_{21}(L) = \frac{2i\sqrt{k^2 - \omega^2\varrho/\mu}\,\mu k \operatorname{sh} p_1 L}{\omega^2\varrho} + \frac{i(\omega^2\varrho - 2\mu k^2)k \operatorname{sh} p_3 L}{\sqrt{k^2 - \omega^2\varrho/(\lambda + 2\mu)}\,\omega^2\varrho}, \tag{4.34}$$

$$\mathbf{T}_{22}(L) = \left(1 - \frac{2\mu k^2}{\omega^2\varrho}\right)\operatorname{ch} p_1 L + \frac{2\mu k^2}{\omega^2\varrho}\operatorname{ch} p_3 L, \tag{4.35}$$

$$\mathbf{T}_{23}(L) = \frac{ik}{\omega^2\varrho}(\operatorname{ch} p_1 L - \operatorname{ch} p_3 L), \tag{4.36}$$

$$\mathbf{T}_{24}(L) = -\frac{\sqrt{k^2 - \omega^2\varrho/\mu}\operatorname{sh} p_1 L}{\omega^2\varrho} + \frac{k^2 \operatorname{sh} p_3 L}{\sqrt{k^2 - \omega^2\varrho/(\lambda + 2\mu)}\,\omega^2\varrho}, \tag{4.37}$$

$$\mathbf{T}_{31}(L) = \frac{4\sqrt{k^2 - \omega^2\varrho/\mu}\,\mu^2 k^2 \operatorname{sh} p_1 L}{\omega^2\varrho} - \frac{(\omega^2\varrho - 2\mu k^2)^2 \operatorname{sh} p_3 L}{\sqrt{k^2 - \omega^2\varrho/(\lambda + 2\mu)}\,\omega^2\varrho}, \tag{4.38}$$

$$\mathbf{T}_{32}(L) = 2i\left(1 - \frac{2\mu k^2}{\omega^2\varrho}\right)k\mu(\operatorname{ch} p_3 L - \operatorname{ch} p_1 L), \tag{4.39}$$

$$\mathbf{T}_{33}(L) = \frac{2\mu k^2}{\omega^2\varrho}\operatorname{ch} p_1 L + \left(1 - \frac{2\mu k^2}{\omega^2\varrho}\right)\operatorname{ch} p_3 L, \tag{4.40}$$

$$\mathbf{T}_{34}(L) = \frac{2i\sqrt{k^2 - \omega^2\varrho/\mu}\,\mu k \operatorname{sh} p_1 L}{\omega^2\varrho} + \frac{i(\omega^2\varrho - 2\mu k^2)k \operatorname{sh} p_3 L}{\sqrt{k^2 - \omega^2\varrho/(\lambda + 2\mu)}\,\omega^2\varrho}, \tag{4.41}$$

$$\mathbf{T}_{41}(L) = 2i\left(1 - \frac{2\mu k^2}{\omega^2\varrho}\right)k\mu(\operatorname{ch} p_3 L - \operatorname{ch} p_1 L), \tag{4.42}$$

$$\text{(4.43)}\qquad \mathbf{T}_{42}(L) = -\frac{(\omega^2\varrho - 2\mu k^2)^2 \operatorname{sh} p_1 L}{\sqrt{k^2 - \omega^2\varrho/\mu}\,\omega^2\varrho} + \frac{4\sqrt{k^2 - \omega^2\varrho/(\lambda+2\mu)}\,\mu^2 k^2 \operatorname{sh} p_3 L}{\omega^2\varrho},$$

$$\text{(4.44)}\qquad \mathbf{T}_{43}(L) = -\frac{i(\omega^2\varrho - 2\mu k^2) k \operatorname{sh} p_1 L}{\sqrt{k^2 - \omega^2\varrho/\mu}\,\omega^2\varrho} - \frac{2i\sqrt{k^2 - \omega^2\varrho/(\lambda+2\mu)}\,\mu k \operatorname{sh} p_3 L}{\omega^2\varrho},$$

$$\text{(4.45)}\qquad \mathbf{T}_{44}(L) = \left(1 - \frac{2\mu k^2}{\omega^2\varrho}\right) \operatorname{ch} p_1 L + \frac{2\mu k^2}{\omega^2\varrho} \operatorname{ch} p_3 L .$$

## 5. Elastic waves in layered media

The transition matrices obtained in Sec. 4 enable us to describe the transition of the two-dimensional elastic wave through a multi-layered medium. In such a case, knowing the transition matrices through individual layers, we can obtain the transition matrix through the whole stratified medium as a product of the matrices.

The transition matrix $\mathbf{T}(\cdot)$ enables us to express the wave field $\hat{\mathbf{u}}$,

$$\text{(5.1)}\qquad \hat{\mathbf{u}} = \begin{bmatrix} \hat{u} \\ \hat{\tau} \end{bmatrix} \qquad \text{or} \qquad \hat{\mathbf{u}} = \begin{bmatrix} \hat{u}_1 \\ \hat{u}_2 \\ \hat{\tau}_1 \\ \hat{\tau}_2 \end{bmatrix},$$

at any point $x = L \in \mathbb{R}^+$ in a homogeneous medium, provided the boundary condition $\hat{\mathbf{u}}_0 = \hat{\mathbf{u}}(0)$ at $x = 0$ is known in the form (3.13).

Consider at the moment the multi-layered medium (slab) built of $N$ layers of elastic materials, with thicknesses $\Delta_j$, $j = 1, 2, \ldots, N$. Assume that the stratified medium is surrounded by the homogeneous elastic environment, at $x < 0$ and $x > L = \sum_{j=1}^{N} \Delta_j$. Since the wave field $\hat{\mathbf{u}}$ must be continuous at the interfaces of the layers in the stratified medium, we can express the wave, generated by some boundary conditions $\hat{\mathbf{u}}_0$ at $x = 0$, after it reaches the point $L$, in the form

$$\text{(5.2)}\qquad \hat{\mathbf{u}}(L) = \mathbf{T}_N(\Delta_N)\mathbf{T}_{N-1}(\Delta_{N-1}) \ldots \mathbf{T}_2(\Delta_2)\mathbf{T}_1(\Delta_1)\hat{\mathbf{u}}_0,$$

or, in a more convex form, by

$$\text{(5.3)}\qquad \hat{\mathbf{u}}(L) = \prod_{j=1}^{N} \mathbf{T}_j(\Delta_j)\hat{\mathbf{u}}_0,$$

where $\hat{\mathbf{u}}_0$ is the vector describing the incident and reflected wave, $\hat{\mathbf{u}}(L)$ is the vector of the transmitted wave, $\mathbf{T}_j(\cdot)$ is the transition matrix through $j$-th layer, for $j = 1, 2, \ldots, N$, depending on the material parameters of the layer.

In the above equation all the material properties of the multi-layered medium are completely described by the $4 \times 4$ matrix $\mathcal{T}$, being the product of the transition matrices through the individual layers and interpreted as a transition matrix through the slab built of $N$ layers of homogeneous elastic materials,

$$\mathcal{T} = \prod_{j=1}^{N} \mathbf{T}_j(\Delta_j). \tag{5.4}$$

Let us remark that vector $\hat{\mathbf{u}}_0$ describes jointly the (Fourier transforms of) incident wave pulse (going to the right), and all the reflected pulses leaving the slab (going to the left), generated by all the reflections at the interfaces of the layers, measured at the plane $x \equiv 0$. Similarly, $\hat{\mathbf{u}}(L)$ represents the transmitted pulses, generated by all the reflections and transmissions at the internal interfaces of the layers, measured at the plane $x \equiv L$.

## 6. The limiting case – homogenization

Assume that the slab is built of $2K$ layers with thicknesses $l_1(\gamma), l_2(\gamma), \ldots, l_{2K}(\gamma)$, where $l_i(\gamma)$, $i = 1, 2, \ldots, 2K$ are random variables. In the above $\gamma \in \Gamma$ is an elementary event and $(\Gamma, \mathcal{F}, \mathcal{P})$ is the complete probabilistic space. Assume additionally that the material parameters of the layers and their thicknesses $(\varrho_{2j-1}(\gamma), \lambda_{2j-1}(\gamma), \mu_{2j-1}(\gamma), l_{2j-1}(\gamma), \varrho_{2j}(\gamma), \lambda_{2j}(\gamma), \mu_{2j}(\gamma), l_{2j}(\gamma))$ are, as the vector random variables, independent and identically distributed for $j = 1, 2, \ldots, K$. Moreover, we assume that the thicknesses of the layers have the following particular property:

$$(l_{2j-1}(\gamma), l_{2j}(\gamma)) = \left( \frac{L_{2j-1}(\gamma)}{2K} \frac{L_{2j}(\gamma)}{2K} \right), \tag{6.1}$$

for $j = 1, 2, \ldots, K$, are independent, identically distributed two-dimensional random variables with the given mean values:

$$E\{L_{2j-1}(\gamma)\} = L^1, \qquad E\{L_{2j}(\gamma)\} = L^2. \tag{6.2}$$

In this particular case the periodically repeated segments of the bar are built of the couples of the elements with lengths $l_{2j-1}(\gamma), l_{2j}(\gamma)$, $j = 1, 2, \ldots, K$. For such segments the transition matrices $\mathbf{M}_j(\gamma)$ are the products of the pairs of the transition matrices through the individual layers,

$$\mathbf{M}_j(\gamma) = \mathbf{T}_{2j-1}(l_{2j-1}(\gamma))\mathbf{T}_{2j}(l_{2j}(\gamma)), \qquad j = 1, 2, \ldots, K, \tag{6.3}$$

and the Eq. (5.3) for the Fourier transform of the amplitudes takes the following form ($2K = N$):

$$\hat{\mathbf{u}}(L) = \prod_{j=1}^{K} \mathbf{M}_j(\gamma)\, \hat{\mathbf{u}}_0, \tag{6.4}$$

where $L = L(\gamma) = \sum_{j=1}^{N} l_j(\gamma)$.

To study the asymptotic behaviour of the randomized equation for the amplitudes of the waves, we apply the law of large numbers for the products of random matrices obtained in [3]. This theorem can be written in the following form.

*Consider the sequence of the products of real random matrices*

$$\mathbf{P}_K(\gamma) = \prod_{j=1}^{K} \mathbf{M}_{j,K}(\gamma). \tag{6.5}$$

*It is assumed that for $K$ tending to infinity the matrices $\mathbf{M}_{j,K}$ can be represented by*

$$\mathbf{M}_{j,K}(\gamma) = \mathbf{Id} + \frac{1}{K}\mathbf{B}_{j,K}(\gamma) + \mathbf{R}_j(K,\gamma), \tag{6.6}$$

*where $\mathbf{B}_{j,K}(\gamma)$ for $j = 1, 2, \ldots, K$ are independent, identically distributed random matrices, integrable with respect to probability measure $\mathcal{P}$ and $|\mathbf{R}_j(K,\gamma)| = o(K^{-1})$ for large $K$. Under these conditions, the law of large numbers holds true and*

$$\lim_{K\to\infty} \mathbf{P}_K(\gamma) = \exp\left(E\{\mathbf{B}_{j,K}(\gamma)\}\right), \tag{6.7}$$

*in the sense of convergence in distribution of all the vectors obtained by multiplication of the random matrix by an arbitrary deterministic vector.*

The presented method makes it possible to obtain the effective transition matrices in both cases of the anti-plane (Sec. 3) and the plane (Sec. 4) state of deformation. Let us begin the considerations from the more complicated, second example.

To analyze the limiting case of Eq. (6.4) when $K$ tends to infinity, we expand, at the beginning, the transition matrix defined in (4.30)–(4.45) under the assumption (6.1) on the thickness of the layers, with respect to the powers of $1/K$:

$$\mathbf{T}_j\left(\frac{L_j}{K}\right) = \begin{bmatrix} 1 & 0 & 0 & 0 \\ 0 & 1 & 0 & 0 \\ 0 & 0 & 1 & 0 \\ 0 & 0 & 0 & 1 \end{bmatrix} + \frac{L_j}{K}\begin{bmatrix} 0 & -ik\alpha_j & \kappa_j & 0 \\ -ik & 0 & 0 & \eta_j \\ -\omega^2\varrho_j & 0 & 0 & -ik \\ 0 & 4k^2\beta_j - \omega^2\varrho_j & -ik\alpha_j & 0 \end{bmatrix} + o\left(\frac{L_j}{K}\right). \tag{6.8}$$

Multiplying the matrix $\mathbf{T}_1(L_1)$, corresponding to the transition matrices with odd indices by $\mathbf{T}_2(L_2)$ – with even indices, we obtain, that the matrices $\mathbf{B}_j$ required

in formula (6.7) are defined as (we have changed the numeration of the random variables being the material parameters and the thicknesses of the layers according to the following rule: $b_{2j-1} = b_j^1$, $b_{2j} = b_j^2$ for any parameter ($b$ is $\alpha, \beta, \kappa, \eta, \varrho$ or $L$) and $j = 1, 2, \ldots, K$, so the parameters with identical superscripts – 1 or 2 – have identical distributions):

$$\mathbf{B}_j = \begin{bmatrix} 0 & -ik\left(\alpha_j^1 L_j^1 + \alpha_j^2 L_j^2\right) \\ -ik\left(L_j^1 + L_j^2\right) & 0 \\ -\omega^2\left(\varrho_j^1 L_j^1 + \varrho_j^2 L_j^2\right) & 0 \\ 0 & 4k^2\left(\beta_j^1 L_j^1 + \beta_j^2 L_j^2\right) - \omega^2\left(\varrho_j^1 L_j^1 + \varrho_j^2 L_j^2\right) \end{bmatrix} \tag{6.9}$$

$$\begin{bmatrix} \kappa_j^1 L_j^1 + \kappa_j^2 L_j^2 & 0 \\ 0 & \eta_j^1 L_j^1 + \eta_j^2 L_j^2 \\ 0 & -ik\left(L_j^1 + L_j^2\right) \\ -ik\left(\alpha_j^1 L_j^1 + \alpha_j^2 L_j^2\right) & 0 \end{bmatrix}.$$

The common average value of the matrices $\mathbf{B}_j$ is

$$E\{\mathbf{B}_j\} = \begin{bmatrix} 0 & -ik\,E(\alpha_j^1 L_j^1 + \alpha_j^2 L_j^2) \\ -ik\,E(L_j^1 + L_j^2) & 0 \\ -\omega^2 E(\varrho_j^1 L_j^1 + \varrho_j^2 L_j^2) & 0 \\ 0 & 4k^2 E(\beta_j^1 L_j^1 + \beta_j^2 L_j^2) - \omega^2 E(\varrho_j^1 L_j^1 + \varrho_j^2 L_j^2) \end{bmatrix} \tag{6.10}$$

$$\begin{bmatrix} E(\kappa_j^1 L_j^1 + \kappa_j^2 L_j^2) & 0 \\ 0 & E(\eta_j^1 L_j^1 + \eta_j^2 L_j^2) \\ 0 & -ikE(L_j^1 + L_j^2) \\ -ikE(\alpha_j^1 L_j^1 + \alpha_j^2 L_j^2) & 0 \end{bmatrix},$$

where in the above formulae the parameters and the thicknesses are random variables with distributions identical for all couples of layers.

The matrix $e^{E\{\mathbf{B}_j\}}$ is of the form analogous to (4.30)–(4.45) where, instead of the parameters $\alpha(\gamma), \beta(\gamma), \kappa(\gamma), \varrho(\gamma), \eta(\gamma), p_1(\gamma), p_3(\gamma)$, being random variables,

one has the effective constant parameters $\alpha^{\text{eff}}, \beta^{\text{eff}}, \kappa^{\text{eff}}, \varrho^{\text{eff}}, \eta^{\text{eff}}, p_1^{\text{eff}}, p_3^{\text{eff}}$, defined as

$$\alpha^{\text{eff}} = \frac{E\left\{\alpha^1(\gamma)L^1(\gamma) + \alpha^2(\gamma)L^2(\gamma)\right\}}{L}, \tag{6.11}$$

$$\beta^{\text{eff}} = \frac{E\left\{\beta^1(\gamma)L^1(\gamma) + \beta^2(\gamma)L^2(\gamma)\right\}}{L}, \tag{6.12}$$

$$\kappa^{\text{eff}} = \frac{E\left\{\kappa^1(\gamma)L^1(\gamma) + \kappa^2(\gamma)L^2(\gamma)\right\}}{L}, \tag{6.13}$$

$$\eta^{\text{eff}} = \frac{E\left\{\eta^1(\gamma)L^1(\gamma) + \eta^2(\gamma)L^2(\gamma)\right\}}{L}, \tag{6.14}$$

$$\varrho^{\text{eff}} = \frac{E\left\{\varrho^1(\gamma)L^1(\gamma) + \varrho^2(\gamma)L^2(\gamma)\right\}}{L}, \tag{6.15}$$

where

$$\alpha^1 = \frac{\lambda^1}{(\lambda^1 + 2\mu^1)}, \qquad \alpha_2 = \frac{\lambda^2}{(\lambda^2 + 2\mu^2)}, \tag{6.16}$$

$$\beta^1 = \frac{4\mu^1(\lambda^1 + \mu^1)}{(\lambda^1 + 2\mu^1)}, \qquad \beta^2 = \frac{4\mu^2(\lambda^2 + \mu^2)}{(\lambda^2 + 2\mu^2)}, \tag{6.17}$$

$$\kappa^1 = \frac{1}{(\lambda^1 + 2\mu^1)}, \qquad \kappa^2 = \frac{1}{(\lambda^2 + 2\mu^2)}, \tag{6.18}$$

$$\eta^1 = \frac{1}{\mu^1}, \qquad \eta^2 = \frac{1}{\mu^2}, \tag{6.19}$$

$$L = L^1 + L^2 \tag{6.20}$$

and

$$p_{1,3}^{\text{eff}} = \sqrt{2k^2 - \omega^2 A_2^{\text{eff}} \pm \omega^2 A_3^{\text{eff}}}/\sqrt{2}, \tag{6.21}$$

with the parameters $A_2^{\text{eff}}$ and $A_3^{\text{eff}}$ which are defined as:

$$A_2^{\text{eff}} = \varrho^{\text{eff}}(\kappa^{\text{eff}} + \eta^{\text{eff}}) = \varrho^{\text{eff}} \frac{\lambda^{\text{eff}} + 3\mu^{\text{eff}}}{\mu^{\text{eff}}(\lambda^{\text{eff}} + 2\mu^{\text{eff}})}, \tag{6.22}$$

$$A_3^{\text{eff}} = \varrho^{\text{eff}}(\kappa^{\text{eff}} - \eta^{\text{eff}}) = \varrho^{\text{eff}} \frac{\lambda^{\text{eff}} + \mu^{\text{eff}}}{\mu^{\text{eff}}(\lambda^{\text{eff}} + 2\mu^{\text{eff}})}. \tag{6.23}$$

Similarly in the case of anti-plane deformation, the transition matrix through the individual layer (3.18) can be written in the form (6.6),

$$\mathbf{T}_j\left(\frac{L_j}{K}\right) = \begin{bmatrix} 1 & 0 \\ 0 & 1 \end{bmatrix} + \frac{L_j}{K}\begin{bmatrix} 0 & \frac{1}{\mu} \\ \mu k^2 - \varrho\omega^2 & 0 \end{bmatrix} + o\left(\frac{L_j}{K}\right). \tag{6.24}$$

The matrix $\mathbf{B}_j$ is, in the case of the anti-plane wave pulses, of the form

$$\mathbf{B}_j = \begin{bmatrix} 0 \\ \left(\mu^1(\gamma)L^1(\gamma)+\mu^2(\gamma)L^2(\gamma)\right)k^2-\left(\varrho^1(\gamma)L^1(\gamma)+\varrho^2(\gamma)L^2(\gamma)\right)\omega^2 \\ \dfrac{L^1(\gamma)}{\mu^1(\gamma)}+\dfrac{L^2(\gamma)}{\mu^2(\gamma)} \\ 0 \end{bmatrix}. \tag{6.25}$$

By averaging the matrix $\mathbf{B}_j$ we can see that the effective transition matrix depends now on three parameters: $\kappa^{\text{eff}}$ and $\varrho^{\text{eff}}$, defined in (6.14), (6.15), and on the additional parameter $\mu^{\text{eff}}$, defined as:

$$\mu^{\text{eff}} = \frac{E\left\{\mu^1(\gamma)L^1(\gamma)+\mu^2(\gamma)L^2(\gamma)\right\}}{L}. \tag{6.26}$$

The transition matrix has the form analogous to (3.18) with suitable effective parameters, where

$$p^{\text{eff}} = \sqrt{k^2-\varrho^{\text{eff}}\omega^2/\mu^{\text{eff}}}\,. \tag{6.27}$$

As a conclusion of the above considerations we can say that the elastic homogenized medium (obtained by the homogenization procedure from a randomly stratified medium) conducting wave pulses is completely described by six parameters: $\alpha^{\text{eff}}, \beta^{\text{eff}}, \kappa^{\text{eff}}, \eta^{\text{eff}}, \mu^{\text{eff}}$ and $\varrho^{\text{eff}}$, defined in (6.11)–(6.15) and (6.26).

## 7. Closing remarks

In the paper we have considered the model of stratified medium, that is the slab built of a number of isotropic, homogeneous elastic layers. Such a medium, globally, is both anisotropic and nonhomogeneous. After the presented averaging procedure, it becomes homogeneous but remains anisotropic (locally and globally transversally isotropic). The elastic properties of such a medium are described by a tensor, whose 5 elements are independent (see [22]). However, as we have seen from the considerations of the previous sections, to describe the elastic waves in the case of the plane state of deformation we need four elastic constants, while in the anti-plane state only two elastic constants are necessary (one of them – different than in the plane state). This statement remains valid both in the dynamic nonstationary case, studied in this paper, and in the stationary one (see [14]).

The above considerations were performed analytically. Solution of the equations, that is calculation of the resulting waves (reflected and transmitted) generated by some incident pulse needs numerical calculations. The most effective way

of doing this is calculating the inverse Fourier transform using the Fast Fourier Transform algorithm (see [20]). Effective results in this field require precise specification of the incident pulse (that is, its shape, caused by the form of the source generating the disturbance).

Let us finally remark that the model of stratified medium considered in this paper is an idealization of a real physical medium. Therefore it neglects many effects observed in nature (like dissipation of energy or dispersion of waves in layered media) and needs some modifications. However, the improvement of the model of two-dimensional stratified medium is connected with the growth of the dimension of the system of the corresponding partial differential equations and is connected with numerical difficulties.

## References


1. L.-E. ANDERSON and B. LUNDBERG, *Some fundamental transmission properties of impedance transitions*, Wave Motion, 6, pp. 389-406, 1984.
2. G. BECUS, *Wave propagation in imperfectly periodic structures: a random evolution approach*, ZAMP, 29, pp. 252–261, 1978.
3. M.A. BERGER, *Central limit theorem for products of random matrices*, Trans. A.M.S., 285, pp. 777–803, 1984.
4. L.M. BREKHOVSKIKH and O.A. GODIN, *Acoustics of layered media I, II*, Springer-Verlag, Berlin 1990.
5. J.F. DOYLE, *Wave propagation in structures. An FFT-based spectral analysis methodology*, Springer-Verlag, Berlin 1989.
6. N.A. HASKELL, *Crustal reflection of plane SH waves*, J. Geophys. Res., 65, pp. 4147–4150, 1960.
7. N.A. HASKELL, *Crustal reflection of plane P and SV waves*, J. Geophys.Res., 67, pp. 4751–4769, 1962.
8. N.A. HASKELL, *Radiation pattern of surface waves from point sources in a multi-layered medium*, Bull. Seismol. Soc. of America, 54, pp. 377–393, 1964.
9. S. KALISKI [Ed.], *Vibrations and waves in solids*, PWN, Warszawa 1966.
10. B.L.N. KENNETT, *Elastic wave propagation in stratified media*, [in:] Advances in Applied Mech., 21, pp. 79–167, 1981.
11. B.L.N. KENNETT, *Seismic wave propagation in stratified media*, Cambridge University Press, London 1983.
12. Z. KOTULSKI, *On the effective reflection properties of the randomly stratified elastic slab*, ZAMM, 70, T211-T213, 1990.
13. Z. KOTULSKI, *Wave propagation in randomly stratified media and the law of large numbers*, J. Sound and Vibration, 158, pp. 93–104, 1992.
14. Z. KOTULSKI, *Elastic waves in randomly stratified medium, Part 1. Analytical results*, Acta Mech., 83, pp. 61–75, 1990; *Part 2. Numerical results*, Acta Mech., 85, pp. 111–222, 1992.
15. Z. KOTULSKI, *On the effective reflection properties of the randomly segmented elastic bar*, European J. Mech., A/Solids, 13, 5, pp. 677–696, 1994.
16. Z. KOTULSKI, *On the effective reflection properties of the randomly segmented elastic bar. Formulation and final results*, ZAMM, 74, T149-T151, 1994.
17. R.B. LINDSAY, *Filtration of oblique elastic waves in stratified media*, J. Acous. Soc. Am., 11, pp. 178–183, 1939.
18. B. LUNDBERG, R. GUPTA and L.-E. ANDERSON, *Optimum transmission of elastic waves through joints*, Wave Motion, 1, pp. 193–200, 1979.
19. W. NOWACKI, *Theory of elasticity*, PWN, Warsaw 1970.
20. W.H. PRESS, B.F. FLANNERY, S.A. TEUKOLSKY and W.T. VETTERLING, *Numerical recipes. The art of scientific computing*, Cambridge University Press, London 1986.
21. H. REISSNER, *Der senkrechte und schräge Durchtritt einer in einem flüssigen Medium erzeugten ebenen Dilatations-Welle durch eine in diesem Medium befindliche planparallele feste Platte*, Helv. Phys. Acta, 11, pp. 140–155, 1938.

22. G.P. SENDECKYJ [Ed.], *Mechanics of composite materials*, vol. 2, Academic Press, New York 1974.
23. V.I. SMIRNOV, *Course of higher mathematics*, vol. 3, part 2, State Editors of Physical and Mathematical Literature, Moscov 1961.
24. J.B. SMYTH and R.B. LINDSAY, *Supersonic transmission at oblique incidence through a solid plate in water*, J. Acous. Soc. Am., 16, pp. 20–25, 1944.
25. F. ZIEGLER, *Wave propagation in periodic and disordered layered composite elastic materials*, Int. J. Solids Structures, 13, pp. 293–305, 1977.

POLISH ACADEMY OF SCIENCES,
INSTITUTE OF FUNDAMENTAL TECHNOLOGICAL RESEARCH, WARSZAWA.

*Received October* 12, 1994.

*Centre International des Sciences Mecaniques*

*International Centre for Mechanical Sciences*

# PRELIMINARY PROGRAMME 1995

*Courses*

New Design Concepts for High Speed Air Transport
Coordinator: H. Sobieczky (Göttingen) — June 5 - 9, 1995

Bone Cell and Tissue Mechanics
Coordinator: S.C. Cowin (New York) — July 10 - 14, 1995

Liquid Bridge Theory and Applications
Coordinator: J. Meseguer (Madrid) — July 17- 21, 1995

Mathematical Modelling for Arch Dam design and Safety Control
Coordinators: M. E.R. de Arantes e Oliveira, J.O. Pedro (Lisboa) — Sept. 4 - 8, 1995

Mechanics of Solids with Phase Changes
Coordinators: M. Berveiller (Metz), F.D. Fischer (Leoben) — Sept. 11 - 15, 1995

Modelling and Simulation of Hypersonic Flows for Spatial Flights
Coordinator: R. Brun (Marseille) — Sept. 18 - 22, 1995

Control of Flow Instabilities and Unsteady Flows
Coordinators:
G.E.A. Meier (Göttingen), G.H. Schnerr (Karlshruhe) — Sept. 18 - 22, 1995

Advanced Methods of Tunnelling
Coordinator: K. Kovari (Zürich) — Sept. 25 - 29, 1995

Earthquake Resistant Design
Coordinator: R.T. Duarte (Lisboa) — Oct. 2 - 6, 1995

The Flow of Particles in Suspension
Coordinator: G. Cognet (Grenoble) — Oct. 9 - 13, 1995

*Meetings Hosted by CISM*

Workshop on "Multimedia GIS Data"
International Society for Photogrammetry and Remote Sensing – Commission I
Coordinators: R. Galetto (Pavia), F. Crosilla (Udine) — June 12 - 16, 1995

10th International Conference on Artifical Intelligence in Engineering
Chairmen: C.A. Brebbia (Southampton), C. Tasso (Udine) — July 4 - 6, 1995

I-33100 Udine (Italy), Palazzo del Torso, Piazza Garibaldi, 18
Tel: + 39 0432 - Secretariat 294989 or 508251 - Administration 294795 - Printing Office 45533 - Fax 501523
Partita I.V.A. 00401650304

**Computer Assisted Mechanics and Engineering Sciences (CAMES)**

to be published quarterly starting in 1994

Editor: M. Kleiber, Warsaw Associate Editor: H.A. Mang, Vienna

Scope of the Journal

Computer Assisted Mechanics and Engineering Sciences (CAMES) is a refereed international journal, published quarterly, providing an international forum and an authoritative source of information in the field of computational mechanics and related problems of applied science and engineering.

The specific objective of the journal is to support researchers and practitioners based in Central Europe by offering them a means facilitating (a) access to newest research results by leading experts in the field (b) publishing their own contributions and (c) dissemination of information relevant to the scope of the journal.

Papers published in the journal will fall largely into three main categories. The first will contain state-of-the-art reviews with the emphasis on providing the Central European readership with a guidance on important research directions as observed in the current world literature on computer assisted mechanics and engineering sciences.

The second category will contain contribution presenting new developments in the broadly understood field of computational mechanics including solid and structural mechanics, multi-body system dynamics, fluid dynamics, constitutive modeling, structural control and optimization, transport phenomena, heat transfer, etc. Variational formulations and numerical algorithms related to implementation of the finite and boundary element methods, finite difference method, hybrid numerical methods and other methodologies of computational mechanics will clearly be the core areas covered by the journal.

The third category will contain articles describing novel applications of computational techniques in engineering practice; areas of interest will include mechanical, aerospace, civil, naval, chemical and architectural engineering as well as software development.

The journal will also publish book reviews and information on activities of the Central European Association of Computational Mechanics.

Subscription and sale of single issues is managed by the Editorial Office.
Price of single issue: 25 USD (in Poland: 7,00 zł)

Address: Editorial Office, CAMES
Polish Academy of Sciences
Institute of Fundamental Technological Research
ul. Świętokrzyska 21, PL 00-049 Warsaw, Poland
Our Bankers: IV Oddz. Pekao SA Warszawa 501132-40054492-3111

**INSTITUTE OF FUNDAMENTAL TECHNOLOGICAL RESEARCH**
is publishing the following periodicals:

ARCHIVES OF MECHANICS — bimonthly (in English)
ARCHIVES OF ACOUSTICS — quarterly (in English)
ARCHIVES OF CIVIL ENGINEERING — quarterly (in English)
ENGINEERING TRANSACTION — quarterly (in English)
COMPUTER ASSISTED MACHANICS AND ENGINEERING SCIENCES — quarterly (in English)
JOURNAL OF TECHNICAL PHYSICS — quarterly (in English)

Subscription orders for all the magazines published in Poland available trought the local press distributors or directly trought the *Foreign Enterprise ARS POLONA*, Krakowskie Przedmieście 7, 00-068 Warszawa, Poland.

**Address of the Editorial Office:**

Institute of Fundamental Technological Research,
Świętokrzyska 21, p. 508,
00-049 WARSZAWA, Poland.

## DIRECTIONS FOR THE AUTHORS

The periodical *ARCHIVES OF MECHANICS (ARCHIWUM MECHANIKI STOSOWANEJ)* deals with the printing of original papers which should not appear in any other publications. The authors may publish in the Bull. Acad. Polon. Sci. short papers only, announcing the solutions of any problems as well as informing that the full text will be inserted in the columns of the *ARCHIVES OF MECHANICS (ARCHIWUM MECHANIKI STOSOWANEJ)*.

As a rule, the volume of a paper should not exceed 40 000 typographic signs, that is about 20 type-written pages, format: 210 × 297 mm, leaded. The papers should be submitted in two copies. They must be set in accordance with the norms established by the Editorial Office. Special importance is attached to the following directions:

1. The title of the paper should be as short as possible.

2. The text should be preceded by a brief introduction; it is also desirable that a list of notations used in the paper be given.

3. Short papers should be divided into sections and subsections, long papers into sections, subsections and points. Each section, subsection or point must bear a title.

4. The formula number consists of two figures: the first represents the section number and the other the formula number under that section. Thus the division into subsections does not influence the numbering of formulae. Only such formulae should be numbered to which the author refers throughout the paper, also the resulting formulae. The formula number should be written on the left-hand side of the formula; brackets are to be only to avoid any misunderstanding. For instance, if the author refers to formula 3 of the set (2.1), a subscript should be added to denote the set of formula, viz. $(2.1)_3$.

5. All the notations should be written very distinctly. Special care must be taken to write small and capital letters as precisely as possible. Semi-bold type must be underlined in black pencil. Explanations should be given on the margin of the manuscript in case of special type face.

6. It has been established to denote vectors semi-bold type, transforms of the corresponding functions by tilded symbols. Trigonometric functions are denoted by sin, cos, tg and ctg, inverse functions – by arc sin, arc cos, arc tg and arc ctg; hyperbolic functions are denoted by sh, ch, th and cth, inverse functions – by Arsh, Arch, Arth and Arcth.

7. Figures in brackets denote reference titles. Items appearing in the reference list should include the initials of the first name of the author and his surname, also the full title of the paper (in the language of the original paper); moreover;

a) in the case of books, the publisher's name, the place and year of publication should be given, e.g.,
5. S. Ziemba, *Vibration analysis*, PWN, Warszawa 1970;

b) in the case of a periodical, the full title of the periodical, consecutive volume number, current issue number, pp. from ... to ..., year of publication should be mentioned; the annual volume number must be marked in black pencil so as to distinguish it from the current issue number, e.g.,
6. M. Sokołowski, *A thermoelastic problem for a strip with discontinuous boundary conditions*, Arch. Mech., **13**, 3, 337–354, 1961.

8. The authors should enclose a summary of the paper. The volume of the summary is to be about 100 words.

Upon receipt of the paper, the Editorial Office forwards it to the reviewer. His opinion is the basis for the Editorial Committee to determine whether the paper can be accepted for publication or not.

The printing of the paper completed, the author receives 25 copies of reprints free of charge. The authors wishing to get more copies should advise the Editorial Office accordingly, not later than the date of obtaining the galley proofs.

**The papers submitted for publication in the journal should be written in English. No royalty are paid to the authors.**

**Please send us, in addition to the typescript, the same text prepared on a diskette (floppy disk) 3 1/2″ or 5 1/4″ as an ASCII file, in Dos or Unix format.**

*EDITORIAL COMMITTEE*
*ARCHIVES OF MECHANICS*
*(ARCHIWUM MECHANIKI STOSOWANEJ)*